Mechanische und spektroskopische Eigenschaften von seltenerd-dotierten Aluminosilicatgläsern

Kumulative Dissertation

zur Erlangung des akademischen Grades
doctor rerum naturalium (Dr. rer. nat.)

seit 1558

vorgelegt dem Rat der Chemisch-Geowissenschaftlichen Fakultät
der Friedrich-Schiller-Universität Jena

von Diplom-Chemiker Mirko Tiegel
geboren am 09.09.1986 in Zeitz

Gutachter:

1. Prof. Dr. Dr. Dr. Christian Rüssel (FSU Jena)
2. Hdoz. Dr. Doris Ehrt (FSU Jena)

Tag der öffentlichen Verteidigung: 29.04.2015

Meiner lieben Familie.

Inhaltsverzeichnis

1. Einleitung / Motivation

1960 wurde von Maiman [1] der weltweit erste Laser mit einem Rubinkristall ($Cr^{3+} : Al_2O_3$) und Blitzlampenanregung realisiert. Noch im selben Jahr wurden weitere Materialien gefunden, die Laseraktivität zeigen ($U^{3+} : CaF_2$ [2], He-Ne-Gaslaser [3]). Schließlich konnte Snitzer [4] ein Jahr später auch einen Glaslaser verwirklichen ($Nd^{3+} : BaO\text{-}K_2O\text{-}SiO_2$), auf dessen Realisierung viele weitere Entwicklungen in den Bereichen von Lasern, optischen Bauelementen und Faserkommunikation beruhen.

Im einfachsten Aufbau besteht ein Laser aus einem aktiven Verstärkermaterial in einem optischen Resonanzraum. Das Verstärkermaterial kann ein Festkörper, Flüssigkeit, Gas oder Plasma sein, in das zunächst Energie von einer externen Energiequelle gepumpt wird. Die Pumpenergie führt zu Rotations-, Vibrations- und / oder elektronischen Übergängen von niedrigen zu hohen Energiezuständen in Atomen oder Molekülen, wobei unter bestimmten Bedingungen eine, für die Laseraktivität notwendige, Besetzungsinversion zwischen zwei Energiezuständen erreicht wird. Der Resonanzraum sorgt für eine Lichtzirkulation im Verstärkermaterial, von der entweder kontinuierliches oder gepulstes Licht ausgekoppelt wird. Dieses Lasersystem, bestehend aus Verstärkermaterial, Pumpquelle und optischen Resonanzraum, wird auch als Oszillator bezeichnet. Daneben gibt es auch noch sogenannte Verstärker, die einen Laserstrahl modifizieren und dessen Energie weiter erhöhen. Mit einem gepulsten System aus Oszillator und darauffolgenden Verstärkerstufen können in Hochleistungslasern Spitzenleistungen von mehr als 10^{15} Watt (Petawatt) erzeugt werden [5]. Die Methode der Verstärkung von gechirpten Pulsen ermöglicht die Erzeugung dieser hohen Energiedichten. Dabei wird ein Lichtpuls zeitlich mit Hilfe von Gittern und Prismen gestreckt und kann danach weiter in Resonatoren verstärkt werden, ohne dass nichtlineare Effekte aufgrund zu hoher Intensitäten das Verstärkermaterial schädigen. Anschließend wird der verstärkte Puls wieder komprimiert, sodass höchste Spitzenleistungen im Tischgerätemaßstab erzeugt werden können. Diese Systeme ermöglichen ein breites Untersuchungsgebiet von Laser-Materie-Wechselwirkungen im Labormaßstab mit Anwendungen in Kernfusionsexperimenten, relativistischer Plasmaphysik, Röntgenstrahlerzeugung und vieles mehr. [6, 7]

Aktive Verstärkermaterialien für den Laserbetrieb müssen schmalbandige Fluoreszenzlinien, starke Absorptionsbanden und angemessen hohe Quantenausbeuten für den gewünschten Fluoreszenzübergang besitzen. Im Allgemeinen erfüllen Festkörper (Glas oder kristalline Materialien), die in geringen Mengen Ionen der Seltenerdmetalle enthalten, diese Voraussetz-

ungen. Deren optische Übergänge finden, bis auf wenige Ausnahmen, in der 4f-Schale ihrer Elektronenhülle statt. Die Abschirmung des umgebenden Ligandenfeldes der f-Elektronen durch weiter außen liegende s-, p- und d-Elektronen bewirkt vergleichsweise diskrete Energieniveaus und damit spektral schmale Absorptions- und Fluoreszenzemissionslinien. Neben den schmalen Emissionslinien werden Absorptionsübergänge für das Pumpen des Lasers benötigt, deren Anregungswellenlänge im Bereich des Emissionsspektrums von verfügbaren Pumpquellen wie Bogenlampen oder Laserdioden liegen.

Der herausragende praktische Vorteil von Glas gegenüber kristallinen Materialien ist die Möglichkeit enorme Dimensionen zu produzieren. Des Weiteren kann Glas mit weniger Aufwand in exzellenten Qualitäten mit feiner optischer Politur und Beschichtung hergestellt werden. Jedoch zeigen im Allgemeinen mit Laserionen dotierte Gläser größere Linienbreiten als entsprechend dotierte Kristalle, aufgrund der fehlenden Fernordnung der Glasstruktur und damit einer uneinheitlicheren Umgebung der dotierten Ionen. Deshalb sind bspw. Laserschwellen in Gläsern höher als in kristallinen Materialien. Auch besitzt Glas eine wesentlich geringere Wärmeleitfähigkeit als die meisten kristallinen Wirtsmaterialien. Dies kann bei hohen Pumpleistungen zu hohen Temperatur- und daraus resultierend zu Brechzahlgradienten führen, die wie eine zusätzliche Linse wirken (thermische Linse). [8]

Am Institut für Optik und Quantenelektronik in Jena wird ein vollständig Laserdiodengepumptes Lasersystem mit fs-Pulsen, Spitzenleistungen von mehreren 100 TW und Wiederholraten von 0,025 Hz betrieben. Als aktives Lasermaterial werden Ytterbium dotiertes Fluorid-Phosphatglas und CaF_2 verwendet. Wesentlicher Gegenstand der Weiterentwicklung des Lasersystems bildet die Erhöhung der Pulsenergie [9]. Da die Pulse dieses Lasersystems nicht einzeln ausgelöst werden, sondern relativ hohe Wiederholraten angestrebt werden, führen die Energieverluste im Verstärkermaterial während der Pulsextraktion zu einem erheblichen Wärmeeintrag und daraus folgend zu einer starken thermomechanischen Belastung in diesem. Wenn die thermomechanischen Belastungen zu groß für die mechanische Festigkeit des Materials werden, führt dies zu einem Spannungsbruch im Material, bevorzugt an Schwachstellen wie Verunreinigungen und Einschlüssen. Um dies zu vermeiden, wird der Wärmeeintrag begrenzt, wodurch die Pulsenergie des Lasersystems limitiert ist. Um diese erhöhen zu können, muss entweder die thermomechanische Spannung verringert oder die Widerstandskraft des Materials erhöht werden, ohne wesentliche Lumineszenzparameter zu verschlechtern. Dabei spielen der thermische Ausdehnungskoeffizient, die Bruchzähigkeit sowie die Festigkeit des Materials eine Rolle, wobei der thermische Ausdehnungskoeffizient hierbei am wichtigsten ist.

CaF_2 und Fluoridphosphatglas besitzen hohe thermische Ausdehnungskoeffizienten von 19 und $14 \cdot 10^{-6}$/K [10]. Aluminosilicatgläser können im Vergleich hierzu deutlich geringere Ausdehnungskoeffizienten [11] aufweisen. Des Weiteren besitzt dieses Glassystem für große Zusammensetzungsbereiche eine geringe Kristallisationsanfälligkeit [12], eine hohe Bruchzähigkeit [13], eine hohe chemische Beständigkeit [14] sowie eine geringe OH^-- und Platin-Löslichkeit [15]. Auch wird der Cluster-Effekt von Seltenerdionen durch Aluminium im Silicatnetzwerk unterdrückt [16-18]. Alle diese Eigenschaften zeigen, dass Aluminosilicatgläser eine vielversprechende Alternative zum verwendeten Fluoridphosphatglas in Hochenergielasern ist und dabei die Möglichkeit bietet, die Pulsenergie zu erhöhen.

Da Aluminosilicate in einem weiten Zusammensetzungsbereich Gläser bilden können, untersucht ein Teil dieser Arbeit den Einfluss der Glaszusammensetzung auf die anwendungsrelevanten Eigenschaften. Dazu wurde zunächst das, für andere Anwendungen gut untersuchte, MgO-Al_2O_3-SiO_2-System betrachtet und vor allem der Einfluss der Konzentration des Netzwerkwandlers analysiert. Schließlich wurden unterschiedliche Netzwerkwandler und Kombinationen aus mehreren Netzwerkwandlern betrachtet. Um fern von Effekten der Art der dotierten Seltenerdionen den Einfluss der Glaszusammensetzung auf die Lumineszenzeigenschaften zu diskutieren, wurden die Gläser, neben Ytterbium, auch mit Samarium und Europium dotiert.

Die relativ guten Lumineszenzeigenschaften, kostengünstigen Herstellungsbedingungen und vorteilhaften chemischen Beständigkeiten der betrachteten Aluminosilicatgläser ließen sich auch auf ein weiteres Anwendungsgebiet im Bereich der Lumineszenzmaterialien übertragen. Cer dotierte Gläser besitzen ein breites Anwendungsgebiet. In möglichen Quantum-Cutting-Systemen mit Ce^{3+} und Yb^{3+} diene Ce^{3+} als Sensibilisator und überträge absorbierte Energie aus dem UV-Spektralbereich auf Yb^{3+} [19]. In dieser Arbeit wurden spektroskopische Effekte der optischen Basizität und des Ce^{3+}/Ce^{4+}-Redoxgleichgewichtes untersucht um Schlußfolgerungen für die Optimierung des Wirtsglases für Ce^{3+}-Yb^{3+}-Quantum-Cutting-Systemen zu treffen.

Die vorliegende Arbeit beruht auf sechs Publikationen deren Ergebnisse im dritten Abschnitt dargelegt werden. Im nächsten Abschnitt sollen zunächst wichtige Grundlagen erläutert und eine Zusammenfassung bisheriger, für diese Arbeit relevanter Forschungsarbeiten vorgestellt werden. Der letzte Abschnitt fasst abschließend nochmals alle Ergebnisse zusammen und gibt einen Ausblick.

2. Grundlagen

2.1. Struktur von Aluminosilicatgläsern

In Aluminosilicatgläsern sind sowohl Silicium als auch Aluminium Netzwerkbildner und koordinieren mit Sauerstoff tetraedrisch [20-23]. Diese Tetraeder sind durch gemeinsame Sauerstoffatome verbunden, die auch als Brückensauerstoffe (BO) bezeichnet werden und bilden ein amorphes Netzwerk, in dem Netzwerkwandlerionen (Li^+, Na^+, K^+, Ca^{2+}, ...) dispergiert sind. Die im Jahre 1953 von Walter Loewenstein [24] aufgestellte Regel zur chemischen Zusammensetzung von Alumosilicaten besagt, dass die Verbindung von zwei Aluminiumatomen über ein Sauerstoffatom (Al-O-Al) instabil ist. In Aluminosilicatgläsern mit einem Al/Si-Verhältnis kleiner eins sollten demnach keine Al-O-Al-Strukturen vorliegen. Jedoch zeigen neuere NMR-Untersuchungen, dass in geringen Anteilen Al-O-Al-Strukturen auch in solchen Aluminosilicatgläsern existieren [25, 26].

Die $[SiO_4]$- und $[AlO_4]^-$-Tetraeder bilden im Glasnetzwerk Ringe unterschiedlicher Größen. Die Größenverteilung dieser Ringe wurde mittels molekulardynamischer Berechnungen ermittelt [27]. Dabei wurden hauptsächlich fünf bis sieben Tetraeder je Ring bestimmt. Untersuchungen an Aluminosilicatgläsern mit Hilfe von spektroskopischen Methoden zeigen eine ähnliche Verteilung von hauptsächlich 6 Tetraedern je Ring [28, 29].

Die formal negativen Ladungen der $[AlO_4]^-$-Tetraeder werden durch die positiv geladenen Netzwerkwandlerionen ausgeglichen. Ein Überschuss an Netzwerkwandlerionen führt zu Trennstellen im Netzwerk durch die Bildung von Trennstellensauerstoffen (NBO), die Ionenbindungen mit den Netzwerkwandlerionen bilden. Peralumische Glaszusammensetzung besitzen nicht genügend Netzwerkwandlerionen um die negativen Ladungen aller möglichen $[AlO_4]^-$-Tetraeder zu kompensieren und enthalten fünf- ($^{[5]}Al$) und sechsfach koordiniertes Aluminium ($^{[6]}Al$) [30, 31]. In ladungsbedingt ausgeglichenen Zusammensetzungen (wie zum Beispiel in $NaAlSi_3O_8$ oder $CaAl_2Si_2O_8$) sollten theoretisch alle Netzwerkwandlerionen zum Ladungsausgleich der $[AlO_4]^-$-Tetraeder verwendet werden und damit ein hochvernetztes Netzwerk ohne Trennstellen vorliegen. Jedoch zeigen Untersuchungen mittels Kernspinresonanzspektroskopie (NMR), dass ein geringer Anteil an Trennstellen in ausgeglichenen Aluminosilicatgläsern vorzufinden ist [32]. Auch belegen weitergehende Untersuchungen, dass selbst in Gläsern mit hohem Überschuss an Netzwerkwandlern $^{[5]}Al$ zu finden ist. Dabei ist die Konzentration von bis zu 8 % $^{[5]}Al$ abhängig von der SiO_2-Konzentration [33, 34]. Auch zeigen La- und Y-haltige Aluminosilicatgläser relativ hohe Konzentrationen von $^{[5]}Al$ und $^{[6]}Al$ [35, 36].

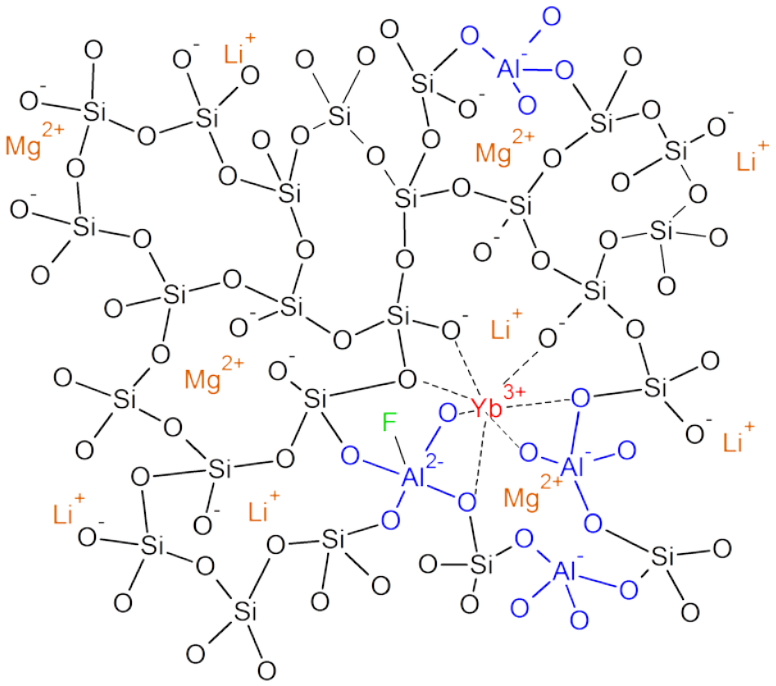

Abbildung 1: Model des Einbaus eines Seltenerdions in die Glasstruktur eines Aluminosilicates mit Fluorid

Die Zugabe von Fluoriden zur Glaszusammensetzung führt dazu, dass ein Teil der eingebrachten Fluoride als SiF_4 und/oder HF während des Schmelzprozesses abdampfen, sodass die H^+/OH^--Konzentration sinkt. Gleichzeitig wird Fluorid in das Aluminosilicat-Glasnetzwerk eingebaut und bildet Oxifluoridgruppen, wobei das Fluorid ausschließlich mit Aluminium koordiniert ist ($[AlO_xF_y]^{n-}$) Dabei steigt der Anteil an fünf- und sechsfach koordiniertem Aluminium im Glasnetzwerk [21, 37, 38].

Seltenerdionen (siehe Abb. 1) besitzen eine hohe positive Ladung sowie einen relativ kleinen Radius und haben somit hohe Feldstärken. Sie zeigen hohe Koordinationszahlen in Aluminosilicatgläsern von fünf bis neun in Abhängigkeit von der Zusammensetzung des Wirtsglases und dem Radius des Ions [39, 40]. Für den Ausgleich der positiven Ladungen besetzen die Seltenerdionen Plätze in depolymerisierten Zonen in der Nähe von Trennstellensauerstoffen und/oder $[AlO_4]^-$-Tetraedern. Dabei besteht eine Präferenz gegenüber $[AlO_4]^-$-Tetraedern. Also wirken sie selbst im Allgemeinen in der Glasstruktur als Netzwerkwandler. Des Weiteren wurden als übernächste Nachbarn Netzwerkwandlerionen nachgewiesen [41].

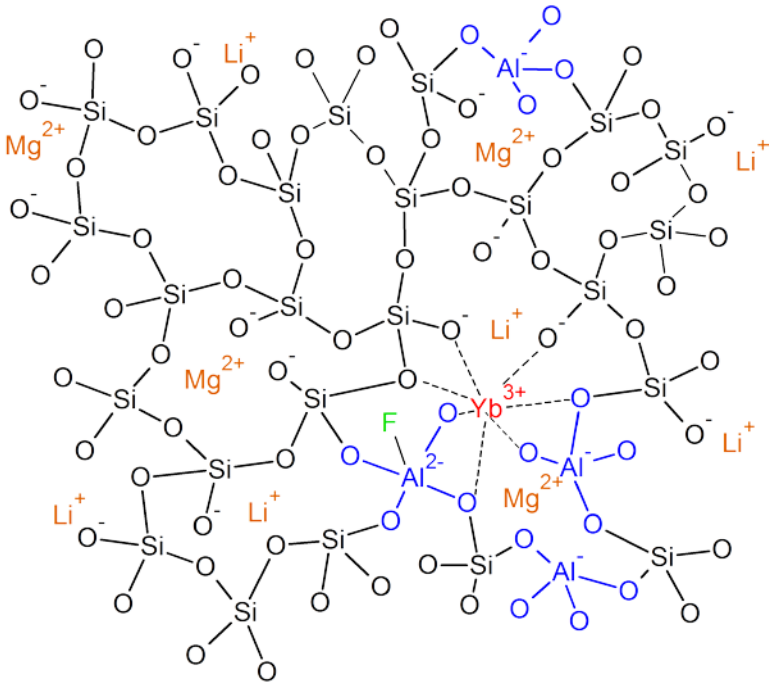

Abbildung 1: Model des Einbaus eines Seltenerdions in die Glasstruktur eines Aluminosilicates mit Fluorid

Die Zugabe von Fluoriden zur Glaszusammensetzung führt dazu, dass ein Teil der eingebrachten Fluoride als SiF_4 und/oder HF während des Schmelzprozesses abdampfen, sodass die H^+/OH^--Konzentration sinkt. Gleichzeitig wird Fluorid in das Aluminosilicat-Glasnetzwerk eingebaut und bildet Oxifluoridgruppen, wobei das Fluorid ausschließlich mit Aluminium koordiniert ist ($[AlO_xF_y]^{n-}$) Dabei steigt der Anteil an fünf- und sechsfach koordiniertem Aluminium im Glasnetzwerk [21, 37, 38].

Seltenerdionen (siehe Abb. 1) besitzen eine hohe positive Ladung sowie einen relativ kleinen Radius und haben somit hohe Feldstärken. Sie zeigen hohe Koordinationszahlen in Aluminosilicatgläsern von fünf bis neun in Abhängigkeit von der Zusammensetzung des Wirtsglases und dem Radius des Ions [39, 40]. Für den Ausgleich der positiven Ladungen besetzen die Seltenerdionen Plätze in depolymerisierten Zonen in der Nähe von Trennstellensauerstoffen und/oder $[AlO_4]^-$-Tetraedern. Dabei besteht eine Präferenz gegenüber $[AlO_4]^-$-Tetraedern. Also wirken sie selbst im Allgemeinen in der Glasstruktur als Netzwerkwandler. Des Weiteren wurden als übernächste Nachbarn Netzwerkwandlerionen nachgewiesen [41].

2.2. Seltenerdionen als Fluorophore

Die Gruppe der 14 Elemente des Periodensystems, die auf das Lanthan (Ordnungszahl 57) folgen, werden als Seltene Erdmetalle, Seltenerdmetalle oder Lanthanoide bezeichnet. Zu ihnen gehören die Elemente der Ordnungszahlen 58-71: Cer (Ce), Praseodym (Pr), Neodym (Nd), Promethium (Pm), Samarium (Sm), Europium (Eu), Gadolinium (Gd), Terbium (Tb), Dysprosium (Dy), Holmium (Ho), Erbium (Er), Thulium (Tm), Ytterbium (Yb) und Lutetium (Lu). Alle Elemente der Gruppe besitzen in der zweitäußersten Schale (5.) jeweils zwei s- und sechs p-Elektronen, sowie kein d-Elektron, außer Lanthan, Cer, Gadolinium und Lutetium, die jeweils über ein d-Elektron verfügen. Die mit steigender Ordnungszahl neu hinzukommenden Elektronen werden in der drittäußersten (4.) Schale als f-Elektronen eingebaut. Durch die Ladung der besetzten, weiter außen liegenden 5. Schale werden die f-Elektronen abgeschirmt. Dementsprechend unterscheiden sich die Seltenerdmetalle chemisch außerordentlich wenig. Die Seltenerdmetalle treten in ihren Verbindungen in der Regel dreiwertig auf, ihr Ionenradius nimmt mit wachsender Kernladungszahl, aufgrund der festeren Bindung der Elektronenunterschalen an den Kern (Lanthanoid-Kontraktion), ab.

Dreiwertige Lanthanoid-Ionen mit nicht-, halb- und vollbesetzter 4f-Schale (La^{3+}, Gd^{3+}, Lu^{3+}) sind farblos und auch im Periodensystem unmittelbar benachbarte Ionen (Ce^{3+}, Tb^{3+}, Eu^{3+}, Yb^{3+}) weisen praktisch keine Farbe auf. Dagegen zeigen die übrigen dreiwertigen Ionen mit zunehmender Entfernung von den genannten Ionen eine charakteristische Färbung. Die durch Lichtabsorption hervorgerufenen Farben gehen in der Regel auf f-f-Übergänge, seltener auf f-d-Übergänge zurück. Dabei führt das Ligandenfeld nur zu vernachlässigbar kleinen Termaufspaltungen, da die f-Elektronen durch die s-, p- und d-Elektronen wirksam von ihrer chemischen Ligandenumgebung abgeschirmt werden. Spektroskopisch dokumentiert sich dies in sehr schmalen, wenige Nanometer breiten Absorptions- und Emissionsbanden der Elektronenübergänge innerhalb der f-Schale. Die f-f-Absorptionen sichtbaren Lichts beruhen auf verbotenen Übergängen zwischen multiplizitätsgleichen Termen unterschiedlicher Gesamtbahndrehimpuls-Quantenzahlen, hervorgerufen durch Bahn-Bahn-Kopplung und sind demgemäß von geringer Intensität und die Lebensdauer des angeregten Zustandes von langer Dauer ($\sim 10^{-3}$ s). [42, 43]

2.2.1. Samarium(III)

Samarium ist das 62. Element des Periodensystems und hat die Elektronenkonfiguration $[Xe]4f^6 6s^2$. Es ist neben Cer, Yttrium, Lanthan, und Neodym das vierthäufigste Seltenerdmetall und mit $6 \cdot 10^{-4}$ Gew.% der Erdhülle häufiger als Silber und Gold. Mögliche Oxidationsstufen

sind +2 und +3, wovon +3 (Elektronenkonfiguration $[Xe]4f^5$ mit dem Grundzustand $^6H_{5/2}$) die beständigere ist. Sm^{3+} wird als Sensibilisator für IR-Strahlung in optischen Gläsern eingesetzt. Die Emission vom Sm^{3+} erstreckt sich über den orange-roten Spektralbereich und beruht auf f-f-Übergängen vom angeregten Zustand $^4G_{5/2}$ zum Grundzustand $^6H_{5/2}$ und höheren Zuständen ^6H_J. [42, 43]

2.2.2. Europium(III)

Europium ist das 63. Element des Periodensystems und hat die Elektronenkonfiguration $[Xe]4f^76s^2$. Es ist neben Promethium das zweitseltenste Seltenerdmetall und mit $1{,}1\cdot10^{-4}$ Gew.% der Erdhülle immer noch häufiger als Silber und Gold. Mögliche Oxidationsstufen sind wie bei Samarium +2 und +3, wovon +3 (Elektronenkonfiguration $[Xe]4f^6$ mit dem Grundzustand $^7F_0$) die beständigere ist. Eu^{3+} besitzt große Bedeutung als Dotand in Leuchtstoffen für Kathodenstrahlröhren, Leuchtstoffröhren und Plasmabildschirmen und wird auch als aktives Ion in Lumineszenzfarbstoffen zur Erhöhung der Fälschungssicherheit von EURO-Banknoten eingesetzt. Die Emission vom Eu^{3+} erstreckt sich über den roten Spektralbereich und beruht auf f-f-Übergängen vom angeregten Zustand $^5D_0$ zu den Zuständen ^7F_J (J = 0, 1, 2, 3, 4, 5, 6) und zusätzlich mitunter auf Übergängen aus höheren ^5D-Zuständen. [42-44]

2.2.3. Ytterbium(III)

Ytterbium ist das 70. Element des Periodensystems und hat die Elektronenkonfiguration $[Xe]4f^{14}6s^2$. Es ist mit $3{,}3\cdot10^{-4}$ Gew.% etwas häufiger als Europium in der Erdhülle vertreten. Mögliche Oxidationsstufen sind wie bei Samarium und Europium +2 und +3, wovon +3 (Elektronenkonfiguration $[Xe]4f^{13}$ mit dem Grundzustand $^2F_{7/2}$) die beständigere ist. Da Yb^{3+} über keine Anregungsbanden im sichtbaren Spektrum verfügt, war es lange Zeit als Dotierungsmittel für aktive Lasermaterialen, aufgrund des Fehlens geeigneter Pumpquellen, bedeutungslos. Erst mit der Entwicklung von leistungsstarken, im Wellenlängenbereich zwischen 900 und 1000 nm emittierenden InGaAs-Laserdioden, die effektiv Yb^{3+}-dotierte Lasermedien pumpen können, änderte sich die Relevanz zu einem bedeutsamen Dotierungsmittel für optische Verstärkermaterialien [45]. Dabei besitzt es gegenüber Nd^{3+}, dem wichtigsten Laserfluorophor, entscheidende Vorteile. Der kleine Quantendefekt von nur 9 % führt zu einem geringen thermischen Energieverlust, sodass während des Laserbetriebs die thermische Belastung geringer ist als in Nd^{3+}-dotierten Lasermedien. Desweiteren besitzt Yb^{3+} eine breite Absorption für die typischen Emissionswellenlänge von InGaAs-Laserdioden, eine lange Lebensdauer des angeregten Zustands und ein Quasi-Drei-Niveau Verhalten, sodass es ein Erfolg versprechendes Dotierungsmittel für Hochleistungs- und Hochenergieanwendungen

darstellt. Die Emission von Yb^{3+} beruht auf nur einem f-f-Übergang vom angeregten Zustand $^2F_{5/2}$ zum Grundzustand $^2F_{7/2}$ bei ~1030 nm. Die Aufspaltung der Zustände aufgrund des Stark-Effektes führt zu einem Quasi-Drei-Niveau-Laserssystem. [8, 42-44]

2.2.4. Cer(III/IV)

Cer ist das 58. Element des Periodensystems und hat die Elektronenkonfiguration $[Xe]4f^15d^16s^2$. Es ist das häufigste Seltenerdmetall und mit 0,006 Gew.% der Erdhülle häufiger als Kupfer. Mögliche Oxidationsstufen sind +3 und +4, wovon +3 (Elektronenkonfiguration $[Xe]4f^1$ mit dem Grundzustand $^2F_{5/2}$) die beständigere ist [42]. Cer wird als UV-Schutz und Hemmstoff von Photodarkening-Effekten in optischen Gläsern, als Entfärbemittel im Behälterglas, sowie als Sensibilisator in Fluoreszenz- und Lasergläsern verwendet [46].

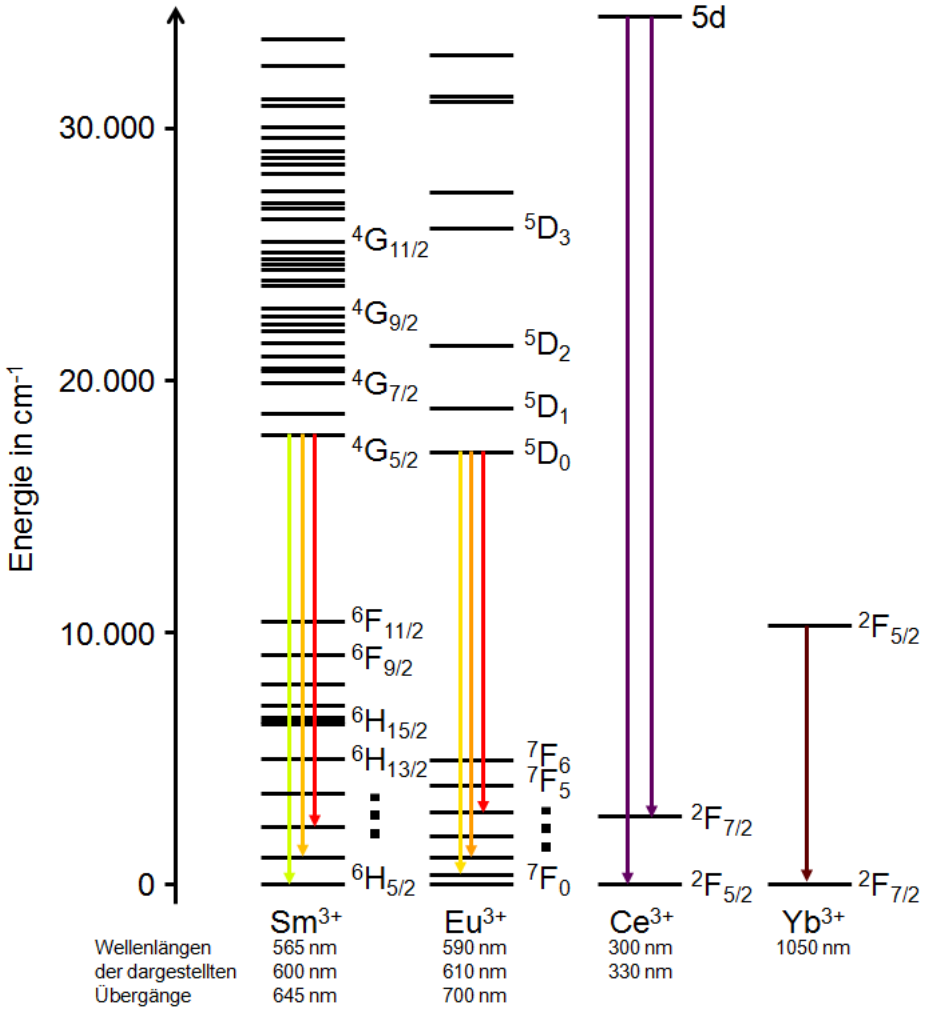

Abbildung 2: Elektronische Energieniveaus für verschiedene freie Seltenerdionen [47-49] und die jeweils stärksten Fluoreszenzübergänge

Die Emission des Ce^{3+}-Ions beruht auf d-f-Übergängen von der angeregten Konfiguration $5d^1$ zur Grundzustandskonfiguration $4f^1$. Die Konfiguration $4f^1$ ist aufgrund von Spin-Bahn-Kopplung in zwei Niveaus geteilt, $^2F_{5/2}$ sowie $^2F_{7/2}$ und die Konfiguration $5d^1$, aufgrund des Ligandenfeldes, in zwei bis fünf Niveaus. d-f-Übergange sind quantenmechanisch erlaubte Übergänge und damit ist die Lebensdauer des angeregten Zustandes kurz. Die spektrale Position der Emissionsbanden hängt ab von der effektiven Ladung, dem Ligandenfeld und der Stokes-Verschiebung. Typische Emissionen des Ce^{3+} liegen im ultravioletten bis blauen Bereich. [43]

Ce^{3+} kann relativ leicht oxidiert werden. Deshalb kann in Gläsern neben Ce^{3+} auch Ce^{4+} vorliegen, welche ein Gleichgewicht mit dem, physikalisch in der Schmelze, gelösten Sauerstoff bilden. Die Oxidationsstufe ist dabei abhängig von der Zusammensetzung [50, 51], der Sauerstoffaktivität der Schmelze [51-53] und der Temperatur [51, 53, 54]. Das Gleichgewicht wird mit steigender Temperatur, sinkender Basizität und unter Verwendung von reduzierenden Schmelzbedingungen in Richtung Ce^{3+} verschoben. Ce^{4+} ($[Xe]4f^0$) zeigt breite und intensive Charge-Transfer-Absorptionen im nahen UV-Bereich [55-57], die sich mit den Absorptionen von Ce^{3+} überlagern [46, 58, 59].

2.2.4.1. Quantum-Cutting in Ce^{3+}-Yb^{3+}-kodotierten Systemen

Aufgrund des hohen Absorptionswirkungsquerschnitts und der breiten Emission wurde Ce^{3+} als Sensibilisator für Yb^{3+}-kodotierte Quantum-Cutting Materialien vorgeschlagen. Beim Quantum-Cutting Mechanismus werden zwei oder mehr niederenergetische Photonen nach Anregung mit einem hochenergetischen Photon emittiert. Effizientes Quantum-Cutting in einem mittels UV-Licht angeregten Material würde die Quanteneffizienz auf größer Eins ansteigen lassen. Mögliche Anwendungen sind zum Beispiel die Effizienzsteigerung von Solarzellen oder Wellenlängenkonverter für optische Sensoren. [19, 60, 61]

Bei kodotierten Ce^{3+}-Yb^{3+}-Systemen werden Ce^{3+}-Ionen im nahen UV-Bereich angeregt und übertragen die Energie mittels eines Donor-Akzeptor-Mechanismus auf Yb^{3+}-Ionen. Die Energietransfereffizienz zwischen kodotierten Fluorophoren hängt hauptsächlich vom spektralen Überlapp der Emission des Donors und der Absorption des Akzeptors ab [62, 63]. Grundsätzlich gilt dies auch für Energietransfers in Quantum Cutting Materialien [64], jedoch muss hier das selbstgefaltete Absorptionsspektrum des Akzeptors verwendet werden [65], sodass die Lage der Ce^{3+}-Emission entscheidend für die Effizienz des Energietransfer ist.

2.3. Fluoreszenzabklingverhalten

Die Emission von Fluoreszenzlicht erfolgt in der Regel vom vibratorischen Grundzustand des ersten elektronisch angeregten Zustands, der für die meisten dreiwertigen Seltenerdionen aufgrund der involvierten, quantenmechanisch verbotenen f-f-Übergänge eine vergleichsweise große Lebensdauer von etwa 10^{-3} s hat und dabei zum elektronischen Grundzustand relaxiert. Diverse parasitäre Zerfallsmechanismen wie Elektronentransfer, Intersystem Crossing und interne Konversion konkurrieren mit der radiativen Fluoreszenz. Die sichtbare Lebensdauer τ des ersten angeregten Zustandes, welche allein direkt experimentell zugänglich ist, ist im Allgemeinen aufgrund dieser nichtradiativen Löschprozesse kleiner als die intrinsische (natürliche) Lebendauer τ_0. Für die Abnahme der Anzahl angeregter Fluorophore x mit der Zeit t gilt:

$$dx = -k\, x\, dt \tag{1}$$

Dabei setzt sich die Zerfallskonstante k aus den Reaktionskonstanten für den radiativen Fluoreszenzübergang k_{rad}, interne Konversion k_{IC}, Intersystem Crossing k_{ISC} und Energietransfer k_{ET} zusammen:

$$k = k_{\mathrm{rad}} + k_{\mathrm{IC}} + k_{\mathrm{ISC}} + k_{\mathrm{ET}} \tag{2}$$

Die Integration der Gleichung (1) liefert:

$$x = x_0\, e^{-kt} \tag{3}$$

Die Fluoreszenzlebendauer τ ist definiert als Zeitpunkt, zu dem die Anzahl angeregter Fluorophore bzw. die Fluoreszenzintensität auf den 1/e-ten Teil (~ 37 %) ihres Anfangswertes n_0 gesunken sind. Sie ist damit der Kehrwert der Zerfallskonstante k:

$$\tau = \frac{1}{k} = \frac{1}{k_{\mathrm{rad}} + k_{\mathrm{IC}} + k_{\mathrm{ISC}} + k_{\mathrm{ET}}} \tag{4}$$

2.3.1. Abhängigkeit der intrinsischen Lebensdauer

Desweiteren gilt für die intrinsische Lebendauer τ_0 [66, 67]:

$$\tau_0 = \frac{1}{k_{\mathrm{rad}}} \tag{5}$$

Die radiative Zerfallskonstante k_{rad} eines Fluorophors ist abhängig vom Brechungsindex *n* der umgebenden dielektrischen Matrix [68]:

$$k_{\mathrm{rad}} = \frac{1}{\tau_0} \propto n^3 \tag{6}$$

Theoretischen Modellen der genauen Abhängigkeit liegen Betrachtungen der Kavitätsstruktur zwischen Fluorophor und Matrix zugrunde, die im Allgemeinen geschrieben werden können als [69-75]:

$$k_{\mathrm{rad}} = \frac{1}{\tau_0} \propto n \cdot l(n)^2 \tag{7}$$

Für das reale Kavitätsmodell gilt [74, 75]:

$$l(n) = \frac{3\,n^2}{2\,n^2 + 1} \tag{8}$$

2.3.2. Abhängigkeit nichtradiativer Relaxationsprozesse

Angeregte elektronische Zustände von Seltenerdionen in Festkörpern können durch Anregung von Gitterschwingungen (Phononen) auch nichtradiativ relaxieren. Die Seltenerdionen haben Sauerstoff oder andere Anionen als nächste Nachbarn, deren Schwingungen und die Schwingungen weiterentfernter Ionen leisten einen Beitrag zum schwingenden Stark-Feld, welches nichtradiative Übergänge induziert. Wenn der Energieabstand zwischen dem angeregten Zustand und dem nächstniedrigeren Zustand größer als die maximale Phononen-Energie des Materials ist, werden mehrere Phononen für diesen Relaxationsmechanismus benötigt (Multiphononenrelaxation). Dabei sinkt die Wahrscheinlichkeit für Multiphononenrelaxation je mehr Phononen für den Übergang benötigt werden. Deshalb sind die Energieabstände der elektronischen Zustände der Seltenerdionen und die maximale Phononen-Energie des Wirtsmaterials von Bedeutung für nichtradiative Relaxationen [76, 77]. Nach [78] hängt die nichtradiative Reaktionskonstante k_{IC} vom Energieabstand der Zustände des Seltenerdions ΔE_o und der maximalen Phononenenergie $\hbar\omega_{max}$ ab:

$$k_{\mathrm{IC}} = \beta_{\mathrm{el}} \cdot e^{-(\Delta E_0 - 2\hbar\omega_{\mathrm{max}})\alpha} \tag{9}$$

mit α und β_{el} als materialabhängige Konstanten. Die hochenergetischen Phononen des Glasnetzwerkes bestehen aus örtlich begrenzten Schwingungen der Glasbildnergruppen (SiO_4, AlO_4, ...) mit Frequenzen nahe der X-O-Bindungsschwingungen. Die höchsten maximalen

Phononenenergien werden in Boraten sowie Phosphaten und die niedrigsten in Germanaten, Fluoriden sowie Telluriten gefunden [79].

2.4. Optische Basizität

Der Säure-Base-Charakter von Schmelzen und Gläsern beeinflusst stark die chemischen und physikalischen Eigenschaften. 1971 wurde von Duffy und Ingram die „optische Basizität“ als spektroskopisch messbare Größe für die Lewis Basizität von Schmelzen und Gläsern eingeführt [80]. Die optische Basizität Λ kann mit verschiedenen Methoden bestimmt werden. Dabei werden Probeionen mit umgebungssensitiven Elektronenübergängen wie z.B. Pb^{2+} oder Tl^{+} dotiert und die Verschiebung der Absorption dieser Ionen in der Matrix ν im Vergleich zur Absorption in einer basischen Umgebung $\nu_{O^{2-}}$ (CaO) und in der Gasphase ν_f bestimmt[81]:

$$\Lambda = \frac{\nu_f - \nu}{\nu_f - \nu_{O^{2-}}} \tag{10}$$

Untersuchungen an vielen Glassystemen und Schmelzen zeigten, dass eine theoretische optische Basizität Λ_{th} aus der stöchiometrischen Zusammensetzung berechnet werden kann [82]:

$$\Lambda_{th} = X(AO_{a/2}) \cdot \Lambda(AO_{a/2}) + X(BO_{b/2}) \cdot \Lambda(BO_{b/2}) + \cdots \tag{11}$$

Dabei sind $\Lambda(AO_{a/2})$, $\Lambda(BO_{b/2})$, … die optischen Basizitäten der verwendeten Oxide $AO_{a/2}$, $BO_{b/2}$ und $X(AO_{a/2})$, $X(BO_{b/2})$, … die Anteile der verwendeten Oxide an der gesamten Sauerstoffanzahl.

2.5. Thermomechanische Eigenschaften

Hochenergielaser werden dazu entwickelt um kontinuierlich im gepulsten Modus bei Wiederholungsraten von ~ 0,1-10 Hz zu arbeiten. Aus diesem Grund sind gute thermomechanische Eigenschaften, wie eine hohe Bruchzähigkeit K_C, hohe thermische Leitfähigkeit k und ein niedriger thermischer Ausdehnungskoeffizienten α, wichtig. Zusammen mit der Poissonzahl ν werden diese Eigenschaften durch die Temperaturwechselbeständigkeit R_T beschrieben [83]:

$$R_T = \frac{k \cdot (1-\nu) \cdot K_C}{E \cdot \alpha} \tag{12}$$

Die Temperaturwechselbeständigkeit berechnet die maximale thermische Belastung einer oberflächengekühlten Glasscheibe. In aktiven Lasermaterialien entstehen große Wärmebelastungen durch den Energieeintrag, der nicht in Laserlicht umgewandelt wird und durch nichtradiative Prozesse in Gitterschwingungen bzw. Wärmeenergie umgewandelt wird. Der Quantendefekt und die Anregung von Multiphononenübergängen sind dabei Ursachen für die Laserenergieverluste. Durch den Wärmeeintrag und die Oberflächenkühlung des aktiven Lasermaterials wird ein Temperaturgradient ΔT erzeugt, der eine thermomechanische Spannung σ im Material verursacht [84]:

$$\frac{\sigma}{\Delta T} = \frac{E \cdot \alpha}{1-\nu} \tag{13}$$

Da der thermische Ausdehnungskoeffizient die höchsten Größenänderungen zeigt, ist ein kleiner Ausdehnungskoeffizient maßgebend für geringe thermomechanische Spannungen.

3. Eigene Arbeiten

Für die vorliegenden Arbeiten wurden verschiedene Aluminosilicatgläser mit 50-70 mol% SiO_2 sowie 5-25 mol% Al_2O_3 hergestellt und spektroskopisch sowie mechanisch untersucht. Die Konzentration von Netzwerkwandlerionen multipliziert mit deren Wertigkeit war gleich oder größer als die Al^{3+}-Konzentration. Zunächst wurden ternäre Magnesium-Aluminosilicatgläser (MgAS), dotiert mit $1{\cdot}10^{20}$ Sm^{3+}/cm^3, untersucht, deren Mg^{2+}-Konzentration von 15 bis 45 mol% variiert wurde. Zusätzlich wurde in einer Reihe mit 20 mol% Mg^{2+}, dieses zur Hälfte durch Ba^{2+}, Zn^{2+}, Sr^{2+} und Ca^{2+} ersetzt. In einer weiteren Reihe wurden bis zu 9 mol% MgO durch MgF_2 substituiert (MT1). Anschließend wurde in ausgewählten MgAS-Zusammensetzungen Mg^{2+} komplett durch andere Netzwerkwandler bzw. Zwischenoxide ersetzt (Li^+, Na^+, K^+, Sr^{2+}, Ca^{2+}, Ba^{2+}, Zn^{2+}, Pb^{2+}, Y^{3+}, La^{3+}) und mit $1{\cdot}10^{20}$ Sm^{3+}/cm^3 (MT2) sowie $1{\cdot}10^{20}$ Eu^{3+}/cm^3 (MT2, MT4) dotiert. Ausgewählte Wirtsgläser mit La^{3+}, Li^+, Mg^{2+} und/oder Zn^{2+} wurden mit $1{\cdot}10^{20}$ Yb^{3+}/cm^3 dotiert und ebenfalls spektroskopisch untersucht (MT3). Weiterhin wurden auch mechanische Untersuchungen an den Wirtsgläsern durchgeführt (MT6). Schließlich wurde das MgAS-Wirtsglas mit 20 mol% MgO, 20 mol% Al_2O_3 und 60 mol% SiO_2 mit Cerionen dotiert und mit dotierten Calcium-, Calcium/Natrium-, Calcium/Barium- und Barium-Aluminosilicatgläsern spektral verglichen (MT5).

In den folgenden Abschnitten werden die Beobachtungen und Ergebnisse zusammengefasst. Zunächst werden die schwingungsspektroskopischen Untersuchungen der Arbeiten MT1 und MT2 dargelegt, die Informationen über die Glasstruktur bzw. das Glasnetzwerk geben. Im nächsten Abschnitt sollen die Ergebnisse der mechanischen Untersuchungen (Dilatometrie, Eindruck- und Ultraschallverfahren) der Wirtsgläser in Abhängigkeit von der chemischen Zusammensetzung und der Glasstruktur betrachtet werden (MT1, MT6). Schließlich werden die Ergebnisse der Fluoreszenz- und Absorptionsspektroskopie von Sm^{3+} (MT1, MT2), Eu^{3+} (MT2, MT4), Yb^{3+} (MT3) und $Ce^{3+/4+}$ (MT5) korreliert mit der Glaszusammensetzung und –struktur, sowie im Fall von Cer-dotierten Gläsern zusätzlich mit den Schmelzbedingungen.

3.1. Schwingungsspektroskopie [MT1, MT2]

Im mittleren Infrarotbereich von 400 bis 4.000 cm^{-1} zeigen die Aluminosilicatgläser vier charakteristische Bereiche: Dreh- bzw. Kippschwingungen des Si-O-(Si,Al)-Netzwerkes bei etwa 480 cm^{-1}, Biegeschwingungen des Si-O-(Si,Al)-Netzwerkes bei 600-850 cm^{-1}, Streckschwingungen des Si-O-(Si,Al)-Netzwerkes bei 850-1.300 cm^{-1} und Streckschwingungen der (–OH)-Gruppen bei 2.500-4.000 cm^{-1} [85-87]. Die Magnesium-Aluminosilicatgläser zeigen in Abhängigkeit von der Mg^{2+}-Konzentration nur geringe Unterschiede im untersuchten Infrarotbereich. Deutliche Änderungen sind im Bereich der Streckschwingungen des Si-O-(Si,Al)-Netzwerkes bei 850-1.300 cm^{-1} zu finden (MT1, Fig. 3).

Ein Überschuss an Mg^{2+} führt zur Bildung von Trennstellen, die Konzentration von Q4-Gruppen sinkt und es werden Q3-, Q2- und Q1-Gruppen mit endständigen $Si\text{-}O^-$-Gruppen gebildet. Je mehr Trennstellen an der Si-O-(Si,Al)-Gruppe sind, desto geringer ist die Streckschwingungsenergie. Im Bereich der Streckschwingungen des Si-O-(Si,Al)-Netzwerkes kann eine Verschiebung des Hauptpeaks zu niedrigeren Schwingungsenergien mit steigender Mg^{2+}-Konzentration beobachtet werden. Dennoch sind auch bei einem hohem Mg^{2+}-Konzentrationsüberschuss (MAS45) Streckschwingungen mit hohen Wellenzahlen zu finden, die auf eine statistische Verteilung von Q4-, Q3-, Q2- und Q1-Gruppen hindeuten, sodass die Phononen-Energie der Aluminosilicatgläser kaum durch die Konzentration (MT1) und die Art der Netzwerkwandler (MT2) beeinflusst werden kann.

Glaszusammensetzungen mit bis zu 9 mol% MgF_2 zeigen keine Änderungen der Absorption im Bereich von 400-2.000 cm^{-1} (MT1, Fig. 5). Die Glasstruktur mit $[AlO_{4/2}]$- und $[SiO_{4/2}]$-Tetraedern wird durch die Zugabe von Fluorid kaum beeinflusst. Es werden Aluminiumoxifluorid-Gruppen $[AlO_xF_y]^{n-}$ gebildet. Die Intensität der OH-Absorptionsbande bei etwa 3.600 cm^{-1} sinkt exponentiell mit steigender Fluoridkonzentration (MT1, Fig. 6), da durch die Bildung von flüchtigen HF oder SiF_4 während des Schmelzvorganges die OH-Konzentration sinkt (MT1).

3.2. Mechanische Eigenschaften [MT1, MT6]

Die linearen thermischen Ausdehnungskoeffizienten und Glastransformationstemperaturen der ternären MgAS-Gläser sind abhängig von der Mg^{2+}-Konzentration (MT1). Mit steigender Konzentration steigt der Ausdehnungskoeffizient annähernd linear von 3,22 (15 mol% MgO) auf 6,45 10^{-6}/K (45 mol% MgO) und die Glastransformationstemperatur sinkt. Gläser mit einer hohen Mg^{2+}-Konzentration (>35 mol%) haben einen Glastransformationsbereich bei etwa 780 °C, wohingegen niedrigere Mg^{2+}-Konzentrationen (<25 mol%) zu Transformationstemperaturen bis 830 °C führen. Dieses Verhalten wurde durch die Bildung von Trennstellen durch Mg^{2+}-Ionen im Glasnetzwerk erklärt, die die molekulare Vernetzung und damit die Versteifung des Glasnetzwerkes verringern. In den Glasnetzwerken von Aluminosilicaten befinden sich $[AlO_{4/2}]^-$-Tetraeder deren negative Ladung durch Ionen der Netzwerkwandler oder Zwischenoxide wie zum Beispiel Mg^{2+} ausgeglichen wird. Dies führt zu einer stärkeren Vernetzung, da $[AlO_{4/2}]^-$-Tetraeder über Al-O-Si-Brücken vernetzt werden. Eventuell überschüssige Kationen bilden Trennstellen die (Al, Si)-O-Si-Brücken aufbrechen und negativ geladene Trennstellensauerstoffe absättigen. Je größer der Überschuss an Netzwerkwandlerionen, desto mehr Trennstellen werden gebildet und desto geringer ist der Vernetzungsgrad. Dabei sind die linearen thermischen Ausdehnungskoeffizienten und Glastransformationstemperaturen der MgAS-Gläser nicht ausschließlich vom Vernetzungsgrad abhängig. Es zeigt sich, dass bei theoretisch ladungsausgeglichenen Zusammensetzungen mit höherer SiO_2-Konzentration der Ausdehnungskoeffizient abnimmt und die Temperatur des Glastransformationsbereichs zunimmt (siehe Tabelle).

Probe	SiO_2-Konzentration (mol%)	linearer Ausdehnungskoeffizient (10^{-6}/K)	Glastransformationstemperatur (°C)
MAS15	71	3,22	831
MAS20	60	4,06	827
MAS22	56	4,49	824

Die Poissonzahlen der untersuchten MgAS-Gläser zeigen einen ähnlichen Zusammenhang. Je weniger Trennstellen und je größer der SiO_2-Anteil am Glasnetzwerk ist, desto geringer ist die Poissonzahl und desto starrer die Glasstruktur (MT6). Der Elastizitätsmodul zeigt einen gegensätzlichen Verlauf. Hohe Elastizitätsmoduli repräsentieren starre Glasstrukturen. Es wurden niedrigere Werte für Gläser mit hohem SiO_2-Anteil und wenigen Trennstellen bestimmt. Die Ergebnisse der Eindruckprüfung zeigen ein noch inhomogeneres Bild. Einerseits

steigt die Bruchzähigkeit, je größer der Vernetzungsgrad der Glasstruktur ist. Andererseits bleibt die Härte relativ konstant (mit einem Ausreißer, Mg37). Dieses Glas beruht auf einer eutektischen Schmelze mit 37 mol% MgO, 13 mol% Al_2O_3 und 50 mol% SiO_2. Das Eindruckverhalten eines Glases wird durch drei verschiedene Prozesse – plastisches Fließen, Verdichtung und elastischer Verformung – beeinflusst, wobei sich die genannten Effekte stark überlagern können (MT6).

Die mechanischen Eigenschaften der Lanthan Aluminosilicat (LaAS) Gläser verhalten sich ähnlich. Der Verlauf der Poissonzahl in Abhängigkeit von der Glaszusammensetzung ist sowohl vom SiO_2-Anteil am Glasnetzwerk, als auch von der Zahl der Trennstellen im Glasnetzwerk abhängig (MT6, Fig. 3a). Je weniger Trennstellen und je mehr SiO_2 enthalten sind, desto starrer wird die Glasstruktur und die Poissonzahl sinkt. Wieder sind die Elastizitätsmodulwerte niedrig für Gläser mit hohem SiO_2-Anteil und wenigen Trennstellen (MT6, Fig. 3b). Auch zeigen die Eindruckprüfungen (Vickers Härte und Bruchzähigkeit) ein ähnliches Bild in Abhängigkeit von der chemische Zusammensetzung und Glasstruktur.

Im Vergleich von Aluminosilicatgläsern gleicher molarer Zusammensetzung (60 mol% SiO_2, 20 mol% Al_2O_3 und 20 mol% M_xO) aber mit unterschiedlichen Netzwerkwandlerionen bzw. Zwischenoxiden (Li^+, Na^+, K^+, Sr^{2+}, Ca^{2+}, Ba^{2+}, Zn^{2+}, Pb^{2+}) kann eine direkte Abhängigkeit der mechanischen Eigenschaften von der Feldstärke der Netzwerkwandlerionen erkannt werden (MT6, Figs. 1a-d). Je größer die Feldstärke der Netzwerkwandlerionen, desto größer sind die Werte von Elastizitätsmodul, Bruchzähigkeit und Härte. Es besteht jeweils ein nahezu linearer Zusammenhang mit wenigen Ausreißern. Die Feldstärke der Netzwerkwandlerionen beeinflusst die Glasstruktur, sodass bei höherer Feldstärke eine starrere Struktur gebildet wird. Das Lithium-haltige Glas besitzt relativ zum linearen Verlauf höhere Werte für Bruchzähigkeit und Elastizitätsmodul. Im Vergleich dazu zeigen die Blei- und Lanthan-haltigen Gläser niedrigere Werte von Elastizitätsmodul, Härte und Bruchzähigkeit. Lithium ist das einzige Netzwerkwandlerion, das in der zweiten Periode des Periodensystems steht. Es besitzt kein vollständiges Elektronenoktett, bevorzugt niedrige Koordinationszahlen und wirkt stark polarisierend [42]. Hingegen gehören Blei und Lanthan zu den schwersten der hier verwendeten Netzwerkwandlerionen. Blei ist leicht polarisierbar und gehört, wie auch das Lanthan, zu den Zwischenoxiden, d.h. dass sie sowohl als Netzwerkwandler als auch als –bildner agieren können. Des Weiteren bevorzugen beide Ionen relativ hohe Koordinationszahlen [42].

Die Untersuchung von Aluminosilicatgläser mit zwei Netzwerkwandlerionen (Li/Mg, Mg/Zn, Li/Zn) mit gleichen molaren Konzentrationen ergeben, dass diese Mischgläser Glastransforma-

tionstemperaturen, thermische Ausdehnungskoeffizienten und Elastizitätsmoduli zwischen den reinen ternären Gläsern besitzen (MT3). Um den Einfluss von Mischeffekten der Netzwerkwandler genauer zu untersuchen, wurden Gläser mit 20 mol% Al_2O_3, 60 mol% SiO_2 sowie 20 mol% ZnO und MgO in verschiedenen Verhältnissen (Zn:Mg, 0:1, 1:6, 1:3, 1:1, 3:1, 1:0) untersucht. Dabei zeigten sich für Härte und Bruchzähigkeit in Abhängigkeit von der Art der Netzwerkwandler und ihrer Konzentration positive Abweichungen von den linearen Verläufen (MT6, Figs. 4b, c). Ein solches Verhalten wird als Mischoxid- bzw. Mischalkalieffekt bezeichnet und ist typisch für Transporteigenschaften, wie Diffusion und Ionenleitfähigkeit [88]. Es wurden schon ähnliche Verhalten, bezogen auf mechanische Eigenschaften wie Elastizitätsmodul und Härte, in der Literatur nachgewiesen. Zum Beispiel wurden in Mg/Ca- und Ca/Li-Natrium-Aluminosilicatglassystemen negative Abweichungen von der Linearität nachgewiesen [89, 90], als auch positive Abweichungen in einem Na/K-Aluminosilicatglassystem [91].

Die partiellen Substitutionen von MgO durch MgF_2 in einem Magnesium-Aluminosilicatglas mit 20 mol% Al_2O_3, 60 mol% SiO_2 sowie 20 mol% MgO, zeigten, dass Poissonzahl, Elastizitätsmodul, Härte und Bruchzähigkeit kaum beeinflusst werden (MT6). Gleichzeitig sinkt die Glastransformationstemperatur um mehr als 100 K (bei Substitution von 9 mol% MgF_2). Der lineare Ausdehnungskoeffizient ist für geringe Substitutionen (bis 3 mol% MgF_2) größer als für die fluorid-freie Glasprobe. Mit einer Substitution von 9 mol% MgF_2 ist der lineare Ausdehnungskoeffizient um mehr als 4 % kleiner (MT1). Fluorid wird in Al_2O_3-haltigen Gläsern in Form von Aluminiumoxifluorid-Gruppen $[AlO_xF_y]^{n-}$ ins Glasnetzwerk eingebaut, wobei Aluminium überwiegend vierfach koordiniert vorliegt [21, 37, 38]. Dadurch gehen Sauerstoffbrücken zum Aluminium verloren und der Vernetzungsgrad der Glasstruktur sinkt, weshalb die Glastransformationstemperatur mit zunehmender Fluoridkonzentration sinkt. Allerdings muss beachtet werden, dass die tatsächlichen Fluoridkonzentrationen im Glas niedriger sind, als es der Einwaage entspricht, da etwa 35 % während des Schmelzens als HF und SiF_4 abdampft.

Thermomechanische Spannungen σ, die durch Temperaturgradienten ΔT im Glas erzeugt werden, können durch folgende Formel abgeschätzt werden:

$$\frac{\sigma}{\Delta T} = \frac{E \cdot \alpha}{1 - \nu} \tag{14}$$

Für die untersuchten Aluminosilicatgläser wurden thermomechanische Spannungen von 0,5-1,0 MPa/K bestimmt (MT3). Je kleiner der Elastizitätsmodul, die Poissonzahl und der thermische Ausdehnungskoeffizient sind, desto geringer sind die, bei Temperaturwechsel oder bei

inhomogener Temperatur gebildeten, thermomechanischen Spannungen. Dabei werden alle drei Eigenschaften durch die chemische Zusammensetzung der Gläser beeinflusst. Die höchsten Größenänderungen zeigt der thermische Ausdehnungskoeffizient, sodass ein kleiner Ausdehnungskoeffizient als maßgebend für geringe thermomechanische Spannungen angesehen werden kann. Die kleinsten thermischen Ausdehnungskoeffizienten und damit auch die geringsten thermomechanischen Spannungen wurden für Zn- und Mg-haltige Aluminosilicatgläser bestimmt. Dabei sinken die Spannungswerte mit steigendem Vernetzungsgrad der Gläser und werden kaum durch den Zusatz von Fluorid beeinflusst.

3.3. Fluoreszenzeigenschaften

3.3.1. Samarium(III) [MT1, MT2]

Im Vergleich zu Phosphat- und Fluoridphosphatgläsern sind die Peaks der Emissionsspektren der Sm^{3+}-dotierten Aluminosilicatgläser aufgrund der hohen optischen Basizität und des stärkeren Ligandenfeldes um die Sm^{3+}-Ionen, breiter und um wenige Nanometer zu höheren Wellenlängen verschoben (MT1, Fig. 8). Die Anregungsspektren der einzelnen Aluminosilicatzusammensetzungen zeigen aber kaum sichtbare Unterschiede. Des Weiteren ist die Fluoreszenzlebensdauer 15–35 % kürzer als in Fluoridphosphatgläsern.

Die Lage und Form der Fluoreszenzanregungspeaks der untersuchten, Sm^{3+}-dotierten Aluminosilicatgläser wird ebenfalls kaum von deren Zusammensetzung beeinflusst. Lediglich für Zink-haltige Gläser wurden niedrigere Intensitäten der Übergänge kleiner 400 nm gemessen, da Zn^{2+}-Ionen eine breite Absorptionsbande im Bereich von 200 bis 400 nm besitzen. In den Emissionssprektren kann eine geringe Verschiebung (≤ 2 nm) der Peaks zu größeren Wellenlängen, mit sinkendem Atomgewicht der Netzwerkwandler, beobachtet werden (MT2, Fig. 3). Auf die Fluoreszenzlebensdauer hat die Glaszusammensetzung jedoch einen größeren Einfluss. Mit sinkendem mittleren Atomgewicht der Zusammensetzung steigt die Sm^{3+}-Fluoreszenzlebensdauer (MT2, Fig. 4). Der Einfluss auf die Sm^{3+}-Fluoreszenz von nicht-radiativen Relaxationsprozessen wie Multiphononen- und OH-Quenching werden als gering erachtet. Es wurde gezeigt, dass nur ein geringer Zusammenhang zwischen den OH-Konzentrationen bzw. den Phononen-Energien der Aluminosilicatgläser und der Sm^{3+}-Fluoreszenzlebensdauer besteht.

In ternären Magnesium-Aluminosilicatgläsern wird das Fluoreszenzabklingverhalten kaum durch die Zusammensetzung beeinflusst (MT1, Fig. 9), da Magnesium, Aluminium und Sili-

cium benachbarte Elemente im Periodensystem sind, unterscheiden sie sich kaum in ihrer Ordnungszahl und Atomgewicht, sodass Zusammensetzungsänderungen in diesem System kaum Einfluss auf das mittlere Atomgewicht haben. Entsprechend ist die Sm^{3+}-Fluoreszenzlebensdauer der Magnesium-Aluminosilicatgläser im angegebenen Zusammensetzungsbereich konstant bei 2,4 ms. Da kaum parasitäre Energietransfermechanismen auftreten, wird ein nahezu monoexponentieller Abfall beobachtet. Die leichte Krümmung der Abklingkurven wird durch Kreuzrelaxationsprozesse zwischen angeregten Sm^{3+}-Ionen und solchen im Grundzustand hervorgerufen, welche bei ca. 10^{19} Sm^{3+} cm^{-3} einsetzen [92]. Die Phononen-Energien wurden mit Hilfe der Infrarotspektroskopie untersucht. Durch einen Überschuss an Magnesiumionen werden Trennstellen im Glasnetzwerk gebildet. Die weniger vernetzte Struktur besitzt eine leicht geringere maximale Phononen-Energie. Dabei konnte kein Zusammenhang zwischen Fluoreszenzlebensdauer und der Phononen-Energie nachgewiesen werden.

Der Einbau von Fluorid ins Glasnetzwerk beeinflusst die Sm^{3+}-Fluoreszenzlebensdauer stark. Es wurden bis zu 9 mol% MgF_2 verwendet. Durch die Verwendung von Fluorid wird das Phononenspektrum nicht beeinflusst (MT1, Fig. 5), die Höhe der Wasserbande kann um bis zu 2/3 gesenkt werden (MT1, Fig. 6) und damit werden mögliche OH-Relaxationsprozesse verringert. Es wird gezeigt, dass mit steigender Fluoridkonzentration die Sm^{3+}-Fluoreszenzlebensdauer steigt (MT1, Fig. 11). Im Vergleich zum Fluorid-freien Glas mit derselben Konzentration an Mg^{2+} besitzt die Probe mit 9 mol% MgF_2 eine um 14 % gesteigerte Fluoreszenzlebensdauer. Dieser Anstieg der Fluoreszenzlebensdauer durch Einbau von Fluorid ins Glassystem wurde auch bereits bei Phosphatgläsern beschrieben [92]. Durch die Änderung der Koordinationspartner der Sm^{3+}-Ionen zu Aluminiumoxifluorid-Gruppen $[AlO_xF_y]^{n-}$ wird das Ligandenfeld stark beeinflusst, sodass sich das Fluoreszenzabklingverhalten ändert.

3.3.2. Europium(III) [MT2, MT4]

Um den Einfluss von OH- und Kreuzrelaxationsprozessen, wie sie bei Sm^{3+} dotierten Gläsern vorkommen, auszuschließen, wurden Aluminosilicatgläser mit Eu^{3+} dotiert, da Eu^{3+}, aufgrund seiner größeren Bandlücke im Energieniveauschema, weniger anfällig für diese beiden strahlungslosen Desaktivierungsprozesse ist. Außerdem besitzt Eu^{3+} einen hypersensitiven, elektrischen Dipolübergang ($^5D_0 \rightarrow {}^7F_2$ bei 613 nm), der stark von der Koordinationsumgebung des Ions abhängt. Der Intensitätsvergleich mit einem reinen magnetischen Dipolübergang ($^5D_0 \rightarrow {}^7F_1$ bei etwa 590 nm) kann als Indikator für die umgebende Ligandenfeldsymmetrie der Eu^{3+}-Ionen verwendet werden. Je größer das Verhältnis der Intensitäten I_{590}/I_{613}, desto höher ist die Ligandenfeldsymmetrie [93].

Die Form der Anregungs- und Emissionsspektren der Eu^{3+}-dotierten Aluminosilicatgläser wird kaum durch die chemische Zusammensetzung beeinflusst. Unterschiede findet man für Barium- und Kalium-haltige Aluminosilicatgläser. Der Hauptpeak im Emissionsspektrum dieser Gläser bei 613 nm und der Peak bei etwa 590 nm haben sich sichtbar verschmälert. Außerdem finden sich leichte Änderungen der Intensitätsverhältnisse im Kalium-haltigen Glas. Im nahen UV-Bereich bei Wellenlängen kleiner 400 nm sind niedrigere Intensitäten für Gläser mit relativ niedriger optischer Basizität zu finden. In diesen Gläsern wird ein deutlicher Anteil an Eu^{3+} zu Eu^{2+} in der Schmelze reduziert. Eu^{2+} absorbiert UV-Strahlung und verringert so die Anregung der Eu^{3+}-Ionen in diesem Wellenlängenbereich [43]. Zink- und Blei-haltige Gläser zeigen einen ähnlichen Effekt, aufgrund der breiten Absorptionsbanden der Zn^{2+}- [94-96] bzw. Pb^{2+}-Ionen [43, 97] in Gläsern zwischen 200 und 400 nm.

Der Intensitätsvergleich der Übergange im Emissionsspektrum bei 590 und 613 nm belegt im Allgemeinen in den untersuchten Aluminosilicatgläsern eine sehr niedrige Symmetrie am Eu^{3+}. Für Gläser mit schweren Netzwerkwandlerionen (La^{3+}, Ba^{2+}, Sr^{2+} und K^{+}) wurden die höchsten I_{590}/I_{613}-Verhältnisse bestimmt (MT4). Eine Ausnahme ist das Blei-haltige Glas mit einem relativ geringen I_{590}/I_{613}-Verhältnis. Es konnte letztlich keine eindeutige Abhängigkeit der Symmetrie in Umgebung der Eu^{3+} von der Zusammensetzung des Wirtsglases gefunden werden. Jedoch besteht ein Trend zu höherer Symmetrie in Aluminosilicatgläsern mit schwereren Netzwerkwandlerionen.

Das Abklingverhalten der Eu^{3+}-Fluoreszenz ist ähnlich der Sm^{3+}-Fluoreszenz vom Atomgewicht der Netzwerkwandler abhängig. Je größer das mittlere Atomgewicht des Glases ist, desto kürzer ist die mittlere Fluoreszenzlebendauer. Dennoch zeigen Sr^{2+}-, Ba^{2+}- und K^{+}-haltige Gläser im Vergleich zum allgemeinen Trend deutlich längere Lebensdauern (MT4, Fig. 3). Diese Ionen sind deutlich größer als das Eu^{3+}-Ion (Sr^{2+}: 1,32 Å, Ba^{2+}: 1,49 Å, K^{+}: 1,52 Å, vs. Eu^{3+}: 1,09 Å). Dies könnte Einfluss auf den Einbau der ebenfalls relativ großen Seltenerdionen in die Glasstruktur haben, da die großen Netzwerkwandlerionen wie Sr^{2+}, Ba^{2+} und K^{+} mit Eu^{3+} um die gleichen Netzwerkplätze konkurrieren. Mit einem anderen Koordinationsverhalten ergibt sich für das Eu^{3+}-Ion ein verändertes Ligandenfeld. Dies zeigt sich auch anhand des nicht monoexponentiellen Fluoreszenzabklingverhaltens der entsprechenden Gläser. Für einen Teil der dotierten Eu^{3+}-Ionen ändert sich bemerkbar die umgebende Lokalstruktur in diesen Wirtsgläsern. Somit überlagern sich verschiedene Abklingkinetiken der Eu^{3+} Ionen in unterschiedlichen Umgebungen.

Des Weiteren wurde das Fluoreszenzlebensdauerverhalten gegenüber der chemischen Zusammensetzung des Wirtsglases mit Hilfe des realen Kavitätsmodells [74, 75] untersucht, welches

auf dem Purcell-Effekt [68] beruht und die Abhängigkeit einer spontanen Emission eines Atoms von dem Brechungsindex seiner dielektrischen Umgebung beschreibt. Dabei ergibt sich für die radiative Übergangsrate k_{rad} bzw. für die natürliche Fluoreszenzlebensdauer τ_o:

$$k_{\mathrm{rad}} = \frac{1}{\tau_0} \propto \frac{3n^2}{2n^2+1} n \tag{15}$$

Wenn der Brechungsindex $n \geq 1$ ist, steigt die radiative Übergangsrate bzw. sinkt die natürliche Fluoreszenzlebensdauer mit steigendem Brechungsindex des umgebenden Dielektrikums. Der Brechungsindex nimmt mit steigender Polarisierbarkeit und sinkendem Molvolumen zu [98]. Dieses Modell eignet sich gut um die Ergebnisse der Fluoreszenzlebensdauern von Eu^{3+}- als auch Sm^{3+}-dotierten Gläsern zu beschreiben (MT2, Figs. 7, 8). Wie schon angedeutet, weichen Strontium-, Barium- und Kalium-haltige Gläser allerdings stark von dem Trend ab (MT4, Fig. 4). Sie besitzen weitaus längere Eu^{3+}-Fluoreszenzlebensdauern, als das Modell erwarten lässt.

Das auf der Grundlage des Säure-Base-Konzeptes nach Lewis beruhende Modell von Duffy der optischen Basizität [81] wurde schon mit vielen Glaseigenschaften in Verbindung gebracht. Es kann ein Zusammenhang der Eu^{3+}-Fluoreszenzlebensdauer mit der berechneten, theoretischen optischen Basizität der Glaszusammensetzung nachgewiesen werden. Je größer die optische Basizität ist, desto kleiner ist die Fluoreszenzlebensdauer. Dabei weichen wieder Strontium-, Barium- und Kalium-haltige Gläser stark von dem Trend zu längeren Lebensdauerwerten ab (MT4, Fig. 5).

3.3.3. Ytterbium (III) [MT3]

Ausgewählte Aluminosilicatgläser wurden mit $1{\cdot}10^{20}$ cm^{-3} Yb^{3+} dotiert. Die Fluoreszenzlebensdauern variieren zwischen 0,69 ms (Lanthan-Aluminosilicatglas mit höchster La^{3+}-Konzentration) und 1,02 ms (Lithium-Aluminosilicatglas). Wie bereits für Sm^{3+} und Eu^{3+} sinkt auch die Yb^{3+}-Fluoreszenzlebensdauer mit steigendem mittleren Atomgewicht der Glaszusammensetzung (MT3, Fig. 1).

Im Gegensatz zur Fluoreszenzlebensdauer steigen Emissions- und Absorptionswirkungsquerschnitte mit steigendem mittlerem Atomgewicht der Glaszusammensetzung leicht (MT3, Fig. 2). Dieses inverse Verhalten kann mit dem Füchtbauer-Ladenburg-Formalismus erklärt werden, der den Emissionswirkungsquerschnitt σ_e ins Verhältnis mit der Fluoreszenzlebensdauer τ setzt [99]:

$$\sigma_e \propto \frac{1}{n^2 \cdot \tau} \tag{16}$$

Die Peakpositionen der Absorptions- und Emissionsbanden des dotierten Lithium-Aluminosilicatglases ohne weitere Netzwerkwandlerionen sind um etwa 5 nm weiter von der Nullphononenlinie entfernt als in allen anderen Yb^{3+}-dotierten Glasproben (MT3, Fig. 2).

Der Zusatz von Fluorid erhöht die Fluoreszenzlebensdauer um bis zu 7 % bei einer Substitution von 9 mol% MgF_2. Außerdem sinken in geringem Maße die Emissions- und Absorptionswirkungsquerschnitte im Bereich der Nullphononenlinie. Mit relativ hoher Fluoridkonzentration werden die Emissions- und Absorptionsbanden leicht in Richtung der Nullphononenlinie verschoben (MT3, Fig. 3). Fluorid verringert die Konzentration von gebundenem Wasser im Glas durch Abdampfen von HF und SiF_4 während des Schmelzprozesses. Fluorid wird hauptsächlich in Form von Aluminiumoxifluoridgruppen $[AlO_xF_y]^{n-}$ ins Glasnetzwerk eingebaut. Die Senkung der Wasserkonzentration verringert die Wahrscheinlichkeit von Fluoreszenzquenchingprozessen durch OH-Phononen, die aufgrund des geringen Abstandes der Energieniveaus des Yb^{3+} im Vergleich zu Sm^{3+} und Eu^{3+} einen größeren Einfluss auf das Fluoreszenzverhalten haben. Desweiteren ändert der Einbau des Fluorids ins Glasnetzwerk die chemische Umgebung der Yb^{3+}-Ionen und damit deren Fluoreszenzverhalten.

3.3.4. Cer(III/IV) [MT5]

Es wurden Aluminosilicatgläser unterschiedlicher theoretischer optischer Basizität mit $1{\cdot}10^{19}$ Cerionen pro cm^3 dotiert. Die Banden im Anregungs- und Emissionsspektrum verschieben sich zu größeren Wellenlängen mit steigender optischer Basizität bzw. Polarisierbarkeit des Wirtsglases, gleichzeitig sinkt die Fluoreszenzintensität (MT5, Fig. 1). Nach Dorenbos [100, 101] führt das Ansteigen der Polarisierbarkeit in der Umgebung der Ce^{3+}-Ionen zu einer größeren Verschiebung des $5d^1$-Energieniveaus zu niedrigeren Energien, sodass der Abstand zu den zwei $4f^1$-Energieniveaus sinkt, die die Endzustände des Fluoreszenzüberganges sind. Infolgedessen verschieben sich die zwei Fluoreszenzbanden zu größeren Wellenlängen. Gleichzeitig bewirkt eine steigende optische Basizität die Stabilisierung von hohen Oxidationsstufen [50, 51]. Dementsprechend steigt die Ce^{4+}-Konzentration in Gläsern mit hoher optischer Basizität. Aufgrund der spektralen Überlappung der Absorptionsbanden der Ce^{3+}- und Ce^{4+}-Spezies (MT5, Fig. 3) und der starken Charge-Transfer-Absorption von Ce^{4+} wird in den Gläsern mit hoher optischer Basizität die Strahlung von einer höheren Ce^{4+}-Konzentration absorbiert, die in diesen Gläsern keine Fluoreszenzemission zeigen. Unter konstanten Schmelzbedingungen sinkt folglich die Intensität der Ce^{3+}-Fluoreszenz mit steigender optischer Basizität.

Durch Änderung der Schmelzbedingungen kann das Redoxgleichgewicht von Ce^{3+}/Ce^{4+} beeinflusst werden. Durch Entgasen der Glasschmelze mit Argon, Schmelzen unter Argon-Atmosphäre oder Zugabe von Reduktionsmitteln (wie zum Beispiel Kohlenstoff, Aluminiumpulver) wird das Redoxgleichgewicht zugunsten Ce^{3+} verschoben. Es wird gezeigt, dass mit Hilfe von reduzierenden Schmelzbedingungen die Fluoreszenzintensität der Cer-dotierten Gläser erhöht werden kann, da die Konzentration der Ce^{3+}-Spezies zunimmt. Die höchsten Intensitäten und folglich die effektivste Reduktion wird durch Schmelzen unter Argon-Atmosphäre bei gleichzeitigem Entgasen der Glasschmelze mit Argon oder durch Zugabe von 1 mol% Aluminiumpulver, welches 0,5 mol% Al_2O_3 ersetzt, erhalten (MT5, Fig. 2).

Unter der Annahme, dass durch Zugabe von 1 mol% Aluminiumpulver bei einer Dotierungskonzentration von $1{\cdot}10^{19}$ Cerionen pro cm^3 (≈ 0,04 mol%) nur Ce^{3+}-Ionen vorliegen, kann das Absorptionsspektrum, der mit Aluminiumpulver reduzierten Probe, mit fünf Gaußkurven entfaltet werden (MT5, Fig. 4). Alle Kurven liegen im Bereich des $4f^1 \rightarrow 5d^1$-Übergangs der Ce^{3+}-Ionen, dabei spaltet sich das $5d^1$-Energieniveau in 5 Unterniveaus auf. Die entfalteten Kurven bei 30.000, 30.700, 32.000, 37.200 und 45.700 cm^{-1} stimmen gut mit Literaturwerten [47] überein. Für Ce^{3+} konnte bei einer Wellenlänge von 324 nm ein Extinktionskoeffizient von 807 $l{\cdot}mol^{-1}{\cdot}cm^{-1}$ bestimmt werden. In Glasproben gleicher Dotierungskonzentration, jedoch ohne Reduktionsmittel und einerseits geschmolzen an Umgebungsluft und anderseits entgast mit O_2, werden beide Oxidationsstufen von Cer erwartet. Demzufolge erfolgt die Entfaltung dieser Absorptionsspektren mit zwei zusätzlichen Kurven, die für den Charge-Transfer-Übergang der Ce^{4+}-Ionen stehen (MT5, Figs. 5, 6). Da verglichen mit der reduzierten Probe die Intensitäten der entfalteten Kurven der Ce^{3+}-Übergänge auf 67 % (ohne Reduktionsmittel, an Umgebungsluft) bzw. 47 % (mit O_2 entgast) gesunken sind, wird eine Ce^{3+}-Konzentration von 0,67 und $0{,}47{\cdot}10^{19}$ Ionen pro cm^3 in den unter normalen bzw. oxidierenden Schmelzbedingungen erhaltenen Gläsern angenommen. Damit ergibt sich eine Ce^{4+}-Konzentration von 0,33 bzw. $0{,}53{\cdot}10^{19}$ Ionen pro cm^3. Mit Hilfe dieser Ce^{4+}-Konzentration konnte der Extinktionskoeffizient für Ce^{4+} in diesen Glasproben bei 250 nm bestimmt werden, der 4.627 bzw. 4.843 $l{\cdot}mol^{-1}{\cdot}cm^{-1}$ beträgt. Damit ist der Extinktionskoeffizient der Ce^{4+}-Absorption fast sechsmal so groß wie der Koeffizient der Ce^{3+}-Absorption und überlagert die Absorption von Ce^{3+} bis weit in den sichtbaren Spektralbereich.

Unter reduzierenden Schmelzbedingungen ist die Lage und Intensität der Ce^{3+}-Fluoreszenzbanden auch abhängig von der Cer-Konzentration. Je größer die Konzentration ist, desto weiter werden die Banden in den roten Spektralbereich verschoben. Des Weiteren bricht die Fluoreszenzintensität ab einer Cer-Konzentration von $3{\cdot}10^{20}$ Ionen pro cm^3 und bei einem Zusatz

von 1 mol% Aluminiumpulver ein (MT5, Fig. 7). Der nicht proportionale Anstieg der Fluoreszenzintensität im Vergleich zur Cer-Konzentration und die leichte Verschiebung der Fluoreszenzbanden deuten auf eine veränderte chemische Umgebung der Cer-Ionen hin. Eine verstärkte Cluster-Bildung von stark basischen Cer-Ionen mit steigender Cer-Konzentration wird als Ursache für die Verschiebung und Intensitätsänderung der Fluoreszenzbanden angenommen. Schließlich reicht ein Zusatz von 1 mol% Aluminiumpulver nicht aus, um eine Cer-Konzentration von mehr als $3 \cdot 10^{20}$ Ionen pro cm^3 vollständig zu reduzieren und die oben beschriebene Minderung der Fluoreszenzintensität der Ce^{3+} durch die verstärkte Ce^{4+}-Absorption tritt dann ein.

4. Zusammenfassung / Summary

Die dargelegte Arbeit zeigt das hohe Potenzial von seltenerd-dotierten Aluminosilicatgläsern für Lumineszenzanwendungen, die hohe Ansprüche an die mechanische Stabilität fordern. Aufgrund der Vielfalt erzielbarer Materialeigenschaften in Abhängigkeit von der Zusammensetzung, Struktur und Herstellung bietet dieses Glassystem Forschungsansätze für die anwendungsorientierte Entwicklung. In dieser Arbeit wurden Reihen von Glaszusammensetzungen mit spektroskopischen sowie mechanischen Methoden untersucht und Korrelationen zwischen Struktur, Herstellung und Eigenschaften diskutiert. Mit Hilfe der ermittelten Wechselbeziehungen konnten schließlich die Eigenschaften für unterschiedliche Anwendungen systematisch optimiert werden. Dafür wurden verschiedene Aluminosilicatgläser mit 50-70 mol% SiO_2 sowie 5-25 mol% Al_2O_3 hergestellt. Die Konzentration von Netzwerkwandlerionen (Li^+, Na^+, Mg^{2+}, K^+, Sr^{2+}, Ca^{2+}, Ba^{2+}, Zn^{2+}, Pb^{2+}, Y^{3+}, La^{3+}) multipliziert mit deren Wertigkeit war im Verhältnis zur Al^{3+}-Konzentration gleich oder größer.

Die mechanische Charakterisierung konzentrierte sich auf die Untersuchungsmethoden Dilatometrie (linearer Ausdehnungskoeffizient und Glastransformationstemperatur), Ultraschallprüfung (Elastizitätsmodul und Poissonzahl) sowie Eindruckprüfung (Vickers Härte und Bruchzähigkeit). Es wurde gezeigt, dass Elastizitätsmodul, Bruchzähigkeit und Härte von der Feldstärke der Netzwerkwandlerionen abhängig sind, wobei auch die Koordination und Polarisierbarkeit dieser Ionen Einfluss auf die Eigenschaften nimmt (Li^+, La^{3+}, Pb^{2+}). In Mischoxid-Aluminosilicatgläsern liegen alle mechanischen Eigenschaften zwischen den Eigenschaften der ternären Gläser. Für Vickers Härte und Bruchzähigkeit konnten positive Abweichungen von der Linearität im Bezug auf das Netzwerkwandler-Verhältnis (am Beispiel von ZnO/MgO) nachgewiesen werden. Die niedrigsten Ausdehnungskoeffizienten und thermomechanischen Spannungen wurden mit Magnesium- und Zink-Aluminosilicaten gefunden.

Neben der Abhängigkeit von der Art der Netzwerkwandlerionen hat auch die Konzentration Einfluss auf die Eigenschaften. Durch den Überschuss von Netzwerkwandlerionen werden Trennstellen im Glasnetzwerk gebildet. Die geringere Vernetzung führt in den Lanthan- und Magnesium-Aluminosilicatgläsern zu erhöhten thermischen Ausdehnungskoeffzienten, Elastizitätsmoduli und Poissonzahlen, sowie verminderten Glastransformationstemperaturen. Neben dem Vernetzungsgrad bestimmt auch die SiO_2-Konzentration die mechanischen Eigenschaften. Die Substitution von bis zu 9 mol% Netzwerkwandlerfluorid für Netzwerkwandleroxid beeinflusst die untersuchten Eigenschaften kaum, ausschließlich die Transformationstemperatur wird signifikant um mehr als 100 K gesenkt. Da hierdurch auch die Schmelztempe-

ratur gesenkt werden kann und damit geringere Herstellungskosten anfallen, sollten Zusammensetzungen mit Fluorid-Zusätzen bevorzugt werden.

Ebenfalls beeinflusst der Fluorid-Zusatz die Fluoreszenzeigenschaften dotierter Gläser positiv. Die Fluoreszenzlebendauern von Yb^{3+}-, Eu^{3+}- und Sm^{3+}-dotierten Aluminosilicatgläsern werden durch die Zugabe von Fluorid verlängert. Dadurch sinken die Emissions- und Absorptionswirkungsquerschnitte, erklärt durch den Füchtbauer-Ladenburg-Formalismus. Da die Konzentration von Wasser, gebunden im Glasnetzwerk, deutlich mit steigender Fluorid-Konzentration fällt, sinkt die Wahrscheinlichkeit für nicht-radiative Relaxationen durch OH-Oberschwingungen. Des Weiteren werden Aluminiumoxifluoridgruppen $[AlO_xF_y]^{n-}$ im Glasnetzwerk gebildet, die sich in der Umgebung der Seltenerdionen befinden.

Außerdem zeigen die Untersuchungen, dass einerseits das Fluoreszenzverhalten kaum durch die Konzentrationsverhältnisse im ternären Magnesium-Aluminosilicat-Glassystem mit 50-70 mol% SiO_2, 15-45 mol% MgO sowie 5-22 mol% Al_2O_3 beeinflusst werden, obwohl sich die Phononenspektren merklich ändern, andererseits bestimmt die Wahl des Netzwerkwandlerions die Fluoreszenzeigenschaften. Frühere Arbeiten [41] deuten an, dass sich die Netzwerkwandler im Koordinationsfeld der dotierten Seltenerdionen befinden. Dies erklärt, warum das Atomgewicht, die Polarisierbarkeit und somit das Koordinationsverhalten der Netzwerkwandlerionen Auswirkungen auf das Fluoreszenzverhalten der Seltenerdionen haben. Den theoretischen Hintergrund zu diesem Ergebnis liefert der Purcell-Effekt, welcher die Abhängigkeit der Wahrscheinlichkeit spontaner Emission einer Kavität von der umgebenden Matrix mathematisch beschreibt. Dabei steigt die Wahrscheinlichkeit der spontanen Emission mit steigender Brechzahl, was auch in den untersuchten Gläsern nachgewiesen werden konnte.

Im Vergleich zu Phosphat, Alumophosphat- und Fluoridphosphatgläsern sind die Fluoreszenzlebensdauern dotierter Aluminosilicatgläser geringer. Jedoch kann durch Zusatz von Fluorid und durch den Einsatz von leichten Netzwerkwandlerionen die Fluoreszenzlebensdauer soweit erhöht werden, sodass ähnlich gute Werte wie für reine Phosphate und Alumophosphate erzielt werden. Die Lebensdauern für rein fluoridische und Fluoridphosphatgläser liegen in der Regel jedoch noch etwas über den Werten für Aluminosilicatgläser. Im Vergleich dazu sind aber insbesondere die thermischen Ausdehnungskoeffizienten der Aluminosilicatgläser deutlich geringer, sodass eine höhere thermische Belastung der Gläser im Laserbetrieb möglich sein sollte. Basierend auf diesen Erkenntnissen werden zur Zeit Untersuchungen der Stabilität von Aluminosilicatgläsern im Hochenergielaserbetrieb durchgeführt. Desweiteren stehen weitergehende Untersuchungen der Koordinationssphäre der Seltenenerdionen in Aluminosilicatgläsern aus.

Ein weiteres hoch aktuelles Forschungsthema stellen Ce^{3+}/Yb^{3+}-kodotierte Materialien dar. In dieser Arbeit wurden Cer-dotierte Aluminosilicatgläser hergestellt und der Einfluss von Glaszusammensetzung, optischer Basizität und Schmelzbedingungen auf das Ce^{3+}/Ce^{4+}-Gleichgewicht und die spektralen Eigenschaften und Intensitäten der Ce^{3+}-Fluoreszenz untersucht. In Gläsern mit hoher optischer Basizität werden die Emissions- und Absorptionsbanden zu größeren Wellenlängen verschoben, während das Ce^{3+}/Ce^{4+}-Verhältnis sinkt. Es wurde gezeigt, dass die starke Absorption von Ce^{4+} die Anregung von Ce^{3+} beeinträchtigt. Für eine effektive Ce^{3+}-Fluoreszenz wurde das Ce^{3+}/Ce^{4+}-Gleichgewicht durch geeignete Schmelzbedingungen zum Ce^{3+} verschoben. Des Weiteren wurden erstmalig für eine Glaszusammensetzung die Extinktionskoeffizienten von Ce^{3+} und Ce^{4+} bestimmt. Aufbauend erfolgen in kommenden Arbeiten Untersuchungen zu der Wirkung von reduzierenden Schmelzbedingungen in Ce^{3+}/Yb^{3+}-kodotierten Aluminosilicatgläsern mit hohen optischen Basizitäten.

This work demonstrates the high potential of rare-earth-doped alumino silicate glasses for luminescence applications that require high demands on the mechanical stability. Due to the plurality of the material properties, depending on the composition, structure and preparation, this glass system provides approaches for applied research. In this work, variations of glass compositions were examined by using spectroscopic and mechanical methods. Furthermore, correlations between structure, preparation and properties were discussed. Finally, with the aid of the obtained correlations properties for different applications could systematically be optimized. Various alumino silicate glasses were prepared with 50-70 mol% SiO_2 and 5-25 mol% Al_2O_3. The concentrations of network modifier ions (Li^+, Na^+, Mg^{2+}, K^+, Sr^{2+}, Ca^{2+}, Ba^{2+}, Zn^{2+}, Pb^{2+}, Y^{3+}, La^{3+}) multiplied by their valency was equal to or larger than the Al^{3+}-concentration.

The mechanical characterization was focused on the following methods: dilatometry (linear expansion coefficient and glass transition temperature), Ultra-sound examination (elastic modulus and Poisson's ratio) and indentation test (Vickers hardness and fracture toughness). It has been shown that elastic modulus, fracture toughness and hardness are depending on the field strength of the network modifier ions. Also, the coordination and polarizability of modifier ions (Li^+, La^{3+}, Pb^{2+}) affect these properties. In mixed oxide alumino silicate glasses all mechanical properties are between the properties of the ternary glasses. With respect to the Zn^{2+}/Mg^{2+} ratio positive deviations from linearity could be detected for Vickers hardness and indentation fracture toughness. The lowest expansion coefficient and the lowest thermo-mechanical stress values were found for magnesium and zinc alumino silicate glasses.

In addition to the dependence on the type of network modifier ions, also the concentration affects the properties. Non-bridging oxygen sites are formed in the glass network by an excess of network modifier ions. In the lanthanum and magnesium alumino silicate glasses, the lower crosslinking causes an increase of the thermal expansion coefficient, the elastic modulus and the Poisson's ratio, as well as lower glass transition temperatures. In addition to the degree of crosslinks, the SiO_2-concentration is decisive of the mechanical properties. Furthermore, substitutions of up to 9 mol% networkmodifier fluoride for oxides hardly affect the most physical properties, only the transformation temperature is reduced significantly by more than 100 K. As a result, the melting temperature can be lowered and thus lower manufacturing costs arise. Therefore compositions with fluoride additives should be preferred.

Also, the addition of fluoride positively influences the fluorescence properties of doped glasses. The fluorescence lifetimes of Yb^{3+}, Eu^{3+} and Sm^{3+} doped alumino silicate glasses increase by the addition of fluoride. This will reduce the emission and absorption cross sections, explained by the Füchtbauer-Ladenburg formalism. Since the concentration of water dissolved in the glass network significantly decreases with increasing fluoride substitution, the probability of non-radiative relaxations by OH harmonics decreases. Furthermore groups of aluminiumoxy-fluoride $[AlO_xF_y]^{n-}$ are formed in the glass network, which are part of the coordination shell of the rare earth ions.

In addition, the studies show that, within the range of tested compositions, on the one hand the fluorescence behavior of the doped rare earth ions is hardly affected by the concentration ratios in a ternary glass system, although the phonon energy of the glass is significantly changed. On the other hand, the type of network modifier ion determines the fluorescence properties. Previous work suggests that the network modifier ions are in the coordination field of the doped rare earth ions. Thus, the atomic weight, the polarizability and the coordination behavior of the network modifier affect their fluorescence behavior. The theoretical background of this correlation is the Purcell effect which describes the dependence of the probability of spontaneous emission of a cavity on the refractive index of the surrounding matrix. The probability increases with increasing refractive index, which could also be verified for the studied glasses.

In comparison to phosphate, alumino phosphate and fluoride phosphate glasses, the fluorescence lifetimes are mostly lower in doped alumino silicate glasses. By the addition of fluoride and by the use of network modifier ions with small atomic weight, the fluorescence lifetime in alumino silicate glasses can be increased to the extent that similar results as for phosphate and alumino phosphate glasses are obtained. However, fluoride and fluoride

phosphate glasses still show higher lifetime values. But in comparison to phosphate, alumino phosphate, fluoride and fluoride phosphate glasses, the CTE of the alumino silicate glasses are significantly lower, therefore a higher thermal loading in laser operation should be possible. Based on these findings, studies of the thermo-mechanical stability of aluminosilicate should be carried out in a high-power laser operation. In addition, further studies of the coordination sphere of the rare-earth ions in alumino silicate glasses are lying ahead.

Another recent research topic are Ce^{3+} / Yb^{3+} codoped materials. In this work, cerium-doped alumino silicate glasses were prepared and investigated in respect of the effect of glass composition, optical basicity and melting conditions on the Ce^{3+} / Ce^{4+} equilibrium and the spectral characteristics and intensities of the Ce^{3+} fluorescence. In glasses with a high optical basicity, the emission and absorption bands are shifted to longer wavelengths, while the Ce^{3+} / Ce^{4+} ratio decreases. It has been demonstrated that the strong absorption of Ce^{4+} impairs the excitation of Ce^{3+}. For effective Ce^{3+} fluorescence the Ce^{3+} / Ce^{4+} equilibrium was moved by reducing melting conditions. In addition, the extinction coefficient of Ce^{3+} and Ce^{4+} were determined for one AS glass composition. Further studies should examine the effect of reducing melting conditions in Ce^{3+} / Yb^{3+} doped alumino silicate glasses with high optical basicity.

5. Publikationen

5.1. [MT1] Magnesium aluminosilicate glasses as potential laser host material for ultrahigh power laser systems

Mirko Tiegel, Andreas Herrmann, Christian Rüssel, Jörg Körner, Diethard Klöpfel, Joachim Hein, Malte C. Kaluza

Journal of Materials Chemistry C, 1 (2013) 5031-5039, DOI: 10.1039/C3TC30761A

	Mirko Tiegel	Dr. Andreas Herrmann	Prof. Dr. Christian Rüssel	Dr. Jörg Körner	Diethard Klöpfel	Dr. Joachim Hein	Prof. Dr. Malte C. Kaluza
Konzeption des Forschungsansatzes	☒	☒	☒	☒	☒	☒	☒
Planung der Untersuchungen	☒	☐	☐	☐	☐	☐	☐
Datenerhebung	☒	☒	☐	☐	☐	☐	☐
Datenanalyse und -interpretation	☒	☐	☐	☐	☐	☐	☐
Schreiben des Manuskripts	☒	☒	☒	☐	☐	☒	☒
Vorschlag Anrechnung Publikationsäquivalente	1,0						

Journal of Materials Chemistry C

RSC Publishing

PAPER

View Article Online
View Journal | View Issue

Cite this: J. Mater. Chem. C, 2013, 1, 5031

Magnesium aluminosilicate glasses as potential laser host material for ultrahigh power laser systems

Mirko Tiegel,[a] Andreas Herrmann,*[a] Christian Rüssel,[a] Jörg Körner,[b] Diethard Klöpfel,[b] Joachim Hein[bc] and Malte C. Kaluza[bc]

Received 23rd April 2013
Accepted 11th June 2013

DOI: 10.1039/c3tc30761a

www.rsc.org/MaterialsC

Magnesium aluminosilicate glasses doped with 0.2 mol% Sm_2O_3 (1×10^{20} Sm^{3+} cm^{-3}) have been prepared in a very broad compositional range. The effect of the MgO, Al_2O_3 and SiO_2 concentrations as well as the effect of partial substitution of MgO by CaO, SrO, BaO, ZnO or MgF_2 have been studied. Increasing the network modifier concentration results in decreasing the glass transformation temperature and increasing the coefficient of thermal expansion due to the formation of non-bridging oxygen sites and decreasing glass network connectivity. Although the network connectivity is changed substantially by the addition of network modifier oxides, the maximum phonon energy and the fluorescence lifetime of Sm^{3+} are not affected. Equimolar replacement of up to 9 mol% MgO by MgF_2 results in increasing Sm^{3+} fluorescence lifetimes without increasing the coefficient of thermal expansion or decreasing the glass forming ability. Glasses with fairly small thermal expansion coefficients ($\geq 3.2 \times 10^{-6}$ K^{-1}), low thermal stress values (≥ 0.5 MPa K^{-1}), broad fluorescence emission peaks and fluorescence lifetimes in the range from 2.4 to 2.8 ms are obtained. Such glasses are interesting candidates for laser host materials in ultrahigh peak power laser systems.

1 Introduction

Since the realization of the first glass laser in 1961 by Snitzer,[1] rare earth doped glasses have been well established as amplifying media for solid-state lasers. The main advantages of glasses in comparison to single-crystals or polycrystalline materials are their isotropy, quality, size and throughput. Nowadays, for high power glass-based laser systems the glass composition of choice are phosphate glasses due to their high solubility of rare earth ions, their relatively long fluorescence lifetimes of doped ions and their advantageous spectroscopic properties.[2] Other widely used laser glasses are fluoride phosphate glasses. They possess outstanding lasing properties, *i.e.* very high fluorescence lifetimes and high quantum efficiencies of doped rare earth ions.[3–8]

Generally, the predominant disadvantages of these glasses are their thermo-mechanical limitations.[9,10] Their application in high average power laser systems results in substantial thermal loading. This is especially true if high repetition rates are necessary, producing high mechanical stresses within the glass. At ultrahigh power amplification stages, the thermally induced stress may result in the formation of micro-cracks and finally in the destruction of the lasing material. Here the application of glasses with higher thermal shock resistance is required. Therefore the biggest challenge for the development of ultrahigh power glass-based laser systems is the design and development of glasses with much improved thermo-mechanical properties, while good lasing characteristics have to be maintained.

Fused silica has a very high thermal shock resistance but a low solubility for rare-earth ions.[11] Fujimoto and colleagues[12–14] use a zeolite route to incorporate up to 3 ma% Nd_2O_3 into a SiO_2 matrix without clustering of the rare earth ions by adding some Al_2O_3 to the glass composition. For these glasses the thermal shock resistance was reported to be more than 50 times higher than for commercial phosphate laser glasses. Nevertheless, the hallmarks of established optical glass melting in terms of quality, size and throughput cannot be achieved by this production method.

Magnesium aluminosilicate (MAS) glasses are a well studied glass system with a very good glass forming ability and low crystallization tendency in a broad compositional range.[15] Furthermore these glasses possess very good mechanical and thermo-mechanical properties such as high fracture strength, a high Young's modulus and a low coefficient of thermal expansion.[16,17] Therefore these glasses are used *e.g.* for the production of glass-fibre reinforced polymer matrix composites.[18] Glasses in this system can also be used for the preparation of glass-ceramics with best mechanical properties by controlled crystallization which are *e.g.* suitable for hard disc plates[19] or dental materials.[20] For this, nucleation agents have to be added to the glass composition.

[a]Otto-Schott-Institut, Jena University, Fraunhoferstraße 6, 07743 Jena, Germany. E-mail: andreas.herrmann@uni-jena.de
[b]Institute of Optics and Quantum Electronics, Jena University, Max-Wien-Platz 1, 07743 Jena, Germany
[c]Helmholtz Institute Jena, Fröbelstieg 3, 07743 Jena, Germany

View Article Online
Journal of Materials Chemistry C Paper

In addition, MAS glasses have a high chemical durability,[21] a low OH^- and platinum solubility[22] and a high solubility for rare earth compounds. Furthermore, the good glass forming ability of the MAS system allows high compositional variation and therefore permits the tailoring of most physical properties.[23–25] The thermal expansion coefficient, for example, has to be minimized to achieve a high thermal shock resistance.[26] Thus MAS glasses seem to be a very promising laser host material with respect to high power applications.

In this article we report on the effect of compositional changes on the glass structure and on the thermo-mechanical, optical and fluorescence properties of Sm^{3+}-doped MAS glasses. The concentration of MgO, Al_2O_3 and SiO_2 has been varied. Furthermore, MgO has been partly substituted by other earth alkaline metal oxides (CaO, SrO and BaO), by zinc oxide or by MgF_2.

2 Experimental procedures

Glasses were melted from raw materials of especially high purity (Fe <10 ppm, other metals <0.5 ppm) MgO (Merck, Germany), Al_2O_3 (Ceralox, Condea Chemie, Germany), SiO_2 (Sipur A1, Schott, Germany), ZnO (Merck, Germany), $BaCO_3$ (Reachim, Ukraine), $SrCO_3$ (Reachim, Ukraine), $CaCO_3$ (Merck, Germany), and MgF_2 (Chemiewerk Nünchritz, Germany) in batches of 200 to 400 g in a covered platinum crucible. The batch compositions and some physical properties of the undoped base glass samples are summarized in Table 1. Most of the glasses were doped with Sm_2O_3 (Ferak, Germany) at a doping concentration of 1×10^{20} Sm^{3+} cm^{-3}. After keeping the melts for 4 h at 1590 °C, they were cast into water, dried, and subsequently crushed into pieces with a size of about 1 mm. Then the glasses were re-melted at 1590 °C and held for an additional 4 h to improve their homogeneity. The re-melted glasses were cast into a preheated (880 °C) steel mold and placed in a furnace at a temperature of 880 °C. Then the furnace was switched off and the glass was allowed to cool down to room temperature at a cooling rate of about 3 K min^{-1}.

Prepared glass samples with a diameter of 8 mm and a length of 25 mm were characterized by dilatometry at temperatures in the range from 20 to 1000 °C at a heating rate of 5 K min^{-1} (Netzsch Dil 402 PC). The error in the glass-transition temperature measurements is ±5 K.

Young's moduli measurements are done with the ultrasonic detector Krautkramer-Branson USD 15 on glass samples with a diameter of 15 mm and a length of 20 mm. The error of the Young's modulus measurement is ±3 GPa.

In order to record fluorescence emission spectra, polished plates (15×20 mm^2, thickness 10 mm) were prepared from the glass samples. A fluorescence spectrometer (RF-5301PC, Shimadzu, Japan) was used for these studies. The spectra were obtained using an excitation wavelength of 403 nm.

Luminescence lifetime measurements were conducted using a self-made experimental setup. It consists of a pulsed high power LED (LED 395-66-60, Roithner Lasertechnik Vienna, Austria; wavelength: 395 nm), a spectrometer (H.25, Jobin Yvon, France), a photomultiplier tube (R5929, Hamamatsu, Japan) and a digital storage oscilloscope (TDS2012, Tektronix, USA). For the fluorescence lifetime measurements, the samples were excited by an UV light pulse of high power LEDs at a wavelength of 395 nm. The resulting luminescence light was collected and focused to the entrance slit of a spectrometer by a lens array. The spectrum-sliced light was amplified by a photomultiplier tube, which was connected to the oscilloscope. The oscilloscope recorded the luminescence intensity as a function of time. The data obtained were transferred to a PC and later analyzed using commercial scientific graphing software. This type of setup

Table 1 Compositions (mol%) and selected properties of the studied glasses compared to a phosphate glass (P100) and a fluoride phosphate glass (FP20) (reported by Möncke and Ehrt[27]); thermal expansion coefficient α, density ρ, transition temperature T_g, Poisson's ratio ν, Young's modulus E, thermal stress $\sigma/\Delta T$, refractive index n_d (589 nm), and fluorescence lifetime τ (glass samples doped with 1×10^{20} Sm^{3+} cm^{-3})

	Composition (mol%)											
Sample	MgO	Al_2O_3	SiO_2	Substitution of MgO	α (10^{-6}/K)	T_g (°C)	ρ (g cm^{-3})	ν	E (GPa)	$\sigma/\Delta T$ (MPa K^{-1})	n_d	τ (ms)
MAS15	15	14	71		3.22	831	2.44				1.52	2.48
MAS20	20	20	60		4.06	827	2.55	0.255	102	0.55	1.546	2.42
MAS22	22	22	56		4.49	824	2.60				1.56	2.47
MAS30	30	10	60		5.23	796	2.56	0.254	96	0.68	1.546	2.46
MAS37	37	13	50		5.49	780	2.66				1.57	2.45
MAS45	45	5	50		6.45	776	2.70				1.57	
MAS-Zn	10	20	60	10 (ZnO)	3.98	766	2.73	0.249	99	0.52	1.56	2.46
MAS-Ba	10	20	60	10 (BaO)	4.77	841	2.86				1.57	2.39
MAS-Sr	10	20	60	10 (SrO)	4.69	834	2.73				1.549	
MAS-Ca	10	20	60	10 (CaO)	4.62	829	2.61				1.549	
MAS-F1.5	18.5	20	60	1.5 (MgF_2)	4.35	799	2.60				1.542	2.53
MAS-F3	17	20	60	3 (MgF_2)	4.39	779	2.60				1.539	2.59
MAS-F9	11	20	60	9 (MgF_2)	3.88	721	2.58	0.247	98	0.50	1.53	2.81
P_2O_5	SrO	$Sr(PO_3)_2$	AlF_3, Mg/Sr/CaF_2									
P100	50	50			12.5	500	3.15	0.282	50	0.88	1.56	2.60
FP20			20	80	15.0	490	3.54	0.288	76	1.61	1.50	3.50

View Article Online
Paper Journal of Materials Chemistry C

allows wavelength-specific lifetime measurements that enable the discrimination of luminescence light of different origins (*e.g.* different luminescent ions or different local surroundings or even different excitation states). The measurements were carried out for the strongest fluorescence transition of Sm^{3+} at about 598 nm. The relative standard deviation of these measurements could be estimated to less than ±2%.

The refractive indices in the visible range were measured with a refractometer (PR2, Carl Zeiss Jena, Germany) with an error of $\pm 2 \times 10^{-5}$.

The infrared spectra were recorded using polished glass samples (15×20 mm^2, thickness 10 mm) and a Fourier-Transform Spectrometer (Shimadzu IRAffinity-1) in the wavenumber range from 2000 to 4000 cm^{-1} and in the range from 400 to 2000 cm^{-1} with specular reflectance accessories (SRM-8000A).

3 Results and discussion

3.1 General observations

In Table 1 the weighted glass compositions are shown. All cast glasses are visually transparent, clear and show a very light orange color. Element analyses of the fluorine substituted glasses MAS-F revealed a fluorine loss of up to 35% which apparently occurred during the melting of the glasses. These glasses are compared to a pure phosphate glass (P100) and a fluoride phosphate glass (FP20).[27]

3.2 Coefficient of thermal expansion

3.2.1 Unsubstituted MAS glasses. Dilatometric measurements of the cast glasses show a linear thermal expansion coefficient α which depends on the MgO concentration (Fig. 1). When increasing the magnesium oxide concentration a nearly linear increase in the expansion coefficient has been observed. This is due to the formation of more non-bridging oxygen (NBO) sites with increasing magnesium oxide concentration.

3.2.2 Glasses in which MgO is partially substituted by other alkaline earth metals or zinc oxide. In the following, the effect of an equimolar replacement of MgO by other network modifier oxides or ZnO is described. As shown in Table 1 column 6, the coefficients of thermal expansion do not only depend on the quantity of NBO but also on the type of the network modifier ion. The equimolar substitution of Mg^{2+} by Ba^{2+}, Sr^{2+} or Ca^{2+} results in an increase of the coefficients of thermal expansion. This can be explained by reduction of the binding strengths and cation-field strengths Z/r^2 (where Z is the valence number and r is the ionic radius) of the modifier ion.[28] Values for the field strength are in the order: Ba^{2+} (0.99) < Sr^{2+} (1.28) < Ca^{2+} (2.00) < Zn^{2+} (5.56) < Mg^{2+} (5.95) which is the same order as for the reciprocal ionic radius.[29] The zinc substituted glass shows almost the same expansion coefficient as the non-substituted magnesium aluminosilicate glass, which is possibly due to the similar field strength of Mg^{2+} and Zn^{2+}.

3.2.3 Effect of fluorine substitution. In order to improve the luminescence properties of the glasses, MgO was substituted by MgF_2. Here, the MgF_2 concentration was varied between 1.5 and 9 mol% (samples MAS-F). As shown in Table 1, the introduction of fluorine has only a moderate effect on the coefficient of thermal expansion. The latter increased by up to 10% for 1.5 and 3.0 mol% MgF_2. Surprisingly, higher concentrations of MgF_2 lead to a reduction of the expansion coefficient (sample MAS-F9).

3.3 Glass transition temperature

3.3.1 Unsubstituted MAS glasses. Fig. 2 shows the dependence of the glass transition temperature T_g on the MgO concentration in non-substituted MAS glasses. T_g of glasses with a high MgO concentration (>35 mol%) is about 780 °C whereas glasses with a lower MgO concentration (<25 mol%) show T_g values close to 830 °C. Again, the generation of NBO by the introduction of Mg^{2+} into the glass network is responsible for this behavior; the higher the concentration of non-bridging oxygen sites in the glass network, the lower the viscosity of the melt. On the other hand, Mg^{2+} is not only a network modifier. In conjunction with Al_2O_3 it may also compensate the negative charge of $[AlO_{4/2}]^-$ tetrahedra which replace $[SiO_{4/2}]$ in the glass network and hence act as network formers. This means that one

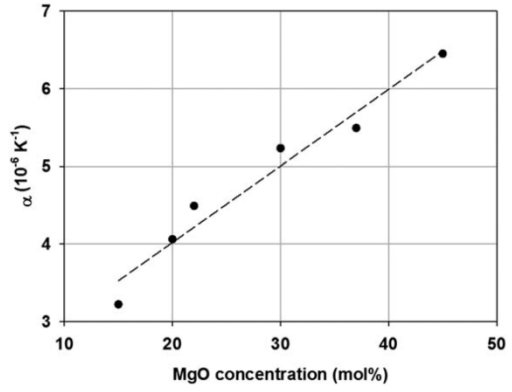

Fig. 1 Dependence of the coefficient of thermal expansion α on the MgO concentration in unsubstituted magnesium aluminosilicate glasses.

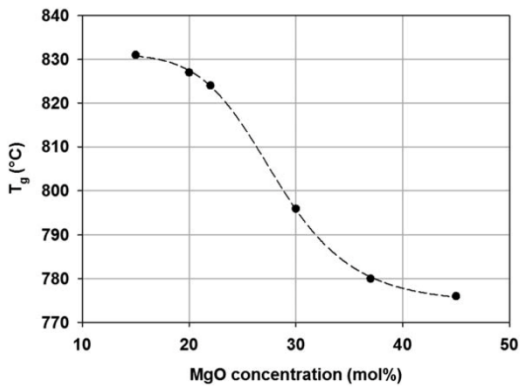

Fig. 2 Dependence of the glass transition temperature T_g on the MgO concentration in unsubstituted magnesium aluminosilicate glasses.

Mg^{2+} ion can stabilize two $[AlO_4]^-$-tetrahedra. If the molar concentration of MgO exceeds that of Al_2O_3, the excess of Mg^{2+} ions will be incorporated as network modifiers into the glass network, creating non-bridging oxygen sites and therefore decreasing the network connectivity. This readily explains the lower T_g values of glasses with a MgO to Al_2O_3 ratio higher than 1 (MAS30, MAS37 and MAS45).

3.3.2 Glasses in which MgO is partially substituted by other alkaline earth metals or by zinc oxide. In comparison to the unsubstituted glass MAS20, the partially substituted glasses show increasing T_g with increasing radius of the substituting ion (Ca^{2+}, Sr^{2+}, and Ba^{2+}). This rise might be explained by decreasing field strengths of the modifier ions which affect the structural rigidity of the glass network.[29] On the other hand the equimolar substitution by zinc oxide results in a notable decrease of T_g to 766 °C in comparison to 827 °C for MAS20 glass.

3.3.3 Effect of fluorine substitution. The substitution of MgO by MgF_2 results in a decrease of T_g. In analogy to the introduction of additional network modifiers, fluorine substitution causes the generation of non-bridging oxygen sites by breaking up potential Si–O–Al crosslinks in the network into $Si–O^-$ and Al–F units.[30]

3.4 Young's moduli and thermal stresses

The measured elastic moduli E of selected glasses are shown in Table 1. All measured MAS glasses have relatively high elastic moduli of about 100 GPa. MAS20 shows the highest stiffness with 102 GPa. A higher concentration of the network former MgO (MAS30) and a partial substitution of MgO by ZnO (MAS-Zn) and MgF_2 (MAS-F9) slightly reduce the stiffness up to 5%. In MAS30 and MAS-F9 more non-bridging oxygen sites are formed in comparison to MAS20. The lower connectivity of the network of these glasses explains the decrease of stiffness. In comparison to P100 and FP20, the elastic moduli of MAS glasses are much higher. This can be explained by the completely different composition and the lower connectivity in the P100 and FP20 glasses.

The thermal stress σ of a material can be calculated by:

$$\sigma = \frac{E\alpha}{1-\nu}\Delta T.$$

Here, E is the Young's modulus, α is the coefficient of thermal expansion and ν is the Poisson's ratio, while ΔT is the induced temperature difference. As Table 1 shows, MAS glasses have thermal stress values of about 0.5–0.7 MPa K^{-1}. The lowest thermal stress is found for the glass with the smallest thermal expansion (MAS-F9). The phosphate (P100) and fluoride phosphate glasses (FP20) show two to three times higher thermal stress values than the MAS glasses because of their high expansion coefficients and low elastic moduli.

3.5 Vibrational spectroscopy

The FTIR absorption spectra obtained from unsubstituted and substituted glasses are shown in Fig. 3–5. In the high energy part of these spectra at wavenumbers in the range between 900 and 1300 cm^{-1}, a broad, strong peak at about 1050–1150 cm^{-1} and another smaller peak at about 950 cm^{-1} are observed. For glasses with high MgO concentration (*e.g.* MAS45 and MAS37)

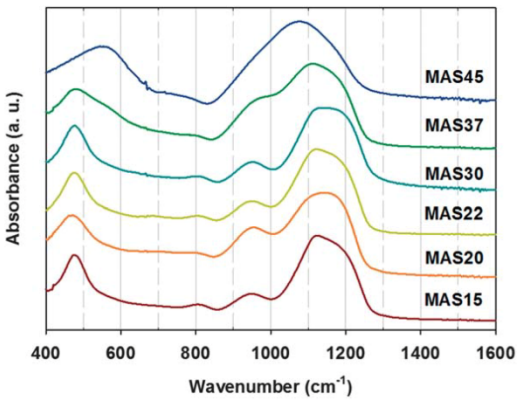

Fig. 3 Infrared absorption spectra of unsubstituted magnesium aluminosilicate glasses.

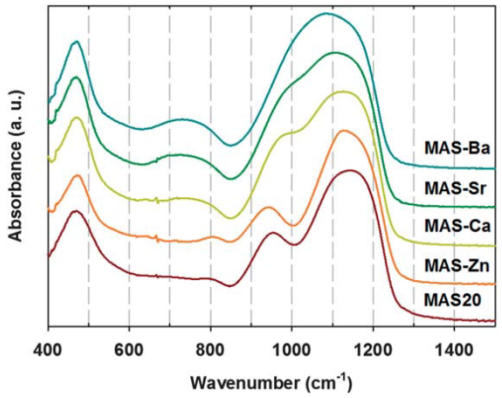

Fig. 4 Infrared absorption spectra of magnesium aluminosilicate glasses substituted with barium, strontium, calcium and zinc oxide in comparison to unsubstituted MAS20 glass.

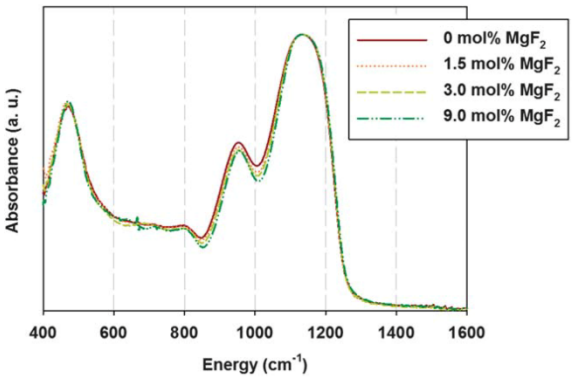

Fig. 5 Effect of MgO substitution by MgF_2 on the infrared absorption spectra of MAS20 glass.

the smaller peak appears as a shoulder of the main peak. Another relatively small peak is observed at about 800 cm^{-1}. In the low energy part of the spectra a strong peak at 480 cm^{-1} appears.

Bell and Dean[6] discussed the MIR spectra of silicates with respect to vibrations of Si–O–Si units. They found three main vibrational bands caused by bridging oxygen at around 1100 cm^{-1} (stretching), at 800 cm^{-1} (bending) and at about 480 cm^{-1} (rocking). Handke and Mozgawa[31] investigated aluminosilicates and distinguished between three structural vibrational units: besides Si–O–Si units, Si–O–Al units which are formed by linkage of $[SiO_4]$ and $[AlO_4]^-$ tetrahedra as well as terminating Si–O^- groups generated by breaking the Si–O–Si units by the introduction of network modifiers are considered. The possibility to distinguish between Si–O–Si and Si–O–Al bands was also discussed by Mozgawa.[32,33] In summary, the broad peak at about 1050–1150 cm^{-1} can be attributed to vibrations of two types of oxygen bridges, Si–O–Si and Si–O–Al. According to Lee and van Deventer,[34] there are two asymmetric stretching bands due to Si–O–(Si, Al) units at 1115–1140 and 1077 cm^{-1}. Additionally, another band due to asymmetric stretching of Si–O–Si units occurs at 1165 cm^{-1}. The band at 950 cm^{-1} is assigned to the stretching vibration of terminal Si–O^- groups, the weak band at about 800 cm^{-1} is attributed to the symmetric vibration of Si–O–Si units and the strong peak at 480 cm^{-1} to the rocking motion of oxygen in both Si–O–Si and Si–O–Al units.[34] In some glasses (*e.g.* MAS-Ba), a relatively broad but mostly very weak peak at around 730 cm^{-1} appears. According to Tarte, this peak is due to Al–O stretching modes of $[AlO_4]^-$ groups.[35]

3.5.1 Unsubstituted MAS glasses. Fig. 3 shows the FTIR spectra of unsubstituted MAS glasses. Most obvious is the effect of the MgO concentration on the intensity of the asymmetric stretching bands of Si–O–(Si, Al) and Si–O^- units at wavenumbers between 1000 and 1300 cm^{-1}. The peak is shifted to lower wavenumbers with increasing network modifier concentration (Mg^{2+}). This effect is most pronounced for glasses with high MgO concentration (*e.g.* MAS45). Here, the Mg^{2+} ions do not only compensate the charge of the $[AlO_4]^-$ tetrahedra but additionally break up the Si–O–(Si, Al) bonds and create non-bridging oxygen sites. This results in increasing concentrations of the Q3, Q2 and Q1 structural units and therefore in a shift of the asymmetric Si–O–(Si, Al) vibrational peak to lower energies. Accordingly the intensity of the band at 950 cm^{-1} which is attributed to the vibrational mode of terminal Si–O^- increases. Nevertheless, the high energy mode of Si–O–Si bonds in Q4 at around 1150 to 1250 cm^{-1} still persists, since the magnesium concentration is not high enough to break up all Si–O–(Si, Al) bonds. Hence, the maximum phonon energy does not decrease. Also the peak of the rocking modes of Si–O–Si and Si–O–Al units at 480 cm^{-1} is shifted towards higher wavelengths with higher magnesium concentrations. This shift is reported by many authors within various glass systems with increasing concentration of different alkaline and alkaline earth oxides. The controversial discussion on the origin of this peak is summarized by McMillan.[36]

3.5.2 Glasses in which MgO is partially substituted by other alkaline earth metals or zinc oxide. In Fig. 4 the effect of network modifier substitution on the FTIR spectra of MAS glasses is shown. Half of the magnesium oxide concentration in the MAS20 glass is replaced by alkaline earth metal oxides of higher atomic weight or by zinc oxide. The substitution of magnesium by zinc hardly affects the FTIR spectra. By contrast, the substitution of Mg^{2+} by Ca^{2+}, Sr^{2+} or Ba^{2+} in the MAS20 glass results in a shift of the asymmetric Si–O–(Si, Al) stretching modes to smaller wavenumbers. Here the shift is obviously more pronounced for ions with higher atomic weight. Zn^{2+}, on the other hand, has a similar cation field strength (5.56) to Mg^{2+} (5.95) and therefore the spectra of the zinc substituted glass do not differ much from those of the unsubstituted glass. The substitution with different network modifiers does not affect the maximum phonon energy.

3.5.3 Effect of fluorine substitution. As shown in Fig. 5, the introduction of fluorine hardly affects the FTIR spectra of the glasses. The spectra of the fluorine substituted glasses are almost the same as for the MAS20 base glass.

Fig. 6 shows the IR absorption spectra of the fluorine substituted glasses in comparison to the unsubstituted MAS20 glass in the range between 2000 and 4000 cm^{-1}. Here broad vibrational bands due to OH^- groups incorporated into the glass network can be seen at wavenumbers in the range from 3000 to 3820 cm^{-1}.[37] With increasing fluorine concentration, the intensity of this band decreases. Harder and Geißler[38] determine the OH^- concentration in glasses by the two-band method of Scholze.[39] Using the stated wavelength-dependent extinction coefficients of OH^- groups $\varepsilon^{3500} = 76$ L mol^{-1} cm^{-1} and $\varepsilon^{2800} = 164$ L mol^{-1} cm^{-1} together with the determined absorption coefficients α^{3500} and α^{2800} at wavenumbers of 3500 and 2800 cm^{-1}, respectively, the OH^- concentration can be calculated using the following equation:

$$c = \frac{\alpha^{3500}}{\varepsilon^{3500}} + \frac{4}{3}\frac{\alpha^{2800}}{\varepsilon^{2800}}$$

Without adding fluoride, the determined OH^- concentration is about 0.09×10^{20} cm^{-3} in all glasses, whereas with increasing fluorine concentration, the OH^- concentration decreases to 0.04×10^{20} cm^{-3}. The concentration of incorporated OH^-

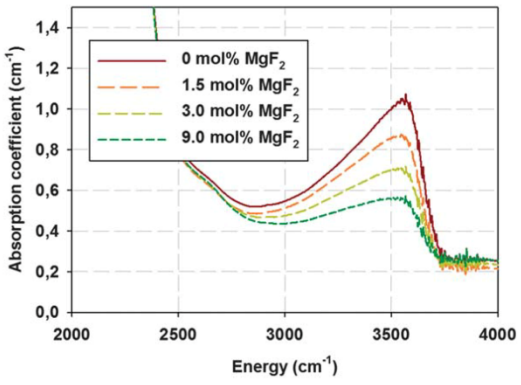

Fig. 6 Infrared absorption spectra in the range of the stretching vibration of OH^- groups for MAS20 glasses. MgO was increasingly substituted by MgF_2.

View Article Online
Journal of Materials Chemistry C Paper

decreases because volatile fluoric acid is formed by the reaction of fluorides with water. However, the concentration of OH^- groups in glasses without fluorine substitution is about one order of magnitude smaller than the samarium concentration.

3.6 Fluorescence investigations

3.6.1 Static fluorescence spectroscopy. Fig. 7 shows the excitation and emission spectra of Sm^{3+} doped unsubstituted MAS glasses. Sm^{3+}, as most trivalent rare-earth ions, is characterized by a partially filled 4f shell which is shielded by $5s^2$ and $5p^6$ electrons located further outside. Hence, the positions of all energy levels and therefore the peak positions of all transitions are hardly affected by changes in the local surrounding of the Sm^{3+} ions. Nevertheless, in comparison to crystals or aqueous solutions, the energy levels of trivalent rare earth ions (and therefore also their fluorescence lines) are somewhat broadened in glasses due to the comparatively irregular glass structure. However, the individual transitions can well be resolved. All transitions observed in Fig. 7 are intra-configurational f–f transitions.

The excitation spectrum (left part of Fig. 7) consists of numerous bands centered at 344, 361, 374, 389, 403, 416, 422, 438, 448, 461, 476, 488 and 502 nm. They can be assigned to the ground state absorption of the $^4K_{17/2}$, $^4D_{3/2}$, $^6P_{7/2}$, $^4L_{15/2}$, $^6P_{3/2}$, $^6P_{5/2}$, $^4G_{9/2}$, $^4M_{17/2}$, $^4F_{5/2}$, $^4I_{13/2}$, $^4I_{11/2}$, $^4M_{15/2}$ and $^4I_{9/2}$ levels, respectively.[40] In order to measure the emission spectra, the prominent excitation peak at 403 nm has been used. The emission spectra exhibit four transitions which can be assigned to $^4G_{5/2} \rightarrow {}^6H_{5/2}$ (563 nm), $^4G_{5/2} \rightarrow {}^6H_{7/2}$ (598 nm), $^4G_{5/2} \rightarrow {}^6H_{9/2}$ (645 nm) and $^4G_{5/2} \rightarrow {}^6H_{11/2}$ (706 nm). All lines are split into at least two components which account for the broadening of the transitions. Since all these transitions are in the yellow to red range of the visible electromagnetic spectrum the fluorescence appears orange to the human eye.

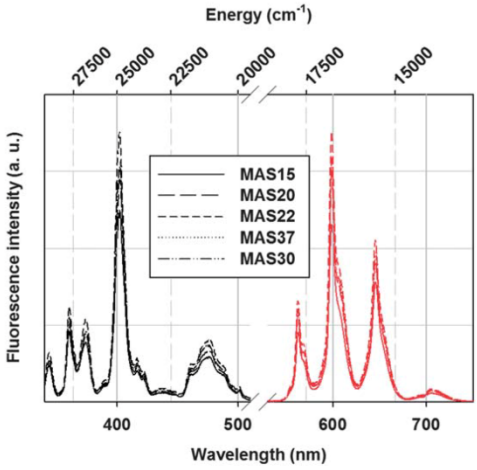

Fig. 7 Fluorescence excitation (λ_{em} = 598 nm) and emission (λ_{ex} = 400 nm) spectra of MAS15, MAS20, MAS22, MAS37 and MAS30 glass samples doped with 1×10^{20} Sm^{3+} cm^{-3}.

In Fig. 8 the normalized emission spectrum of MAS20 is compared to the spectra of a fluoroaluminate glass with 20 mol% strontium phosphate (FP20) and a pure phosphate glass (P100) which were investigated by Herrmann and Ehrt.[41] The peaks of the MAS20 spectrum are broader due to the strong crystal field and the high optical basicity around the Sm^{3+} ions. Furthermore all peaks of the MAS20 spectrum are shifted by 2 nm to higher wavelengths. Both effects are beneficial for the generation of ultrashort laser pulses by the technique of chirped pulse amplification in Ytterbium doped laser glasses.

3.6.2 Dynamic fluorescence spectroscopy. Fig. 9–11 show the fluorescence decay curves for samarium doped unsubstituted and substituted MAS-glasses. In order to facilitate a comparison, all curves have been normalized. The concentration of Sm^{3+} is kept constant at 1×10^{20} cm^{-3} for all studied glass compositions. After excitation by a high power LED pulse at 395 nm, the fluorescence intensity drops with distinct characteristics. In semi-logarithmically scaled diagrams, the slope

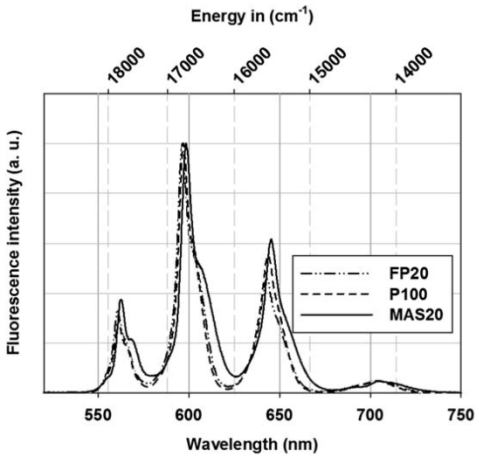

Fig. 8 Normalized fluorescence emission (λ_{ex} = 400 nm) spectra of FP20 (fluoride phosphate), P100 (phosphate) and MAS20 glass samples doped with 1×10^{20} Sm^{3+} cm^{-3}.

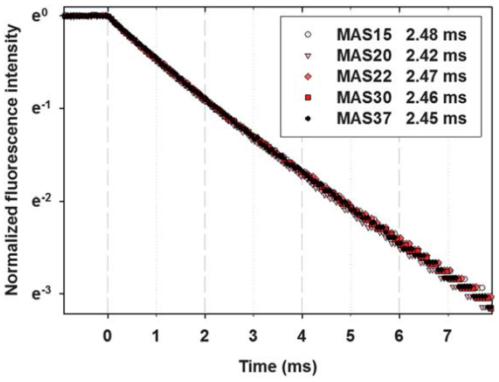

Fig. 9 Normalized fluorescence decay curves and fluorescence lifetimes at 599 nm for unsubstituted magnesium aluminosilicate glasses doped with 1×10^{20} Sm^{3+} cm^{-3}.

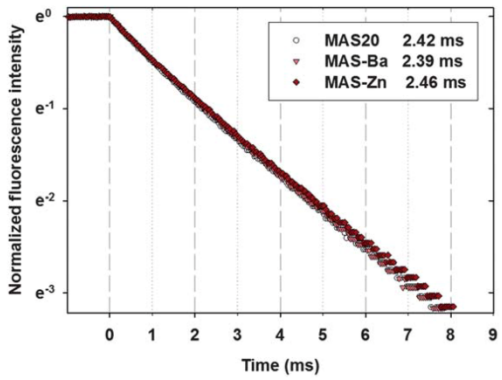

Fig. 10 Normalized fluorescence decay curves and fluorescence lifetimes at 599 nm for Ba-/Zn-substituted magnesium aluminosilicate glasses compared to the unsubstituted MAS20 glass doped with 1×10^{20} Sm^{3+} cm^{-3}.

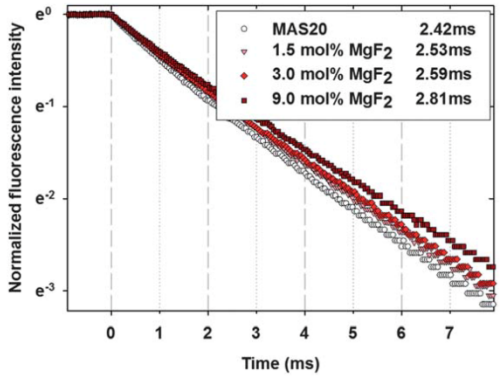

Fig. 11 Normalized fluorescence decay curves and fluorescence lifetimes at 599 nm for magnesium aluminosilicate glasses with increasing substitution of MgO by MgF_2 doped with 1×10^{20} Sm^{3+} cm^{-3}.

of this decay directly represents the (inverse) fluorescence lifetime. A linear gradient represents mono-exponential decay characteristics, *i.e.* the fluorescence is not perturbed by any other deactivation process such as *e.g.* non-radiative energy transfer.

Fig. 9 shows decay curves for non-substituted MAS glasses. Since all curves show approximately the same decay, it can be stated that within the ternary MAS system, the glass composition hardly affects the dynamic fluorescence behavior of the Sm^{3+} ions. The determined lifetimes of all ternary MAS glasses are about 2.4 ms. The almost mono-exponential decay characteristic shows that competing energy transfer hardly occurs. The slight bending of the decay curves is most likely caused by cross-relaxation processes between excited and non-excited Sm^{3+} ions.[41] In contrast to the expectations, lower medium phonon energies do not result in any notable increase of the fluorescence lifetimes.

The partially substituted glasses also show only marginal variations in their fluorescence decays (Fig. 10). Here, within the detection limit a notably advantageous effect of Mg^{2+} substitution by ions with higher atomic number (Ba^{2+} and Zn^{2+} in this case) on the fluorescence lifetime was not observed. Again, the lower medium phonon energies observed for the MAS-Ba glass (Fig. 4) do not affect the dynamic fluorescence behavior.

By contrast, the partial substitution of MgO by MgF_2 leads to pronounced changes in the dynamic fluorescence behavior of the Sm^{3+} ions (Fig. 11), although the phonon spectra of the MAS-F glasses did not show any changes in comparison to the MAS20 base glass (Fig. 5). Nevertheless, the fluorescence lifetime clearly increases with increasing fluoride concentration. For the glass with a MgF_2 concentration of 9 mol%, the fluorescence lifetime of Sm^{3+} is increased by almost 14% (from 2.4 to 2.8 ms). At the same time, the glass transition temperature and the coefficient of thermal expansion decreased, while no negative effect on the glass quality was observed. These increased fluorescence lifetimes are in the same range as for the values found for Sm^{3+}-doped phosphate glasses.[41] The reason for the lifetime improvement might be the coordination of the Sm^{3+} ions with Al–F groups that are formed by the introduction of MgF_2 into the glass network.[7,8]

4 Conclusion

For the magnesium aluminosilicate (MAS) glasses which have been studied here, the following conclusions can be drawn. In non-substituted MAS glasses, the MgO concentration and the MgO/Al_2O_3 ratio control the glass network connectivity as shown by FTIR spectroscopy. Higher molar surplus of MgO reduces the network connectivity by forming non-bridging oxygen sites. Nevertheless, the maximum phonon energy is not affected by the MgO concentration and the fluorescence lifetimes of Sm^{3+}-doped unsubstituted MAS glasses are the same within the limits of error. On the other hand, the coefficient of thermal expansion rises with increasing MgO concentration. Equimolar substitution of magnesium oxide by calcium, strontium or barium oxide results in increasing coefficients of thermal expansion and increasing glass transition temperatures due to the higher binding strengths of these network modifier ions. The zinc magnesium aluminosilicate glass exhibits a lower thermal expansion coefficient and a lower glass transition temperature than the unsubstituted base glass. The maximum phonon energy and fluorescence lifetime of samarium ions are not affected by these substitutions. Partial equimolar substitution of magnesium oxide for magnesium fluoride results in a slight increase of the thermal expansion coefficient and a strong decrease of the glass transition temperature with increasing MgF_2 concentration. Surprisingly, an increase of the concentration of up to 9 mol% MgF_2 results in a reduction of the thermal expansion coefficient (sample MAS-F9). The low OH^- content of the fluorine-free MAS glasses could be further decreased by the fluorine substitution. Although the maximum phonon energy is not affected by the fluorine substitution, the fluorescence lifetime of Sm^{3+} is clearly increased by increasing MgF_2 concentration.

Substitution of MgO by ZnO as well as by MgF_2 results in improved thermo-mechanical and glass processing properties

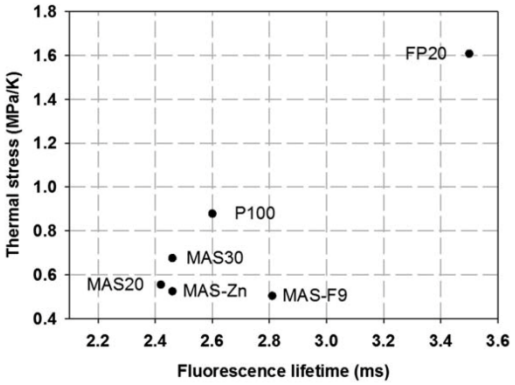

Fig. 12 Thermal stress values *versus* fluorescence lifetime of selected magnesium aluminosilicate glasses, a phosphate glass (P100) and a fluoride phosphate glass (FP20) doped with 1×10^{20} Sm^{3+} cm^{-3}.

of magnesium aluminosilicate glasses. MgF_2 additionally leads to a notable increase of the fluorescence lifetimes of these glasses. The prepared glasses show small coefficients of thermal expansion and relatively broad emission spectra. In Fig. 12 the thermo-mechanical and fluorescence properties of selected MAS glasses, a pure phosphate glass (P100) and a fluoride phosphate glass (FP20) are summarized. It shows the thermal stress values *versus* the fluorescence lifetime of samarium doped glass samples. The figure clearly shows that MAS glasses in general have low thermal stress values while fluorescence lifetimes in the range of pure phosphate glasses can be achieved. Fluoride phosphate glasses on the other hand show very high fluorescence lifetimes but poor thermo-mechanical properties. Hence a magnesium aluminofluoride silicate glass could be a promising laser material especially with respect to ultra-high power systems or applications with high repetition rates.

Acknowledgements

This work was supported by the European Social Fund (ESF) through the Thuringian Ministry of Economy, Employment and Technology (project number 2011 FGR 0122).

References

1 E. Snitzer, *Phys. Rev. Lett.*, 1961, **7**, 444–446.
2 J. H. Campbell, J. S. Hayden and A. Marker, *Int. J. Appl. Glass Sci.*, 2011, **2**, 3–29.
3 J. Hein, S. Podleska, M. Siebold, M. Hellwing, R. Bödefeld, R. Sauerbrey, D. Ehrt and W. Wintzer, *Appl. Phys. B: Lasers Opt.*, 2004, **79**, 419–422.
4 S. Paoloni, J. Hein, T. Töpfer, H. G. Walther, R. Sauerbrey, D. Ehrt and W. Wintzer, *Appl. Phys. B: Lasers Opt.*, 2004, **78**, 415–419.
5 J. F. Philipps, T. Töpfer, H. Ebendorff-Heidepriem, D. Ehrt and R. Sauerbrey, *Appl. Phys. B: Lasers Opt.*, 2001, **72**, 399–405.
6 R. J. Bell and P. Dean, *Discuss. Faraday Soc.*, 1970, **50**, 55.
7 C. Bocker, F. Muñoz, A. Durán and C. Rüssel, *J. Solid State Chem.*, 2011, **184**, 405–410.
8 A. de Pablos-Martín, G. C. Mather, F. Muñoz, S. Bhattacharyya, T. Höche, J. R. Jinschek, T. Heil, A. Durán and M. J. Pascual, *J. Non-Cryst. Solids*, 2010, **356**, 3071–3079.
9 J. H. Campbell and T. I. Suratwala, *J. Non-Cryst. Solids*, 2000, **263–264**, 318–341.
10 H. Weber, J. S. Hayden, D. L. Sapak and H. J. Hoffmann, *Proc. SPIE*, 1989, **1021**, 36–41.
11 S. Sen, R. Rakhmatullin, R. Gubaidullin and A. Pöppl, *Phys. Rev. B: Condens. Matter Mater. Phys.*, 2006, **74**, 100201.
12 Y. Fujimoto and M. Nakatsuka, *J. Non-Cryst. Solids*, 1997, **215**, 182–191.
13 Y. Fujimoto, H. Yoshida, M. Nakatsuka, T. Ueda and A. Fujinoki, *Jpn. J. Appl. Phys.*, 2005, **44**, 1764–1770.
14 T. Sato, Y. Fujimoto, T. Ueda, A. Fujinoki, H. Okada, H. Yoshida, K. Sumimura and M. Nakatsuka, *Jpn. J. Appl. Phys.*, 2006, **45**, 6936–6939.
15 S. M. Logvinkov, G. D. Semchenko and D. A. Kobyzeva, *Refractories*, 1996, **37**, 378–381.
16 P. Wange, T. Höche, C. Rüssel and J. Dieter Schnapp, *J. Non-Cryst. Solids*, 2002, **298**, 137–145.
17 M. Dittmer, M. Müller and C. Rüssel, *Mater. Chem. Phys.*, 2010, **124**, 1083–1088.
18 M. Reben and H. Li, *Int. J. Appl. Glass Sci.*, 2011, **2**, 96–107.
19 A. Hunger, G. Carl, A. Gebhardt and C. Rüssel, *Mater. Chem. Phys.*, 2010, **122**, 502–506.
20 M. Dittmer and C. Russel, *J. Biomed. Mater. Res., Part B*, 2011, 463–470.
21 G. Leturcq, G. Berger, T. Advocat, C. Fillet, C. Halgand and E. Vernaz, *MRS Proceedings*, 2011, vol. 506.
22 T. Izumitani, M. Matsukawa and H. Miyade, *NIST Spec. Publ.*, 1988, **756**, 29–34.
23 M. Dittmer, C. F. Yamamoto, C. Bocker and C. Rüssel, *Solid State Sci.*, 2011, **13**, 2146–2153.
24 A. Hunger, G. Carl, A. Gebhardt and C. Rüssel, *J. Non-Cryst. Solids*, 2008, **354**, 5402–5407.
25 A. Hunger, G. Carl and C. Rüssel, *Solid State Sci.*, 2010, **12**, 1570–1574.
26 D. P. H. Hasselman, *Ceramurgia Int.*, 1978, **4**, 147–150.
27 D. Möncke and D. Ehrt, *Phys. Chem. Glasses*, 2005, **46**, 67–71.
28 H. Scholze, *Glass – Nature, Structure, and Properties*, Springer New York, New York, 1991.
29 S. Toyoda, S. Fujino and K. Morinaga, *J. Non-Cryst. Solids*, 2003, **321**, 169–174.
30 K. Greene, M. J. Pomeroy, S. Hampshire and R. Hill, *J. Non-Cryst. Solids*, 2003, **325**, 193–205.
31 M. Handke and W. Mozgawa, *Vib. Spectrosc.*, 1993, **5**, 75–84.
32 W. Mozgawa, M. Handke and W. Jastrzębski, *J. Mol. Struct.*, 2004, **704**, 247–257.
33 W. Mozgawa, W. Jastrzębski and M. Handke, *J. Mol. Struct.*, 2005, **744–747**, 663–670.
34 W. K. W. Lee and J. S. J. van Deventer, *Langmuir*, 2003, **19**, 8726–8734.
35 P. Tarte, *Spectrochim. Acta, Part A*, 1967, **23**, 2127–2143.
36 P. Mcmillan, *Am. Mineral.*, 1984, **69**, 622–644.

37 N. Kuzuu, Y. Kokubo, T. Nishimura, I. Serizawa, L.-H. Zeng, K. Fujii, M. Yamaguchi, K. Saito and A. J. Ikushima, *J. Non-Cryst. Solids*, 2004, **333**, 115–123.
38 U. Harder and H. Geißler, *Fresenius' J. Anal. Chem.*, 1998, **361**, 585–586.
39 H. Scholze, *Glastech. Ber.*, 1959, **32**, 81–88.
40 C. Srinivasa Rao and C. K. Jayasankar, *Opt. Commun.*, 2013, **286**, 204–210.
41 A. Herrmann and D. Ehrt, *J. Non-Cryst. Solids*, 2008, **354**, 916–926.

5.2. [MT2] Structure and fluorescence properties of ternary aluminosilicate glasses doped with samarium and europium

Andreas Herrmann, Stefan Kuhn, Mirko Tiegel, Christian Rüssel, Jörg Körner, Diethard Klöpfel, Joachim Hein, Malte C. Kaluza

Journal of Materials Chemistry C, 2 (2014) 4328-4337, DOI: 10.1039/C4TC00036F

	Dr. Andreas Herrmann	Stefan Kuhn	Mirko Tiegel	Prof. Dr. Christian Rüssel	Dr. Jörg Körner	Diethard Klöpfel	Dr. Joachim Hein	Prof. Dr. Malte C. Kaluza
Konzeption des Forschungsansatzes	☒	☒	☒	☒	☒	☒	☒	☒
Planung der Untersuchungen	☒	☒	☒	☐	☐	☐	☐	☐
Datenerhebung	☒	☒	☒	☐	☐	☐	☐	☐
Datenanalyse und -interpretation	☒	☒	☒	☐	☐	☐	☐	☐
Schreiben des Manuskripts	☒	☒	☒	☒	☐	☐	☒	☒
Vorschlag Anrechnung Publikationsäquivalente			0,75					

Journal of Materials Chemistry C

PAPER

View Article Online
View Journal | View Issue

Cite this: J. Mater. Chem. C, 2014, 2, 4328

Structure and fluorescence properties of ternary aluminosilicate glasses doped with samarium and europium

Andreas Herrmann,*[a] Stefan Kuhn,[a] Mirko Tiegel,[a] Christian Rüssel,[a] Jörg Körner,[b] Diethard Klöpfel,[b] Joachim Hein[bc] and Malte C. Kaluza[bc]

Received 7th January 2014
Accepted 2nd March 2014

DOI: 10.1039/c4tc00036f

www.rsc.org/MaterialsC

Various ternary aluminosilicate glasses with the molar compositions 20 Al_2O_3–60 SiO_2–20 R_2O (R = Li or Na), 20 Al_2O_3–60 SiO_2–20 RO (R = Mg, Ca or Zn) and 23.1 Al_2O_3–69.2 SiO_2–7.7 R_2O_3 (R = Y or La) doped with 1×10^{20} Sm^{3+} cm^{-3} or 1×10^{20} Eu^{3+} cm^{-3} (about 0.2 mol% Sm_2O_3 or Eu_2O_3) were prepared. The glasses were studied with respect to their molecular structure, and their thermo-mechanical and fluorescence properties. All glasses show relatively broad fluorescence excitation and only a weak effect of the glass composition on the emission spectra is observed. Although the glasses should be structurally very similar, huge differences are found in the coefficients of thermal expansion and the glass transition temperatures. The fluorescence lifetime increases steadily with decreasing mean atomic weight and decreasing refractive index of the glasses, which may be explained by local field effects. The only exception from this rule is the zinc aluminosilicate glass, which shows a relatively high fluorescence lifetime. The highest fluorescence lifetime is found for the lithium aluminosilicate glass. The lowest coefficients of thermal expansion are found for zinc- and magnesium aluminosilicate glasses. A low coefficient of thermal expansion is a prerequisite for a high thermal shock resistance of the material and hence favorable for high-power laser applications.

Introduction

Most glass-based laser amplifiers produced nowadays are realized using silica glass doped with ytterbium, neodymium or erbium oxides. The solubilities of these rare earth oxides in silica glass are comparably small, resulting in clustering of the rare earth ions at relatively low doping concentrations, which strongly decreases the fluorescence parameters such as the fluorescence lifetime of the dopants and the overall quantum efficiency. Therefore laser amplifiers based on silica glass are most commonly used in the form of optical fibers. Here the low rare earth doping concentrations can be compensated by increasing the interaction length *i.e.* the length of the fibers. Nevertheless, for ultra high-power laser applications, where laser pulses with peak powers of terawatt or even petawatt are generated, fiber amplifiers cannot be used since the necessary energy density and intensity in the comparatively small fiber core would exceed the destruction limit by many orders of magnitudes. Furthermore, non-linear effects such as self-phase modulation or self-focussing strongly deteriorate the temporal and spatial distribution of the light pulses which renders most high-power applications impossible.[1] Therefore, bulk glass amplifiers with larger rare earth oxide concentrations are necessary. This, however, cannot be achieved using pure SiO_2 as the host material. Although the solubility of rare earth ions in silica glass can be substantially improved by aluminium codoping,[2,3] a large scale production of rare earth–Al_2O_3 co-doped SiO_2 bulk glass is very cost intensive due to the sophisticated production methods and very high melting temperature.

The amplifier materials used until now in high-power bulk lasers are mostly ytterbium doped phosphate glasses,[4] fluoride phosphate glasses[5,6] or ytterbium doped calcium fluoride single crystals.[7,8] The optical properties of these materials are exceptionally good, *i.e.* they show high fluorescence lifetimes and broad emission spectra[6,9] enabling direct diode pumping and the amplification of sub-ps laser pulses. However, when used in amplification stages where joule-class laser pulses are to be generated, micro-cracks are likely to be formed in the glass, which increase light scattering and finally lead to a complete collapse of the laser operation or – after a further growth of these cracks – a destruction of the material. The cause of this crack generation most likely is the high thermo-mechanical stress that is induced by the intense laser irradiation in conjunction with the high coefficients of thermal expansion, CTE, of these materials.[10] The latter are as large as 15×10^{-6} K^{-1} for fluoride phosphate glasses,[11] around 20×10^{-6} K^{-1} for

[a]Otto-Schott-Institut, Jena University, Fraunhoferstraße 6, 07743 Jena, Germany. E-mail: andreas.herrmann@uni-jena.de
[b]Institute of Optics and Quantum Electronics, Jena University, Max-Wien-Platz 1, 07743 Jena, Germany
[c]Helmholtz Institute Jena, Fröbelstieg 3, 07743 Jena, Germany

CaF_2 (ref. 12) and larger than 12×10^{-6} K^{-1} for phosphate glasses.[4] Furthermore the CTE strongly increases with increasing temperature.

Usually, the thermal shock behaviour of materials is described empirically using an appropriate figure-of-merit. In the literature, different figures-of-merit have been used (for a comparison see *e.g.* Hasselman[13]). In most of these formulae, the coefficient of thermal expansion is part of the denominator, while the thermal conductivity and the mechanical strength are part of the numerator.

Many borosilicate as well as aluminosilicate glasses show comparatively small coefficients of thermal expansion[14–16] and also high Young's moduli and somewhat higher mechanical strengths than phosphate and fluoride phosphate glasses. In certain composition ranges, however, phase separation might occur. Aluminosilicate glasses are widely used as glasses with good mechanical and good thermo-mechanical properties. Especially the $CaO–MgO–Al_2O_3–SiO_2$ system is well studied and is *e.g.* used for high modulus technical fibers which are used for polymer matrix composites. Glasses in the $MgO–(ZnO)–Al_2O_3–SiO_2$ system are used for glass-ceramics with excellent mechanical properties which are *e.g.* suitable as hard disc substrates[17] or as materials in dentistry.[18] Magnesium and zinc aluminosilicates have good glass forming abilities,[14,15] high tensile strengths, high Young's moduli and especially low coefficients of thermal expansion.[19] In addition, aluminosilicate glasses have a high chemical durability, a high solubility for rare earth oxides as well as comparably low OH solubility.[20,21] Thus, aluminosilicate glasses are promising candidates as a laser host material, especially with respect to high-power laser applications. Nevertheless, in the literature the only aluminosilicate glass frequently described as a potential laser host material is the $La_2O_3–Al_2O_3–SiO_2$ system (ref. 22 and references therein).

In this article the effect of the glass composition on the structural, thermo-mechanical and fluorescence properties of rare earth-doped aluminosilicate glasses is described. Li_2O, Na_2O, MgO, ZnO, CaO, Y_2O_3 and La_2O_3 have been used as network modifiers. Sm^{3+} or Eu^{3+} has been used as probing ions since the fluorescence lifetime of Yb^{3+} is difficult to measure because of strong reabsorption effects.

Experimental procedures

The glasses were prepared from high purity raw materials (Fe < 10 ppm, other contaminating metals < 0.5 ppm), SiO_2 (Sipur A1, Schott, Germany), Al_2O_3 (Ceralox, Condea Chemie, Germany), MgO (Merck, Germany), ZnO (Merck, Germany), $CaCO_3$ (Merck, Germany), Na_2CO_3 (Merck, Germany), Li_2CO_3 (Chemapol, Czech Republic), Y_2O_3 (Sigma-Alrich, Germany), $La_2O_3 \cdot H_2O$ (Laborchemie Apolda, Germany), Sm_2O_3 (Ferak, Germany) and Eu_2O_3 (Ferak, Germany). Batches of 100 to 200 g were melted in covered platinum crucibles at temperatures in the range from 1600 to 1650 °C depending on the individual glass composition. Special measures for additional homogenization of the melts have not been applied. After melting for at least 3 hours, the samples were cast into preheated steel moulds and transferred into a muffle furnace, preheated to temperatures in the range from 720 to 920 °C depending on T_g of the glass. Subsequently the cooling furnace was switched off and the samples were allowed to cool down (cooling rate: approximately 3 K min^{-1}).

Table 1 summarizes the chemical compositions of all prepared glasses. The samples were denoted according to their molar chemical composition. Most glasses were doped with samarium using samarium oxide as an additive to the raw materials. Some of the glasses were also prepared with europium doping. The doping concentration of Sm^{3+} or Eu^{3+} was kept constant at 1×10^{20} ions per cm^3 for all glass compositions which corresponds to about 0.2 mol% Sm_2O_3 or Eu_2O_3 depending on the density of the glass.

The glass transition temperatures T_g and the coefficients of thermal expansion CTE were measured using a dilatometer (DIL 402 PC, NETZSCH Gerätebau GmbH, Germany). For that purpose, cylindrical samples with a diameter of 8 mm and a length of about 20 mm had been prepared. The temperature range was 20 to 1000 °C and the heating rate was 5 K min^{-1}. The densities were measured using a helium pycnometer (AccuPyc 1330, Micromeritics GmbH, Germany).

Fluorescence emission spectra were measured using a fluorescence spectrometer (RF-5301PC, SHIMADZU Japan); the samples were polished and had a thickness of 10 mm. Samarium excitation spectra were recorded at an emission wavelength of about 600 nm (615 nm for Eu^{3+}) while emission spectra were obtained using an excitation wavelength of about 400 nm (395 nm for Eu^{3+}) (spectral resolution: 0.2 nm). Fluorescence lifetimes were measured using a home-made experimental setup. For excitation of the glass samples a high intensity pulsed InGaN-diode (LED 395-66-60-110, Roithner Lasertechnik GmbH, Austria) with an emission wavelength of 395 nm was used. The emitted fluorescence light was collected and focused by a lens array onto the entrance slit of a monochromator (H.25, HORIBA Jobin Yvon, France). The spectrum-sliced light is amplified by a photomultiplier tube (R5929, Hamamatsu Photonics K.K., Japan) connected to a digital storage oscilloscope (TDS2012, TEKTRONIX USA). This setup allows for wavelength specific lifetime measurements. Fluorescence lifetimes were measured for the strongest fluorescence transitions ($^4G_{5/2} \rightarrow {}^6H_{7/2}$ of Sm^{3+} at around 600 nm and $^5D_0 \rightarrow {}^7F_2$ of Eu^{3+} at around 615 nm).

Furthermore, Fourier-transformed IR (FTIR) spectra of all samples were recorded using a spectrometer (IRAFFINITY-1, Shimadzu Corp., Japan) with a specular reflectance accessory (SRM-8000A). Reflection spectra were measured on polished glass samples in the wavenumber range from 400 to 2000 cm^{-1}; subsequently the Kramers–Kronig-transformation was applied.

Results and discussion

In Table 1, the as weighted glass compositions are shown. For alkali- and earth alkali aluminosilicate glasses the molar composition is 20% network modifier oxide, 20% Al_2O_3 and 60% SiO_2. The samples are named RAS2020 while R stands for the network modifier ion. To ensure the same network structure for all investigated glasses, those glasses containing Y_2O_3 and La_2O_3 have additionally been prepared with only 6.67 mol%

View Article Online
Journal of Materials Chemistry C Paper

Table 1 Molar compositions, transition temperatures T_g, density, refractive index n_e, coefficients of thermal expansion CTE, fluorescence lifetimes (1×10^{20} Sm^{3+} cm^{-3}) and OH^- absorption coefficients of homogeneous glass samples

Sample name	Composition (mol%) $M_2O/MO/M_2O_3$	Al_2O_3	SiO_2	T_g (°C) ± 3	Density (g cm^{-3}) ± 0.005	n_e ± 0.005	CTE (10^{-6} K^{-1}) ± 0.1	$\tau_{Sm^{3+}}$ (ms) ± 0.03	E_{OH}/d (cm^{-1}) ± 0.05
LiAS2020	Li_2O: 20	20	60	693	2.40	1.531	7.64	2.65	1.27
LiAS1515	Li_2O: 15	15	70	820	2.36	1.521	6.64	2.62	1.06
NaAS2020	Na_2O: 20	20	60	811	2.45	1.507	9.46	2.45	1.37
NaAS1515	Na_2O: 15	15	70	813	2.38	—	7.98	2.56	1.17
MgAS2020	MgO: 20	20	60	827	2.55	1.548	4.06	2.43	0.73
MgAS1515	MgO: 15	15	70	831	2.44	1.520	3.22	2.47	0.37
CaAS2020	CaO: 20	20	60	868	2.61	1.557	5.71	2.37	1.00
CaAS1515	CaO: 15	15	70	876	2.50	—	5.05	2.51	0.85
ZnAS2020	ZnO: 20	20	60	742	2.84	1.573	3.64	2.51	0.99
ZnAS1515	ZnO: 15	15	70	757	2.68	—	3.10	2.47	0.83
YAS0823	Y_2O_3: 7.7	23.1	69.2	899	2.85	1.581	4.31	2.28	1.32
LaAS2020	La_2O_3: 20	20	60	863	4.08	1.709	6.50	2.01	0.76
LaAS1515	La_2O_3: 15	15	70	862	3.57	1.648	5.43	2.12	0.93
LaAS0823	La_2O_3: 7.7	23.1	69.2	875	3.02	1.593	4.43	2.23	0.85

Y_2O_3 and La_2O_3, while keeping the Al_2O_3/SiO_2 ratio constant at 1 : 3. The normalized molar composition of these glasses is 7.7 mol% Y_2O_3/La_2O_3, 23.1 mol% Al_2O_3 and 69.2 mol% SiO_2. These samples are named YAS0823 and LaAS0823 respectively. All prepared glass samples were visually transparent and homogeneous. Furthermore, Table 1 summarizes the glass transition temperatures, T_g, the refractive indices, n_e, the coefficients of linear thermal expansion, CTE, and the densities of all glass compositions. As expected, the density and the refractive index of the glasses increase with increasing atomic weight of the network modifier ion. For laser applications, a high refractive index is likely to be disadvantageous because of increased second order effects[23] which might lead to self-focussing and self-phase modulation which strongly deteriorate the temporal and spatial characteristics of the pulses.[24] The lowest CTE of all investigated glasses are found for the magnesium and the zinc aluminosilicate glasses (4.06 and 3.64 $\times$ 10^{-6} K^{-1}, respectively). The highest CTE are found for the lithium- and sodium aluminosilicate glasses. Low CTE is a prerequisite for a high resistance to thermo-mechanical shock. Glasses of low atomic weight, on the other hand, in general show relatively high thermal conductivity values if glasses of similar structure are discussed.[25] A high thermal conductivity should decrease the thermal stress of the material and therefore is beneficial for high power laser applications. Thermal conductivity is also increased by increasing network connectivity,[25] but for most glasses investigated here, network connectivity should not change much. For that reason thermal conductivity should be similar for most glass compositions that are discussed here. However, there should be a tendency to lower thermal conductivity of glasses of higher atomic weight.

Huge differences were found in the glass transition temperatures. In general, the glass transition temperatures are very high and lie in the range of 693 to 899 °C. The lowest T_g was found for lithium- and zinc-aluminosilicate glasses. This might be advantageous for the glass production because lower melting temperatures are possible. Hence better homogenization of the glasses might be facilitated due to lower viscosities.

The FTIR absorption spectra of all investigated aluminosilicate glasses are shown in Fig. 1. Basically, the spectra can be divided into 3 parts: the high energy part with wavenumbers above 850 cm^{-1}, the low energy part below 600 cm^{-1} and the part of medium energy in between (600 to 850 cm^{-1}).

The high energy part of all spectra is dominated by a high intensity, broad band in the range from 850 to 1250 cm^{-1}. The main peak of this band is located between 1050 and 1200 cm^{-1} and can be attributed to vibrations of two types of oxygen bridges, Si–O–Si and Si–O–Al.[26] According to Lee and Deventer[27] two asymmetric stretching bands due to Si–O–(Si, Al) units are observed at around 1115–1140 and 1080 cm^{-1}. Additionally, another band occurs at around 1165 cm^{-1} due to asymmetric stretching of Si–O–Si units. These bands reflect the "bridging" oxygen atoms (BO) that form the interlinkage of one [SiO_4] group with another [SiO_4] tetrahedron, as well as of a [SiO_4]

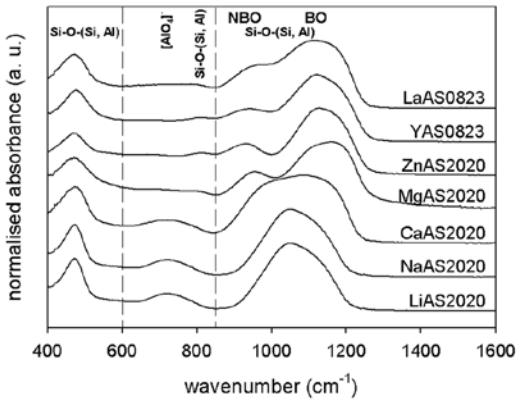

Fig. 1 FTIR absorbance spectra of different ternary aluminosilicate glasses.

tetrahedron with an $[AlO_4]^-$ group. All these $[SiO_4]$ and $[AlO_4]^-$ tetrahedra form the glass network in aluminosilicate glasses. For the occurrence of aluminum in fourfold coordination, *i.e.* as $[AlO_4]^-$ tetrahedra, the compensation of the negative charge is required. This can be achieved by the addition of appropriate quantities of network modifier oxides. Larger concentrations of network modifying oxides can also result in the splitting up of the bridging oxygen Si–O–(Si, Al) bonds and hence in the formation of non-bridging oxygen (NBO). In the IR spectra, the stretching vibrations of these terminating Si–O^- groups are attributed to the peak at around 950 cm^{-1}.[26] Hence, the intensity of this peak directly reflects the breaking of the network forming Si–O–(Si, Al) bonds. Furthermore, the formation of NBO sites also affects the position of the BO peak. The vibrational energy of $[SiO_4]$ tetrahedra coordinated with four bridging oxygen atoms is higher than those of $[SiO_4]$ groups coordinated with two or three bridging oxygen atoms. Hence, a decreasing network connectivity results in the shift of the BO peak to smaller wavenumbers and therefore in a decrease of the maximum phonon energy.[22] For zinc- and magnesium aluminosilicate glasses, the BO peak can be found at around 1150 cm^{-1} (Fig. 1). It is well separated from the NBO peak at around 950 cm^{-1}. For most other glasses, the BO peak is shifted to lower energies and the NBO peak can only be observed as a shoulder of the broadened BO peak.

In the medium energy range of the spectra in Fig. 1 between 600 and 850 cm^{-1}, mainly symmetric Si–O–(Si, Al) stretching modes are observed. As reported for vitreous silica, the symmetric stretching vibrations of Si–O–Si can be found at around 800 cm^{-1}.[28] In calcium aluminosilicate glasses these vibrations are observed at wave numbers between 770 and 833 cm^{-1}.[29] In rare earth and cerium aluminosilicate glasses the band is reported to occur at 780 cm^{-1} (ref. 30) and at 773 to 792 cm^{-1},[31] respectively. These data fit very well to our observations (see Fig. 1). The Al–O stretching vibrations are observed between 650 and 750 cm^{-1}.[30] Tarte found that vibrations in the range from 900 to 700 cm^{-1} can be attributed to "condensed" $[AlO_4]^-$ tetrahedra in crystalline materials.[32] "Isolated" $[AlO_4]^-$ tetrahedra absorb between 800 and 650 cm^{-1}. However, the spectra in Fig. 1 show a broad but mostly very weak band in this wavenumber range. But Al^{3+} ions can also act as network modifiers. In this case $[AlO_6]^{3-}$ octahedra are formed instead of $[AlO_4]^-$ tetrahedra. For "isolated" and "condensed" $[AlO_6]^{3-}$ octahedra the characteristic vibrational energies are reported to be at around 500 to 680 cm^{-1} and 400 to 530 cm^{-1} respectively.[32] Furthemore, in the low energy part of the spectra in Fig. 1 below 600 cm^{-1} rocking vibrations of Si–O–Si and Si–O–Al units are found.[26] These dominate this wavenumber range. In charge compensated aluminosilicate glasses, that means at network modifier oxide to aluminium oxide ratios of about 1, most of the Al^{3+} ions are found in $[AlO_4]^-$ tetrahedra. Shelby estimates the amount of Al^{3+} ions in $[AlO_6]^{3-}$ octahedra to be less than 10% in such glasses.[33] However, within this wavenumber range all spectra in Fig. 1 show approximately the same shape, and almost no variation between glasses of different compositions is found.

The fluorescence excitation and emission spectra of three samarium doped glass types are shown in Fig. 2 and 3,

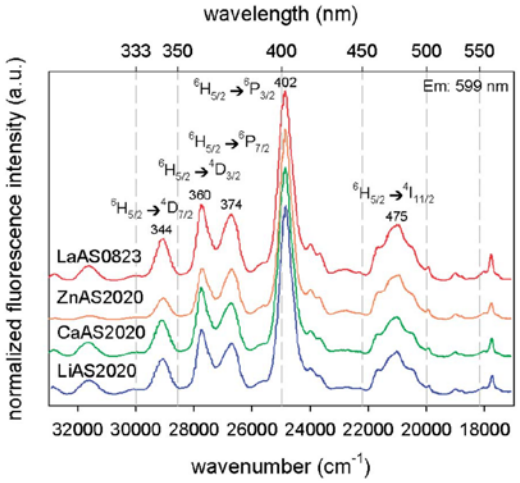

Fig. 2 Sm^{3+} excitation spectra of samples LiAS2020, CaAS2020, ZnAS2020 and LaAS0823 doped with 1×10^{20} Sm^{3+} cm^{-3}. Note that the different spectra have been shifted in vertical direction for clarity.

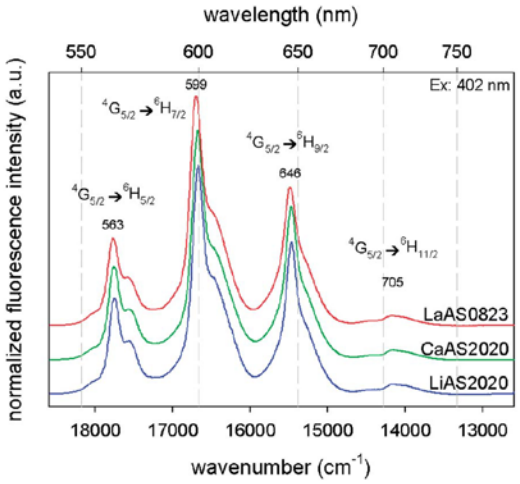

Fig. 3 Sm^{3+} emission spectra of samples LiAS2020, CaAS2020 and LaAS0823 doped with 1×10^{20} Sm^{3+} cm^{-3}. Note that the different spectra have been shifted in vertical direction for clarity.

respectively. For comparison only the lithium-, calcium- and lanthanum aluminosilicate glasses are displayed. All spectra are normalized to their most intense peaks at around 400 nm (excitation) and 600 nm (emission). Furthermore the different spectra are shifted in the vertical direction for clarity. Relatively narrow bands attributed to the f–f-transitions of Sm^{3+} are observed, which are broadened in comparison to the transitions observed in crystals due to the irregular glass structure and the attributed variation in the local sites of the Sm^{3+} ions. In the excitation spectra (Fig. 2) several small and one relatively intense excitation band are present. This intense excitation band is due to the transition of $^6H_{5/2}$ (ground state) to $^6P_{3/2}$ at around 402 nm.[34] In general the excitation spectra of all glasses

View Article Online
Journal of Materials Chemistry C Paper

do not show notable differences. Only for the zinc aluminosilicate glass (ZnAS2020), which is additionally shown in Fig. 2, a decrease in intensity for the transitions below 400 nm is observed in comparison to all other glasses. This effect is due to the broad absorption band of the zinc ions in glasses between 200 and 400 nm, which hinders the excitation of the Sm^{3+} ions in this wavelength range.[35,36]

Fig. 3 shows the typical four fluorescence emission lines of the Sm^{3+} ions. The most intense line at around 600 nm is attributed to the transition $^4G_{5/2} \rightarrow {}^6H_{7/2}$. At 563, 646 and 705 nm, the transitions $^4G_{5/2} \rightarrow {}^6H_{5/2}$, $^4G_{5/2} \rightarrow {}^6H_{9/2}$ and $^4G_{5/2} \rightarrow {}^6H_{11/2}$ are respectively observed.[34,37] The line shapes are hardly affected by compositional variations. A slight but steady shift in the emission spectra to longer wavelengths can be observed with lower atomic weight of the network modifying ion: *e.g.* the highest fluorescence emission peak of LaAS0823 is located at 598 nm while it is observed at 600 nm for the LiAS2020 glass.

Fig. 4 shows the fluorescence decay curves of four Sm^{3+}-doped glass types. After excitation at 395 nm by the high-power LED, fluorescence rises quickly to its maximum value (not shown), which is kept for several milliseconds (normalised fluorescence intensity level at $t < 0$). At $t = 0$, the diode is switched off and the fluorescence intensity of the samples drops with distinct characteristics. Due to the half-logarithmic scale, a mono-exponential decay appears as a straight line. The slope of this line corresponds to the inverse fluorescence lifetime. For all samples an almost mono-exponential decay is observed, which indicates an almost undisturbed fluorescence emission process and homogeneously distributed fluorophores. The slight deviations from mono-exponential decays most likely are due to cross-relaxation processes. For clarity only 4 decay curves are displayed in Fig. 4. The lifetimes vary between 2.2 ms (lanthanum aluminosilicate) and 2.7 ms (lithium aluminosilicate). The fluorescence lifetimes of all glasses are included in Table 1. The fluorescence lifetime decreases steadily with increasing atomic weight of the network modifier ions and therefore also with increasing refractive index of the glasses. The only exception from this rule is, again, the zinc aluminosilicate sample. Its relatively long fluorescence lifetime is only surpassed by the lithium aluminosilicate glass. In general, the same behaviour is also found for Sm^{3+}-doped ternary aluminosilicate glasses of the molar composition 15/15/70 (Table 1). Even lower fluorescence lifetimes were found for glasses with higher lanthanum concentration[22] and tantalum containing aluminosilicate glasses (not shown). According to frequent reports in the literature, the fluorescence lifetime should increase with decreasing phonon energies of the glass network. Hence, it should be assumed that those compositions which show low phonon energies should also show high fluorescence lifetimes. Although Fig. 1 suggests a slightly lower phonon energy for lithium and sodium aluminosilicate glasses in comparison to the other glasses depicted in this figure (peak position and high energy offset of the peak at around 900 to 1300 cm^{-1}), previous detailed studies of magnesium and lanthanum aluminosilicate glasses, however, found no correlation between phonon energy and fluorescence lifetime in Sm^{3+}-doped aluminosilicate glasses.[22,38] For both glass systems the maximum phonon energy could be reduced by increasing the network modifier concentrations. This resulted in a decrease of the fluorescence lifetime in lanthanum aluminosilicate glasses while it did not show a significant effect in the magnesium aluminosilicate glasses. A clear correlation to other parameters of the network modifying ions such as electronegativity, ionic radius or ionization energy can also be ruled out easily by comparing the tabulated data with the measured fluorescence lifetimes. A clear dependency upon the optical basicity of the glass host can also be ruled out, although a general trend to higher lifetimes for low basicity glasses can be observed. Furthermore the OH^- concentrations of all glasses have been measured using IR-spectroscopy (Table 1). In the wavenumber range between 3000 and 3700 cm^{-1} all glasses show low E/d (extinction/thickness) values between 1.4 and 0.4 cm^{-1} which correspond to OH^- concentrations between 1.3 and 0.4×10^{19} cm^{-3} assuming OH^- extinction coefficients to be the same as for soda lime silica glasses.[21,38] The shape of the OH^- absorption band (particularly the high energy offset of the band) also doesn't change for all glasses. A correlation between OH^- concentration and fluorescence lifetime in this concentration range was not found (Table 1). Hehlen *et al.* show that OH^- concentrations in this range have only little influence on the quantum efficiency (and therefore on the fluorescence lifetime) of the $^4I_{13/2}$ level of Er^{3+} in aluminosilicate glasses at relatively low rare earth doping concentrations of around 0.2 mol%.[39] The $^4G_{5/2}$ emission of Sm^{3+} should be even less influenced than the $^4I_{13/2}$ emission of Er^{3+} because of the bigger energy gap to the next lower energy level (around 7400 cm^{-1} and 6500 cm^{-1} respectively[34]). However, all these parameters, especially the ion radius of the network modifier ions and OH^- concentration might have a minor effect on the fluorescence lifetime of the doped rare earth elements. A clear correlation was found for the mean atomic weight of the glass composition and therefore for the mean atomic number of the network modifier ion if glasses of constant molar fractions of the glass components are compared (*e.g.* 20/20/60). Fig. 5 shows the dependency of the Sm^{3+} fluorescence lifetime on the mean atomic weight of ternary aluminosilicate glasses. Data points of

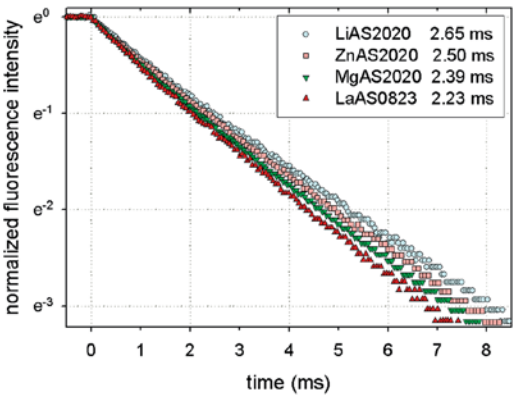

Fig. 4 Fluorescence decay curves of the $4G_{5/2}$ energy level of Sm^{3+} and decay times (inset) for different glass compositions.

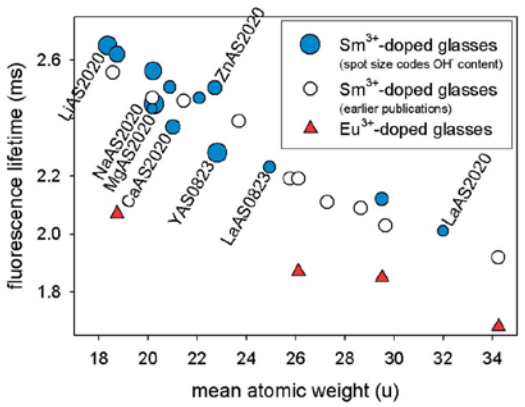

Fig. 5 Fluorescence lifetimes of ternary aluminosilicate glasses doped with 1×10^{20} cm^{-3} Sm^{3+} (circles) and Eu^{3+} (triangles) depending on the mean atomic weight of the glass composition. The filled circles represent the Sm^{3+}-doped samples of this publication. For these, the circle size represents the OH^- concentration of the specific sample.

the glasses reported here are filled, while the additional data (not filled data points) are taken from earlier publications[22,38] and some glasses with a somewhat different molar composition. The systematical error of the lifetime measurements due to sample preparation and experimental setup can be estimated to be less than 2%. The biggest uncertainty is due to cross-relaxation processes and OH^- quenching. While cross-relaxation processes mainly depend on the Sm^{3+} doping concentration which is kept constant and therefore has a consistent influence on all samples, OH^- quenching in this OH^- concentration range causes an error of about 10%.[39] To be able to estimate the influence of OH^- quenching on the measurement, the size of the filled circles represents the OH^- concentration of the specific glass sample. But despite all disturbance, an almost linear dependence of the fluorescence lifetime on the mean atomic weight of the glass composition can be observed. The same dependency was found for Eu^{3+}-doped aluminosilicate glasses which were additionally prepared. These data points (triangles) are also added to the diagram. While the Sm^{3+} measurements might be slightly influenced by OH^- quenching as discussed above, the $^5D_0$ emission of Eu^{3+} should be almost free of any OH^- quenching because of the huge energy gap of around 12 000 cm^{-1}.[45] This can be shown easily by applying the so-called energy-gap law.[39] Also, cross-relaxation processes do not occur for Eu^{3+}-doped materials in this concentration range.[46]

According to Bardez *et al.*, rare earth ions (Nd^{3+} in this case) enter depolymerized regions of the glass matrix (sodium calcium aluminosilicate system in this case).[40] It was shown by extended X-ray absorption fine structure (EXAFS) measurements that sodium and calcium ions are likely to be present in the second coordination shell of the Nd^{3+} ions. A similar behavior of rare earth ions (Er^{3+} and Eu^{3+}) is reported by Du, Cormack and Kokou for binary alkali silicate glasses.[41,42] A very good depiction of such depolymerized regions in alkali silicate glasses can be found in ref. 43. This behavior of rare earth ions could well explain the strong dependence of the fluorescence lifetime on the network modifier, assuming that closely coordinated network modifying ions have a substantial influence on the parameters of the rare earth sites as *e.g.* crystal field strength and symmetry. Unfortunately, the spectra of the Sm^{3+}-doped glasses presented in Fig. 2 and 3 do not show notable variations with the glass composition. For this reason, few Eu^{3+}-doped glasses have additionally been prepared since Eu^{3+} has a hypersensitive transition which is strongly dependent on the local symmetry at the rare earth site.[37,44] Fig. 6 shows fluorescence emission spectra of two Eu^{3+}-doped glasses, a lithium and a lanthanum aluminosilicate glass. Note that the two spectra are shifted vertically for clarity. For excitation, a wavelength of 395 nm was used. Both spectra are normalized to the strongest fluorescence emission line at about 615 nm which is assigned to the transition $^5D_0 \rightarrow {}^7F_2$.[45] This transition is almost entirely electric dipole in nature and therefore sensitive to the local crystal field symmetry.[44] The other peaks are assigned to the transitions $^5D_0 \rightarrow {}^7F_0$ at about 575 nm, $^5D_0 \rightarrow {}^7F_1$ at about 590 nm, $^5D_0 \rightarrow {}^7F_3$ at about 655 nm and $^5D_0 \rightarrow {}^7F_4$ at about 700 nm.[45] The transitions at 575 and 590 nm can hardly be distinguished because of the strong splitting of the 590 nm line. The latter of these two ($^5D_0 \rightarrow {}^7F_1$ at 590 nm) is an almost pure magnetic dipole transition which is not influenced by local site symmetry.[44] Therefore the intensity ratio of the emission peaks at 590 and 615 nm, I_{590}/I_{615}, can be used as a measure of the overall symmetry at the local Eu^{3+} site. A high ratio of I_{590}/I_{615} indicates a high crystal field symmetry and *vice versa*.[44] Unfortunately, a clear differentiation between the intensity ratios of the peaks in the two spectra of Fig. 6 is not possible, although the peak at 590 nm in lanthanum aluminosilicate is slightly higher than that in lithium aluminosilicate which should indicate a slightly higher symmetry in the lanthanum containing glass.[37,44] Nevertheless, because of the relatively low

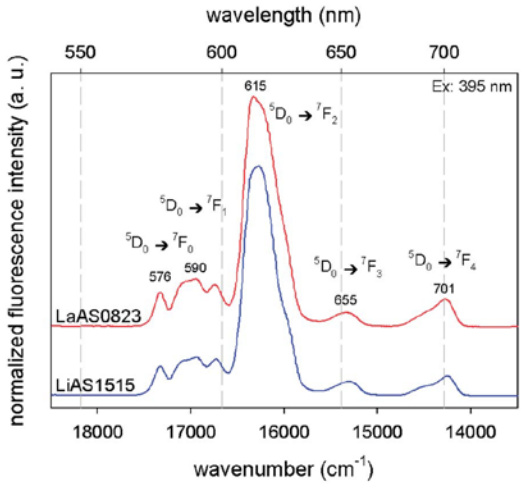

Fig. 6 Eu^{3+} emission spectra of a lithium (LiAS1515) and a lanthanum aluminosilicate glass (LaAS0823) doped with 1×10^{20} Eu^{3+} cm^{-3}. Note that the different spectra have been shifted in the vertical direction for clarity.

View Article Online
Journal of Materials Chemistry C Paper

intensity ratio I_{590}/I_{615} of both glasses (see Fig. 6), it can be stated that the rare earth site symmetry in aluminosilicate glasses is generally very low. This is not surprising since similar observations have been made for other silicate glasses.[46] In contrast to aluminosilicate glasses, fluoride based glasses offer a much higher symmetry at the local Eu^{3+} sites. Here, much higher intensity ratios I_{590}/I_{615} were found.[46] In summary, a clear estimation of individual symmetry or crystal field strength cannot be made for the glasses investigated here. However, Brecher and Riseberg as well as Lochhead and Bray found decreasing fluorescence lifetimes for Eu^{3+} ions at sites with locally increased crystal field by laser-induced fluorescence line narrowing (LFLN) measurements.[47,48] On the other hand it is well known that spontaneous emission can be changed by altering the refractive index of the surrounding dielectric media. Since the first publication of this effect by Purcell[49] many theoretical examples,[50–54] experimental examples (ref. 54 and referenced studies therein) have been published on this topic, although only a few of the experimental works have been performed on glasses so far.[55–57] Among the various theoretical models that predict the dependence of the spontaneous emission rates A^{diel} on the refractive index n of the surrounding dielectric medium are the real-cavity[58] and the virtual-cavity models.[59] In general this dependency can be written as: $A^{diel}(n) = n \times l(n)^2 \times A_0$. Here, A_0 is the vacuum spontaneous emission rate and l is the dielectric local-field correction factor which differs for the various models. For the real-cavity model it is defined as $l(n) = 3n^2/(2n^2 + 1)$ (ref. 58) and for the virtual-cavity model $l(n) = (n^2 + 2)/3$ (ref. 59). Since $n \geq 1$ the spontaneous emission rate is increased (and the lifetime of the excited state is decreased) by the dielectric medium around the emitter with increasing n, and accordingly with increasing interaction of the emitter and the surrounding dielectric medium. Fig. 7 shows the fluorescence lifetimes of Sm^{3+}-doped glasses depending on the measured refractive index n_e of the samples together with the least-square fit of both models. Although both models represent the experimental data about right it is difficult to decide which one fits the data better. As discussed earlier, the fluorescence lifetime of the Sm^{3+}-doped samples is additionally influenced by various effects, most notably OH^- quenching and cross-relaxation processes (slight deviation from mono-exponential fluorescence decay in Fig. 4 (ref. 60)) which distort the relationship between fluorescence lifetime and refractive index for the measurements presented here. Furthermore, the observed fluorescence transition of Sm^{3+} ($^4G_{5/2} \rightarrow {}^6H_{7/2}$) has a notable magnetic dipole contribution and therefore is not entirely electric dipole dominated[61] which is required to apply the two models. Magnetic dipole transitions show a different dependence on the refractive index of the surrounding medium.[50] In analogy to the Sm^{3+}-doped glasses, Fig. 8 shows the fluorescence lifetimes of the Eu^{3+}-doped samples depending on the measured refractive indices. Again, the virtual and real cavity models have been fitted to the data. Here, the real cavity model reproduces the data much better than the virtual cavity model, although the data consist of only 4 samples. Nevertheless, this result is in agreement with previous studies on glasses.[55,56] In contrast to Sm^{3+}, the measured transition of Eu^{3+} ($^5D_0 \rightarrow {}^7F_2$) is much less sensitive to cross-relaxation processes and OH^- quenching.[46] Furthermore, it has an almost entirely electric dipole character.[44]

However, also the theoretical models are based on the variation of the inhomogeneous, time-dependent electromagnetic local field around the emitting atom. Hence, the observations of Brecher and Riseberg as well as Lochhead and Bray[47,48] are not in disagreement with the theoretically derived refractive index-dependency since the average effective field strength is correlated with the density of the surrounding atoms which form the dielectric medium.[53]

Besides their advantageous properties, such as high solubility for rare earth ions, broad excitation and emission spectra of doped rare earth ions, good glass forming ability, low coefficients of thermal expansion and high mechanical strengths, aluminosilicate glasses can also provide relatively long fluorescence lifetimes. Obviously network modifying ions of low

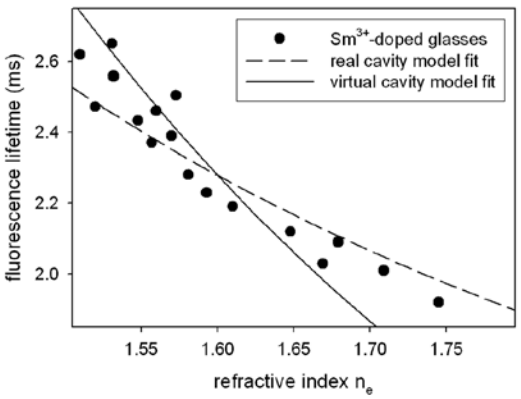

Fig. 7 Fluorescence lifetimes of ternary aluminosilicate glasses doped with 1×10^{20} cm^{-3} Sm^{3+} depending on the refractive index n_e of the glasses. The data have been fitted with the real and virtual cavity models.

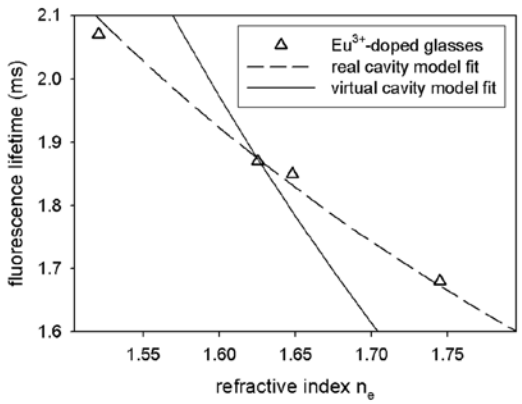

Fig. 8 Fluorescence lifetimes of ternary aluminosilicate glasses doped with 1×10^{20} cm^{-3} Eu^{3+} depending on the refractive index n_e of the glasses. The data have been fitted with the real and virtual cavity models.

atomic weight as well as Zn^{2+} can substantially improve the fluorescence lifetime of doped rare earth ions in this glass system.

Conclusions

Aluminosilicate glasses with the molar compositions 20 Al_2O_3–60 SiO_2–20 R_2O (R = Li or Na), 20 Al_2O_3–60 SiO_2–20 RO (R = Mg, Ca or Zn) and 20 Al_2O_3–73.33 SiO_2–6.67 R_2O_3 (R = Y or La) doped with 1×10^{20} Sm^{3+} cm^{-3} or 1×10^{20} Eu^{3+} cm^{-3} (about 0.2 mol% Sm_2O_3 or Eu_2O_3) were prepared and investigated with respect to their molecular structure and their thermo-mechanical as well as optical properties. The glasses show broad fluorescence excitation and emission spectra that are hardly affected by the glass composition which is a mandatory requirement for chirped pulse laser amplification. Although the glasses should be structurally very similar, significant differences are found in the coefficients of thermal expansion, the glass transition temperatures and the fluorescence lifetimes. The fluorescence lifetime increases steadily with decreasing atomic weight and decreasing refractive index of the glasses. The only exception from this rule is the zinc aluminosilicate glass which shows a longer fluorescence lifetime than the calcium- and magnesium aluminosilicate glasses. Its relatively long fluorescence lifetime is only surpassed by the lithium aluminosilicate glass. The zinc aluminosilicate glass also provides one of the lowest glass transition temperatures which should be beneficial for the production and the optical quality of the glass. Furthermore, it shows the lowest coefficient of thermal expansion of all investigated glasses which is highly advantageous for a high thermal shock resistance. Hence, a zinc aluminosilicate glass could be a promising laser material especially with respect to ultra high-power systems or applications with high repetition rates.

Acknowledgements

This work was supported by the European Social Fund (ESF) through the Thuringian Ministry of Economy, Employment and Technology (project number 2011 FGR 0122).

References

1 J. Limpert, S. Hädrich, J. Rothhardt, M. Krebs, T. Eidam, T. Schreiber and A. Tünnermann, Ultrafast fiber lasers for strong-filed physics experiments, *Laser Photonics Rev.*, 2011, **5**, 634–646.

2 A. J. Kenyon, Recent developments in rare-earth doped materials for optoelectronics, *Prog. Quantum Electron.*, 2002, **26**, 225–284.

3 K. Arai, H. Namikawa, K. Kumata, T. Honda, Y. Ishii and T. Handa, Aluminum or phosphorus co-doping effects on the fluorescence and structural properties of neodymium-doped silica glass, *J. Appl. Phys.*, 1986, **59**, 3430–3436.

4 J. H. Campbell, J. S. Hayden and A. Marker, High-power solid-state lasers: a laser class perspective, *Int. J. Appl. Glass Sci.*, 2011, **2**, 3–29, DOI: 10.1111/j.2041-1294.2011.00044.x.

5 J. Hein, S. Podleska, M. Siebold, M. Hellwing, R. Bödefeld, R. Sauerbrey, D. Ehrt and W. Wintzer, Diode-pumped chirped pulse amplification to the joule level, *Appl. Phys. B: Lasers Opt.*, 2004, **79**, 419–422, DOI: 10.1007/s00340-004-1586-3.

6 D. Ehrt, Fluoroaluminate glasses for lasers and amplifiers, *Curr. Opin. Solid State Mater. Sci.*, 2003, **7**, 135–141.

7 M. Siebold, M. Hornung, R. Bödefeld, S. Podleska, S. Klingebiel, C. Wandt, F. Krausz, S. Karsch, R. Ücker, A. Jochmann, J. Hein and M. C. Kaluza, Terawatt diode-pumped Yb:CaF2 laser, *Opt. Lett.*, 2008, **33**, 2770–2772, DOI: 10.1364/ol.33.002770.

8 J. Körner, C. Vorholt, H. Liebetrau, M. Kahle, D. Klöpfel, R. Seifert, J. Hein and M. C. Kaluza, Measurement of temperature-dependent absorption and emission spectra of Yb:YAG, Yb:LuAG, and Yb:CaF2 between 20 °C and 200 °C and predictions on their influence on laser performance, *J. Opt. Soc. Am. B*, 2012, **29**, 2493–2502, DOI: 10.1364/josab.29.002493.

9 M. Siebold, M. Hornung, S. Bock, J. Hein, M. C. Kaluza, J. Wemans and R. Uecker, Broad-band regenerative laser amplification in ytterbium-doped calcium fluoride (Yb:CaF2), *Appl. Phys. B: Lasers Opt.*, 2007, **89**, 543–547.

10 R. M. Wood, *Laser-induced damage of optical materials*, Institute of Physics Publishing, Bristol and Philadelphia, 2003.

11 D. Möncke, D. Ehrt, L. L. Velli, C. P. E. Versamis and E. I. Kamitsos, Structure and properties of mixed phosphate and fluoride glasses, *Phys. Chem. Glasses*, 2005, **46**, 67–71.

12 S. S. Ballard, S. E. Brown and J. S. Browder, Measurements of thermal-expansion of 6 optical-materials, from room-temperature to 250 degrees C, *Appl. Opt.*, 1978, **17**, 1152–1154, DOI: 10.1364/ao.17.001152.

13 D. P. H. Hasselman, Figures-of-merit for the thermal stress resistance of high-temperature brittle materials: a review, *Ceram. Int.*, 1978, **4**, 147–150.

14 S. M. Logvinkov, G. D. Semchenko and D. A. Kobyzeva, Rearrangement of conodes of the phase diagram of the MgO–Al_2O_3–SiO_2 system and its technological prospects, *CN Refract.*, 1996, **37**, 378–381.

15 D. Ehrt, H. T. Vu, A. Herrmann and G. Voelksch, Luminescent ZnO–Al_2O_3–SiO_2 glasses and glass ceramics, *Adv. Mater. Res.*, 2008, **39-40**, 231–236, DOI: 10.4028/amr.39-40.231.

16 D. Möncke, D. Ehrt, H. Eckert and V. Mertens, Influence of melting and annealing conditions on the structure of borosilicate glasses, *Phys. Chem. Glasses*, 2003, **44**, 113–116.

17 A. Hunger, G. Carl, A. Gebhardt and C. Rüssel, Young's moduli and microhardness of glass–ceramics in the system MgO/Al_2O_3/TiO_2/ZrO_2/SiO_2 containing quartz nanocrystals, *Mater. Chem. Phys.*, 2010, **122**, 502–506, DOI: 10.1016/j.matchemphys.2010.03.034.

18 M. Dittmer and C. Rüssel, Colorless and high strength MgO/Al_2O_3/SiO_2 glass-ceramic dental material using zirconia as nucleating agent, *J. Biomed. Mater. Res., Part B*, 2012, **100B**, 463–470, DOI: 10.1002/jbm.b.31972.

19 M. Dittmer, M. Müller and C. Rüssel, Self-organized nanocrystallinity in $MgO–Al_2O_3–SiO_2$ glasses with ZrO_2 as nucleating agent, *Mater. Chem. Phys.*, 2010, **124**, 1083–1088, DOI: 10.1016/j.matchemphys.2010.08.037.

20 G. Leturcq, G. Berger, T. Advocat, C. Fillet, C. Halgand and E. Vernaz, Chemical durability of aluminosilicate glasses containing low solubility chemical elements, *C-MRS Int. Symp. Proc.*, 1997, **506**, 199, DOI: 10.1557/proc-506-199.

21 H. Scholze, *Glastech. Ber.*, 1959, **32**, 142–152.

22 S. Kuhn, A. Herrmann, J. Hein, M. C. Kaluza and C. Rüssel, Sm^{3+}-Doped $La_2O_3–Al_2O_3–SiO_2$–glasses – structure, fluorescence and thermal expansion, *J. Mater. Sci.*, 2013, **48**, 8014–8022, DOI: 10.1007/s10853-013-7613-1.

23 M. Sheik-Bahae and E. W. Van Stryland, Optical nonlinearities in the transparency region of bulk semiconductors. *Nonlinear Optics in Semiconductors*, 1999, vol. 58, pp. 257–318.

24 T. Töpfer, J. Hein, J. Philipps, D. Ehrt and R. Sauerbrey, Tailoring the nonlinear refractive index of fluoride-phosphate glasses for laser applications, *Appl. Phys. B*, 2000, **71**, 203–206.

25 M. M. Ammar, S. Gharib, M. M. Halawa, K. El Badry, N. A. Ghoneim and H. A. El Batal, Thermal conductivity of some silicate glasses in relation to composition and structure, *J. Non-Cryst. Solids*, 1982, **53**, 165–172, DOI: 10.1016/0022-3093(82)90026-6.

26 M. Handke, W. Mozgawa and M. Nocun, Specific features of the IR spectra of silicate glasses, *J. Mol. Struct.*, 1994, **325**, 129–136.

27 W. K. W. Lee and J. S. J. van Deventer, The use of infrared spectroscopy to study geopolymerization of heterogeneous amorphous aluminosilicates, *Langmuir*, 2003, **19**, 8726–8734, DOI: 10.1021/la026127e.

28 A. Efimov, Quantitative IR spectroscopy: Applications to studying glass structure and properties, *J. Non-Cryst. Solids*, 1996, **203**, 1–11, DOI: 10.1016/0022-3093(96)00327-4.

29 C. Huang and E. Behrman, Structure and properties of calcium aluminosilicate glasses, *J. Non-Cryst. Solids*, 1991, **128**, 310–321, DOI: 10.1016/0022-3093(91)90468-l.

30 J. T. Kohli, R. A. Condrate and J. R. Shelby, Raman and infrared-spectra of rare earth aluminosilicate glasses, *Phys. Chem. Glasses*, 1993, **34**, 81–87.

31 S. Lin, C. Hwang and J. Lee, Characterization of $CeO_2–Al_2O_3–SiO_2$ glasses by infrared and X-ray absorption near edge structure spectroscopies, *J. Mater. Res.*, 1996, **11**, 2641–2650, DOI: 10.1557/jmr.1996.0332.

32 P. Tarte, Infra-red spectra of inorganic aluminates and characteristic vibrational frequencies of AlO_4 tetrahedra and AlO_6 octahedra, *Spectrochim. Acta, Part A*, 1967, **23**, 2127–2143, DOI: 10.1016/0584-8539(67)80100-4.

33 J. E. Shelby, *J. Appl. Phys.*, 1978, **49**, 5885–5891, DOI: 10.1063/1.324553.

34 W. Carnall, P. Fields and K. J. Rajnak, *Chem. Phys.*, 1968, **49**, 4424–4442, DOI: 10.1063/1.1669893.

35 G. Qian, M. Nikl, J. Bei, J. Pejchal, S. Baccaro, R. Giorgi, A. Cecilia and G. Chen, Temperature dependence of photoluminescence in ZnO-containing glasses, *Opt. Mater.*, 2007, **30**, 91–94.

36 G. Chen, M. Nikl, N. Solovieva, A. Beitlerova, J. Rao, Y. Yang, Y. Zhang, X. Jiang and C. Zhu, Photoluminescent properties of nanocrystallized zinc borosilicate glasses, *Radiat. Meas.*, 2004, **38**, 771–774.

37 G. Blasse and B. C. Grabmaier, *Luminescent Materials*, Springer, Berlin and New York, 1994.

38 M. Tiegel, A. Herrmann, C. Rüssel, J. Körner, D. Klöpfel, J. Hein and M. C. Kaluza, Magnesium aluminosilicate glasses as potential laser host material for ultrahigh power laser systems, *J. Mater. Chem. C*, 2013, **1**, 5031–5039, DOI: 10.1039/c3tc30761a.

39 M. P. Hehlen, N. J. Cockroft, T. R. Gosnell and A. J. Bruce, Spectroscopic properties of Er^{3+}- and Yb^{3+}-doped soda-lime silicate and aluminosilicate glasses, *Phys. Rev. B: Condens. Matter Mater. Phys.*, 1997, **56**, 9302–9318.

40 I. Bardez, D. Caurant, P. Loiseau, N. Baffier, J. L. Dussossoy, C. Gervais, F. Ribot and D. R. Neuville, Structural characterisation of rare earth rich glasses for nuclear waste immobilisation, *Phys. Chem. Glasses*, 2005, **46**, 320–329.

41 J. Du and A. N. Cormack, The structure of erbium doped sodium silicate glasses, *J. Non-Cryst. Solids*, 2005, **351**, 2263–2276, DOI: 10.1016/j.jnoncrysol.2005.05.018.

42 L. Kokou and J. Du, Rare earth ion clustering behavior in europium doped silicate glasses: Simulation size and glass structure effect, *J. Non-Cryst. Solids*, 2012, **358**, 3408–3417, DOI: 10.1016/j.jnoncrysol.2012.01.068.

43 B. Vessal, G. N. Greaves, P. T. Marten, A. V. Chadwick, R. Mole and S. Houde-Walter, Cation microsegregation and ionic mobility in mixed alkali glasses, *Nature*, 1992, **356**, 504–506, DOI: 10.1038/356504a0.

44 F. S. Richardson, J. D. Saxe, S. A. Davis and T. R. Faulkner, *Mol. Phys.*, 1981, **42**, 1401–1429.

45 W. Carnall, P. Fields and K. J. Rajnak, *Chem. Phys.*, 1968, **49**, 4450–4455.

46 A. Herrmann, S. Fibikar and D. Ehrt, Time-resolved fluorescence measurements on Eu^{3+}- and Eu^{2+}-doped glasses, *J. Non-Cryst. Solids*, 2009, **355**, 2093–2101.

47 C. Brecher and L. A. Riseberg, Laser-induced fluorescence line narrowing in Eu glass: A spectroscopic analysis of coordination structure, *Phys. Rev. B: Solid State*, 1976, **13**, 81–93.

48 M. J. Lochhead and K. L. Bray, High-pressure fluorescence line narrowing of Eu(III)-doped sodium disilicate glass, *Phys. Rev. B: Condens. Matter Mater. Phys.*, 1995, **52**, 15763–15775.

49 E. M. Purcell, Spontaneous emission probabilities at radio Frequencies, *Phys. Rev.*, 1946, **69**, 674–674, DOI: 10.1103/physrev.69.674.2.

50 R. J. Glauber and M. Lewenstein, Quantum optics of dielectric media, *Phys. Rev. A: At., Mol., Opt. Phys.*, 1991, **43**, 467–491.

51 P. de Vries and A. Lagendijk, Resonant scattering and spontaneous emission in dielectrics: Microscopic derivation of local-field effects, *Phys. Rev. Lett.*, 1998, **81**, 1381–1384.

52 M. E. Crenshaw and C. M. Bowden, Effects of local fields on spontaneous emission in dielectric media, *Phys. Rev. Lett.*, 2000, **85**, 1851–1854, DOI: 10.1103/physrevlett.85.1851.

53 P. R. Berman and P. W. Milonni, Microscopic theory of modified spontaneous emission in a dielectric, *Phys. Rev. Lett.*, 2004, **92**, 0536011–0536014, DOI: 10.1103/physrevlett.92.053601.

54 M. E. Crenshaw, The quantized field in a dielectric and application to the radiative decay of an embedded atom, *Phys. Lett. A*, 2006, **358**, 438–442, DOI: 10.1016/j.physleta.2006.05.049.

55 C.-K. Duan, M. F. Reid and Z. Wang, Local field effects on the radiative lifetime of emitters in sourrounding media: Virtual- or real-cavity model?, *Phys. Lett. A*, 2005, **343**, 474–480, DOI: 10.1016/j.physleta.2005.06.037.

56 G. M. Kumar, D. N. Rao and G. S. Agarwal, Measurement of local field effects of the host on the lifetimes of embedded emitters, *Phys. Rev. Lett.*, 2003, **91**, 2039031–2039034, DOI: 10.1103/physrevlett.91.203903.

57 C.-K. Duan, H. Wen and P. A. Tanner, Local-field effect on the spontaneous radiative emission rate, *Phys. Rev. B: Condens. Matter Mater. Phys.*, 2011, **83**, 2451231–2451235, DOI: 10.1103/physrevb.83.245123.

58 D. Toptygin, Effects of the solvent refractive index and its dispersion on the radiative decay rate and extinction coefficient of a fluorescent solute, *J. Fluoresc.*, 2003, **13**, 201–219.

59 M. Born and E. Wolf, *Principles of Optics*, Cambridge University Press, Cambridge, 1999.

60 A. Herrmann and D. Ehrt, Time-resolved fluorescence measurements on Dy^{3+} and Sm^{3+} doped glasses, *J. Non-Cryst. Solids*, 2008, **354**, 916–926.

61 P. S. May, D. H. Metcalf, F. S. Richardson, R. C. Carter, C. E. Miller and R. A. Palmer, Measurement and analysis of excited-state decay kinetics and chiroptical activity in the $^6H_j \leftarrow {}^4G_{5/2}$ transitions of Sm^{3+} in trigonal $Na_3[Sm(C_4H_4O_5)_3] \cdot 2NaClO_4 \cdot 6H_2O$, *J. Lumin.*, 1992, **51**, 249–268, DOI: 10.1016/0022-2313(92)90076-l.

5.3. [MT3] Fluorescence and thermal stress properties of Yb^{3+}-doped alumino silicate glasses for ultra high peak power laser applications

Mirko Tiegel, Andreas Herrmann, Stefan Kuhn, Christian Rüssel, Jörg Körner, Diethard Klöpfel, Reinhard Seifert, Joachim Hein, Malte C Kaluza

Laser Physics Letters, 11 (2014) 115811, DOI:10.1088/1612-2011/11/11/115811

	Mirko Tiegel	Dr. Andreas Herrmann	Stefan Kuhn	Prof. Dr. Christian Rüssel	Dr. Jörg Körner	Diethard Klöpfel	Reinhard Seifert	Dr. Joachim Hein	Prof. Dr. Malte C. Kaluza
Konzeption des Forschungsansatzes	☒	☒	☒	☒	☒	☒	☒	☒	☒
Planung der Untersuchungen	☒	☒	☒	☐	☐	☐	☐	☐	☐
Datenerhebung	☒	☐	☒	☐	☒	☐	☐	☐	☐
Datenanalyse und -interpretation	☒	☒	☒	☐	☒	☐	☐	☐	☐
Schreiben des Manuskripts	☒	☒	☐	☒	☒	☐	☐	☒	☒
Vorschlag Anrechnung Publikationsäquivalente	1,0								

IOP Publishing | Astro Ltd Laser Physics Letters
Laser Phys. Lett. 11 (2014) 115811 (6pp) doi:10.1088/1612-2011/11/11/115811

Fluorescence and thermal stress properties of Yb^{3+}-doped alumino silicate glasses for ultra high peak power laser applications

Mirko Tiegel[1], Andreas Herrmann[1], Stefan Kuhn[1], Christian Rüssel[1], Jörg Körner[2], Diethard Klöpfel[2], Reinhard Seifert[3], Joachim Hein[2,3] and Malte C Kaluza[2,3]

[1] Otto-Schott-Institut, Jena University, Fraunhoferstraße 6, 07743 Jena, Germany
[2] Institute of Optics and Quantum Electronics, Jena University, Max-Wien-Platz 1, 07743 Jena, Germany
[3] Helmholtz Institute Jena, Fröbelstieg 3, 07743 Jena, Germany

E-mail: andreas.herrmann@uni-jena.de

Received 10 March 2014, revised 14 August 2014
Accepted for publication 15 August 2014
Published 22 September 2014

Abstract

Various alumino silicate glasses (network modifier ions: Li^+, Mg^{2+}, Zn^{2+} and/or La^{3+}) doped with 1×10^{20} Yb^{3+} cm^{-3} (about 0.2 mol% Yb_2O_3) were prepared. The glasses were studied with respect to their thermo-mechanical and fluorescence properties. Huge differences are found for the coefficients of thermal expansion which determine the thermal shock resistance of the material and hence are required for ultra-high power laser applications. Here, zinc and magnesium alumino silicate glasses show the lowest values. The fluorescence lifetimes of the glasses increase with decreasing average atomic weight of the glass composition (685–1020 μs). All glasses show broad and smooth emission spectra with little variations due to compositional changes.

Mixed lithium zinc or lithium magnesium alumino silicate glasses could be promising new laser materials especially with respect to ultra-high peak power systems or applications with high repetition rates.

Keywords: laser material, alumino silicate glass, yb^{3+}, fluorescence, thermo-mechanical properties

(Some figures may appear in colour only in the online journal)

1. Introduction

A fundamental issue for the development of diode pumped high peak power laser systems is the selection of the active medium. Due to the good matching of the absorption bands with the emission wavelengths of available high power InGaAs laser diodes, the low quantum defect and the comparably long excited-state lifetime, Yb^{3+}-doped media are the material of choice for such a task. For the amplification of ultra short pulses with durations as short as 200 fs, a broad and smooth emission band is additionally needed, which further reduces the selection of available materials significantly. Finally, when high pulse energies are also required, this selection is further minimized to materials that are available in high quality and large size of the specimens. So far, only Yb:CaF_2 and Yb^{3+}-doped glasses can fulfill all these conditions at the same time. Though Yb:CaF_2 benefits from its crystalline nature leading to good thermal conductivity in comparison to glasses, most of this advantage is lost when a high doping concentration is required [1, 2]. Furthermore, since the emission spectra of glasses typically exhibit a smoother shape than Yb:CaF_2, glasses are a very interesting alternative.

In addition to laser induced damage typically occurring on nanosecond timescales, which ultimately limits the fluence for the extracting laser pulse, the thermal stress induced by temperature gradients in the laser medium is the main limitation when scaling up the output power of a laser system. The thermal stress σ_{therm} of a material can be calculated by:

$$\sigma_{\text{therm}} = \frac{E \cdot \alpha}{1 - \nu} \Delta T \qquad (1)$$

Here, E is Young's modulus, α is the coefficient of thermal expansion, and ν is Poisson's ratio, while ΔT is the induced temperature difference. The stress induced by temperature gradients in the gain material results in its elastic deformation. After surpassing a certain threshold, micro cracks are likely to be formed in the gain material, which increase light scattering. Finally crack propagation leads to a complete destruction of the laser material.

Therefore glasses with low thermal stress-values are promising candidates for scaling up the output power of a laser amplifier. Phosphate and fluoride phosphate glasses are known for their thermo-mechanical limitations [3, 4] but show exceptionally good optical properties, i.e. high quantum efficiencies, high fluorescence lifetimes and relatively broad emission spectra [3, 5] favouring direct diode pumping and the amplification of sub-ps laser pulses. Furthermore, Yb^{3+}-doped fluoride phosphate glass so far is the only glass used within a laser system reaching an output of more than 10 TW [6].

Fused silica on the other hand in general has a very high thermal shock resistance but a low solubility for rare-earth ions [7]. However, Fujimoto and colleagues [8–10] use a zeolite route to incorporate up to 3 ma% (around 0.55 mol%) Nd_2O_3 into an SiO_2 matrix without clustering of the rare earth ions by adding Al_2O_3 to the glass composition. For these glasses, the thermal shock resistance was reported to be more than 50 times higher than for commercial phosphate laser glasses. Nevertheless, the high optical quality and large sample sizes which are necessary cannot be achieved by this method.

Alumino silicate (AS) glasses are a well-studied glass system with a very good glass forming ability and low crystallization tendency in a broad compositional range [11]. Furthermore these glasses generally exhibit very good mechanical and thermo-mechanical properties such as high fracture strength, a high Young's modulus and a low coefficient of thermal expansion [12, 13]. Therefore, these glasses are used e.g. for the production of glass-fiber reinforced polymer matrix composites [14]. Glasses of this system can also be used for the preparation of glass ceramics with excellent mechanical properties by controlled crystallization which are e.g. suitable for hard disc plates [15] or materials for dentistry [16]. For this purpose, however, nucleation agents have to be added to the glass composition.

In addition, AS glasses have a high chemical durability [17], a low OH^- and a low platinum solubility [18] as well as a high solubility for rare earth ions. Furthermore, the good glass forming ability of the AS system allows large compositional variations and therefore permits the tailoring of most physical properties such as the optical or thermo-mechanical characteristics of the material [19–21].

All these properties indicate that Yb^{3+}-doped alumino silicate glasses are promising materials for high peak power laser amplifiers. In this article, the effect of compositional changes on the thermo-mechanical and optical properties of Yb^{3+}-doped AS glasses is discussed. Li_2O, MgO, ZnO, and La_2O_3 as well as LiF and MgF_2 have been used as network modifiers.

2. Experimental procedures

The glasses were prepared from high purity raw materials (Fe < 10 ppm, other contaminating metals < 0.5 ppm) SiO_2 (Sipur A1, Bremthaler Quarzitwerk, Germany), $Al(OH)_3$ (Sumitomo, Japan), 4 $MgCO_3{\cdot}Mg(OH)_2{\cdot}4$–5 H_2O (Dr P. Lohmann, Germany), ZnO (Heubach, Germany), Li_2CO_3 (Sigma-Aldrich, USA), LiF (Chemiewerk Nünchritz, Germany), MgF_2 (Chemiewerk Nünchritz, Germany) and Yb_2O_3 (Johnson Matthey, Germany). Batches of 200–500 g were melted in covered DPH-platinum crucibles at temperatures in the range from 1500–1550 °C depending on the individual glass composition. After melting for 1 h, the temperature was increased to 1610 °C which was kept for another hour. Afterwards, the melts were homogenized with a screw stirrer for 1 h at 1610 °C. Finally, samples were cast into preheated steel moulds and transferred into a muffle furnace, preheated to temperatures in the range of 750–920 °C depending on the transition temperature T_g of the glasses. Subsequently, the cooling furnace was switched off and the samples were allowed to cool (cooling rate: approximately 3 K min^{-1}).

Table 1 summarizes the chemical compositions of all prepared glasses. In lithium-containing glass compositions 2 mol% of network modifier oxides are replaced by 1.33 mol% lanthanum oxide to suppress volume crystallization. All glasses were doped with Yb^{3+} using ytterbium (III) oxide as an additive to the raw materials. The doping concentration of Yb^{3+} was kept constant at 1×10^{20} ions per cm^3 for all glass compositions which corresponds to about 0.2 mol% Yb_2O_3 depending on the density of the glass. Element analyses of the fluorine containing glasses revealed a fluorine loss of up to 35% which apparently occurred during the melting of the glasses.

The glass transition temperatures T_g and the coefficients of thermal expansion (CTE) were measured by dilatometry in the temperature range of 20–1000 °C using a heating rate of 5 K min^{-1} (dilatometer DIL 402 PC, NETZSCH Gerätebau GmbH, Germany). For that purpose, cylindrical samples with a diameter of 8 mm and a length of about 20 mm had been prepared. The densities were measured using a helium pycnometer (AccuPyc 1330, Micromeritics GmbH, Germany). Young's moduli measurements were done with an ultrasonic detector (USD 15, Krautkramer-Branson, Austria) on glass samples with a diameter of 15 mm and a length of 20 mm.

To evaluate the spectral properties of the different laser glasses, we used a combined setup as described by Körner *et al* [22]. The recording of spectral data was performed with an ANDO A-6315 optical spectrum analyzer. The absorption cross sections σ_a were derived from measured white light transmission spectra using Lambert Beer's law:

$$\sigma_a(\lambda) = \frac{\ln\left(\frac{I_0(\lambda)}{I_t(\lambda)}\right)}{N_d \cdot l}. \quad (2)$$

Here, I_0 is the reference spectral intensity acquired without the sample in the beam path and I_t is the transmitted spectral intensity. N_d denotes the doping concentration of the sample and l the thickness. To compensate for differences in the

Table 1. Molar compositions, average atomic weights Ā, transition temperatures T_g, density, coefficients of thermal expansion (CTE), Young's moduli E, calculated thermal stresses σ_{therm}, and fluorescence lifetimes ($1 \times 10^{20}\,Yb^{3+}cm^{-3}$) of homogeneous glass samples.

	Composition (mol%)			Ā	T_g	Density	CTE	E	σ_{therm}	n_e	τ_{Yb3+}
Sample name	M_xO_y / MF_z	Al_2O_3	SiO_2	(u)	(°C) ± 3	($g\,cm^{-3}$) ± 0.005	($10^{-6}K^{-1}$) ± 0.1	(GPa) ± 3	($MPa\,K^{-1}$) ± 0.05	± 0.001	(ms) ± 0.1
LiAS	Li_2O: 18 La_2O_3: 1.33	20	60	18.4	693	2.40	7.6	90	0.92	1.531	1.02
LiMgAS	Li_2O: 9 MgO: 9 La_2O_3: 1.33	20	60	19.2	709	2.53	5.5	98	0.71	1.541	0.83
MgAS	MgO: 20	20	60	20.2	827	2.55	4.1	102	0.55	1.548	0.80
LiZnAS	Li_2O: 9 ZnO: 9 La_2O_3: 1.33	20	60	20.5	700	2.70	4.7	90	0.56	1.553	0.89
MgZnAS	MgO: 10 ZnO: 10	20	60	21.4	766	2.72	4.0	99	0.53	1.558	0.80
ZnAS	ZnO: 20	20	60	22.7	742	2.84	3.6	94	0.46	1.573	0.80
LaAS-08	La_2O_3: 7.7	23.1	69.2	25.0	875	3.02	4.4	92	0.57	1.593	0.71
LaAS-15	La_2O_3: 15	15	70	29.5	862	3.57	5.4	94	0.71	1.647	0.72
LaAS-25	La_2O_3: 25	25	50	34.2	862	4.28	7.5	94	0.99	1.745	0.69
LiMgAS-F3	Li_2O: 9 MgO: 6 MgF_2: 3 La_2O_3: 1.33	20	60	19.3	670	2.52	6.3	95	0.79	1.538	0.86
LiMgAS-F9	Li_2O: 9 MgF_2: 9 La_2O_3: 1.33	20	60	19.3	636	2.61	6.2	95	0.78	1.546	0.89

amplitudes of the measured intensities originating e.g. from Fresnel losses on the sample surface, the I_0 and I_t values are normalized in non-absorbing parts of the spectrum ranging from 800–820 nm and 1130–1150 nm.

Using σ_a one can apply the so called reprocity relation [23], which allows for a direct calculation of the emission cross sections σ_e:

$$\sigma_e(\lambda) = \frac{\sigma_a(\lambda) \cdot Z_l}{Z_u} \cdot \exp\left[\frac{\left(E_{ZL} - \frac{h \cdot c}{\lambda}\right)}{k_B \cdot T}\right]. \quad (3)$$

Here, E_{ZL} is the energy difference of the transition between the lowest electronic energy levels in the lower and upper manifold. T is the temperature, h Planck's constant, k_B Boltzmann's constant and c the vacuum speed of light. The partition functions of the upper Z_u and lower Z_l manifolds are defined by the individual energy levels of each manifold E_k and their corresponding degree of degeneration d_k:

$$Z_m = \sum_k d_k^m \cdot \exp\left[-\frac{E_k}{k_B \cdot T}\right]. \quad (4)$$

Since for the investigated glasses, the exact values of the energy levels are currently not available, an exact calculation of σ_e using this method alone is not possible. Furthermore, the accuracy of the calculated values of σ_e depends on the relative accuracy of σ_a, which is also rather low for longer wavelengths.

To allow for a more precise determination of σ_e, the so called Fuchtbauer–Ladenburg method (FL) has been used additionally [24]. With this method σ_e can be determined from the fluorescence spectral intensity $I_f(\lambda)$:

$$\sigma_e = \frac{\lambda^5}{8 \cdot \pi \cdot n^2 \cdot \tau_r \cdot c} \cdot \frac{I_f(\lambda)}{\int_0^\infty \lambda \cdot I_f(\lambda)\,d\lambda}. \quad (5)$$

Here, n is the refractive index of the material and τ_r the radiative lifetime of the excited state. A main condition for the applicability of the FL method is that the measured fluorescence spectra are not affected by re-absorption. This condition was met by the geometry of the used setup and the low doping concentration ($1 \times 10^{20}\,cm^{-3}$) of the measured samples. For the calculation of σ_e, the refractive index n, which is known with good accuracy, and the radiative lifetime τ_r are required. Here, the latter is difficult to determine. In order to estimate this parameter, we measured the fluorescence lifetime τ_f (see table 1 for details) within our setup with a photodiode in the position of the spectrum analyzer. Due to the low amount of re-absorption within the setup the measured fluorescence lifetimes will not be influenced significantly. Furthermore, in previous measurements with lower Yb^{3+} concentrations within this glass system, we observed no further increase in lifetime, which indicates that no concentration quenching occurs. Taking this into consideration, we can estimate the measured τ_f to be close to τ_r.

By a comparison of the results of both methods we can estimate the emission cross sections within the relative accuracy of our lifetime measurements of about 10%. The unknown relation of the partition functions was estimated to be 1.1 for all measured glasses. To achieve a good overlap of both methods also τ_r was slightly modified within the accuracy of our measurements.

3. Results and discussion

Table 1 shows the as weighted glass compositions. For alkali and alkaline earth alumino silicate glasses the molar composition is 20 mol% network modifier oxide, 20 mol% Al_2O_3 and 60 mol% SiO_2. For the lanthanum containing glasses different compositions have been prepared. All prepared glass samples were visually transparent and very homogeneous. Furthermore, table 1 summarizes the glass transition temperatures T_g, the coefficients of linear thermal expansion CTE, the Young's moduli, the calculated thermal stresses σ_{therm}, the densities and refractive indices of all glass compositions. As expected, the density and refractive indices of the glasses increase with increasing average atomic weight of the glass composition. The lowest CTE and the lowest thermal stress value of all investigated glasses are found for the magnesium (4.06 $10^{-6}K^{-1}$, 0.55 $MPa\,K^{-1}$), the zinc (3.64 $10^{-6}K^{-1}$, 0.46 $MPa\,K^{-1}$) and the mixed magnesium zinc alumino silicate glasses (3.98

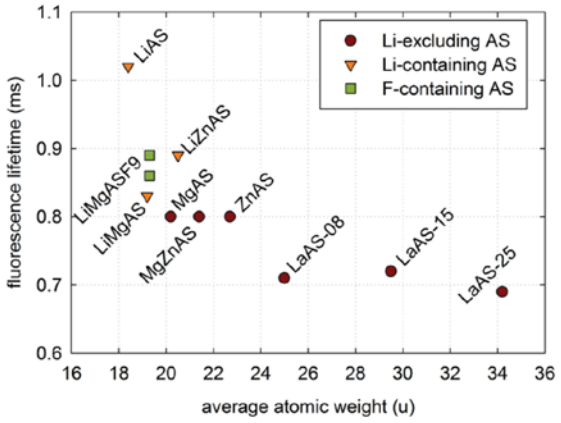

Figure 1. Fluorescence lifetimes of alumino silicate glasses doped with $1{\cdot}10^{20}\,cm^{-3}$ Yb^{3+} as a function of the average atomic weight of the glass composition.

$10^{-6}\,K^{-1}$, 0.53 MPa K^{-1}). Low thermal stress is a prerequisite for a high resistance to thermo-mechanical shock. The highest CTE and thermal stress values are found for the lithium alumino silicate glasses. Substitution of magnesium fluoride for magnesium oxide slightly increases the CTE and thermal stress values. Interestingly, this increase is lower for the glass composition with 9 mol% MgF_2 (6.17 $10^{-6}\,K^{-1}$, 0.78 MPa K^{-1}) than for the sample with only 3 Mol% MgF_2 (6.26 $10^{-6}\,K^{-1}$, 0.79 MPa K^{-1}). Huge differences were also found for the glass transition temperatures. In general, the glass transition temperatures are fairly high and lie in the range between 636 and 875 °C. The lowest T_g of fluorine-free samples was found for lithium and zinc alumino silicate glasses. For magnesium alumino silicate glasses T_g decreases with increasing substitution of MgF_2 for MgO due to the depolymerisation of the glass network. A low glass transition temperature might be advantageous for glass production because of lower viscosities and/or lower melting temperatures. Hence better homogenization of the glasses might be achieved. Furthermore, the quaternary glass compositions LiMgAS, LiZnAS and MgZnAS show CTE-, thermal stress—and T_g values between those of the respective ternary alumino silicate glasses. Hence, the thermal stress and melting properties could be controlled by changing and combining the network modifier oxides without changing the connectivity of the alumino silicate glass network.

Figure 1 shows the fluorescence lifetimes of alumino silicate glasses doped with $1{\cdot}10^{20}\,cm^{-3}$ Yb^{3+} in dependence of the average atomic weight of the glass composition. The lifetimes vary between 0.69 ms (lanthanum alumino silicate LaAS-25) and 1.02 ms (lithium alumino silicate). The fluorescence lifetimes of all glasses are also included in table 1. From the determined lifetimes a general trend to higher values can be seen for a reduced average atomic weight of the glass composition. The same correlation was also found for samarium(III) and europium(III)-doped alumino silicate glasses [25]. In this reference, local field effects e.g. higher polarizability of the network modifying ions that surround the rare earth ions in the glass structure are suggested as the origin of this effect. A correlation with the phonon energy could be ruled out [26, 27]. The phonon energy of lanthanum and magnesium alumino silicates could be reduced by increasing network modifier concentrations. This, however, resulted in a decrease of the fluorescence lifetime in lanthanum alumino silicate glasses while it did not show a significant effect for the magnesium alumino silicate glasses. Here an increasing lanthanum concentration drastically increases the atomic weight of the glass composition while increasing magnesium content does not notably affect the mean atomic weight of the glass. The Yb^{3+} fluorescence lifetimes of the three lanthanum alumino silicate glasses presented in this paper varied between 0.69 and 0.72 ms. Although the lowest lifetime is found for the glass with the highest atomic weight and refractive index it must be stated that all three lifetime values are within the limit of error and no general trend can be deduced from these measurements. For magnesium alumino silicate glasses, the addition of fluoride results in an increase of the fluorescence lifetime. Although this effect is relatively small and within the uncertainty range of the lifetime measurements it could also be found for other alumino silicate glasses (not shown). Most likely, the addition of fluoride to the glass composition reduces the OH^- concentration which reduces OH^- quenching of the Yb^{3+} fluorescence [27]. Another reason for the lifetime improvement might be the coordination of the Yb^{3+} ions with Al–F groups that are formed by the introduction of MgF_2 into the glass network [28, 29].

In figure 2, absorption and emission cross sections of some of the investigated glasses are shown. With increasing atomic weight, an increase in the cross sections is found in the absorption and emission bands, which shows the inverse behavior in comparison to the fluorescence lifetime and the refractive index. This can be explained by equation (5) (FL-Formalism). Here, for a constant spectral distribution the relation

$$\sigma_e \sim \frac{1}{n^2 \cdot \tau_r} \tag{6}$$

can be derived. LiAS again shows a significantly different value in comparison to the other glasses. The spectral peaks of the absorption and emission band are about 5 nm further apart from the zero phonon line in this case. For operation in a laser amplifier this might be advantageous since the reabsorption below the peak emission will be significantly lower in this case. Also the already mentioned higher fluorescence lifetime is advantageous for this material.

The addition of fluorine to the composition has only a minor effect on the cross sections of these glasses (figure 3). In general, increasing fluoride concentrations result in a slightly decreasing peak cross section in absorption and emission at the zero phonon line. In case of the glass containing 3% fluoride, the rest of the spectrum remains unchanged. For the sample containing 9% fluoride also slight shifts of the absorption and emission band in the direction of the zero phonon line are observed.

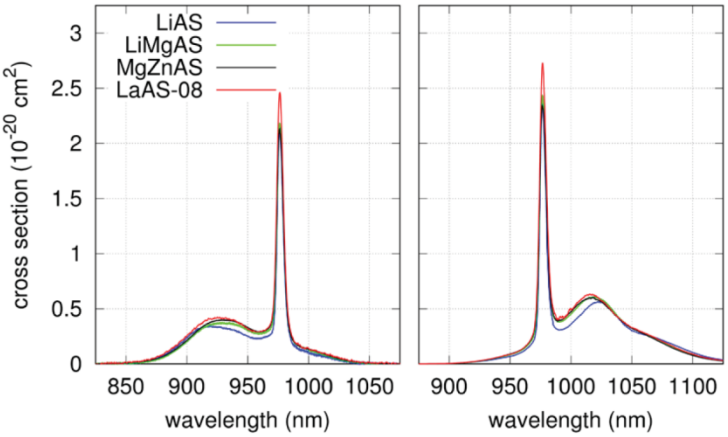

Figure 2. Comparison of cross sections for Yb^{3+}-doped glasses with different average atomic weight. Left: absorption; right: emission.

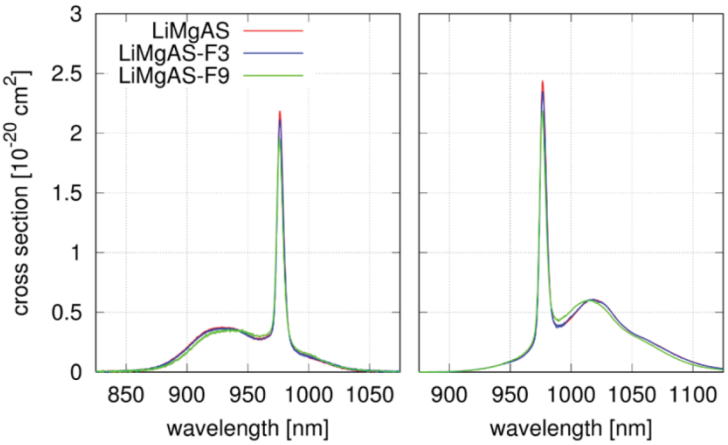

Figure 3. Comparison of cross sections for Yb^{3+}-doped lithium magnesium alumino silicate glasses with different concentrations of fluoride. Left: absorption; right: emission.

4. Conclusions

Alumino silicate glasses of the molar composition 20 Al_2O_3 – 60 SiO_2 – 20 R_xO (R = Li, Mg and/or Zn) and lanthanum alumino silicate glasses with varying composition doped with 1×10^{20} Yb^{3+} cm^{-3} (about 0.2 mol% Yb_2O_3) were prepared and investigated with respect to their thermo-mechanical and optical properties. In general, the fluorescence lifetime increases with decreasing average atomic weight and decreasing refractive index of the glass composition. Simultaneously, a reduction in the absorption and emission cross sections can be seen, while the general spectral shape of the cross sections remains constant for all measured glasses within this glass system. The largest deviations were found for the pure lithium alumino silicate glass which offers a comparably high fluorescence lifetime of 1.02 ms and a slightly shifted spectral distribution. The zinc and magnesium alumino silicate glasses show the smallest coefficients of thermal expansion and therefore the lowest thermal stress values of all investigated glasses,

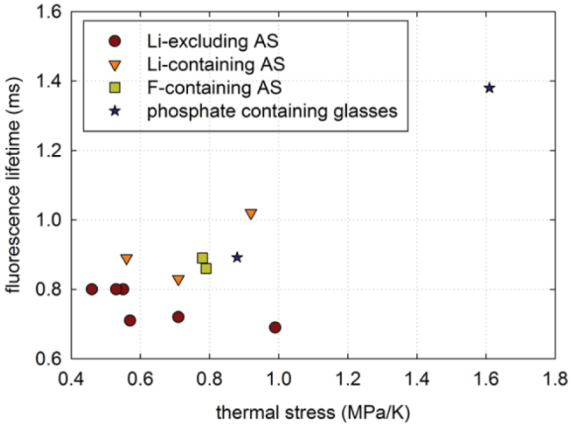

Figure 4. Thermal stress values versus fluorescence lifetime of selected alumino silicate glasses, as well as of phosphate containing glasses (P100 and FP15) all doped with $1{\cdot}10^{20}$ cm^{-3} Yb^{3+}.

which is highly advantageous for a high thermal shock resistance. However, these glasses also show notably lower fluorescence lifetimes than the lithium alumino silicate glass. The partial substitution of lithium for zinc or magnesium increases the fluorescence lifetime, while the good thermo mechanical properties can be maintained. The addition of fluoride to the glasses further increases the fluorescence lifetimes but resulted also in larger coefficients of thermal expansion. Zinc containing glasses provide low glass transition temperatures, which should be beneficial for the production and the optical quality of the glass. In figure 4, the thermo-mechanical and fluorescence properties of the glass samples investigated here as well as of a pure phosphate glass (P100) and of a fluoride phosphate glass (FP15) are summarized. It shows the thermal stress values versus the fluorescence lifetime of ytterbium doped glass samples. The figure clearly shows that alumino silicate glasses in general have low thermal stress values while fluorescence lifetimes in the range of pure phosphate glasses can be achieved. Fluoride phosphate glasses on the other hand show very high fluorescence lifetimes but poor thermo-mechanical properties. In summary it can be stated, that mixed lithium zinc or lithium magnesium alumino silicate glasses with some amount of fluoride could be promising laser materials especially with respect to ultra-high peak power systems or applications with high repetition rates.

Acknowledgments

This work was supported by the European Social Fund (ESF) through the Thuringian Ministry of Economy, Employment and Technology (project number 2011 FGR 0122).

References

[1] Druon F *et al* 2011 On Yb:CaF_2 and Yb:SrF_2: review of spectroscopic and thermal properties and their impact on femtosecond and high power laser performance [Invited] *Opt. Mater. Express*. 1 489
[2] Popov P A *et al* 2008 Thermal conductivity of single crystals of Ca1 − x Yb x F2 + x solid solutions *Dokl. Phys.* **53** 198–200
[3] Campbell J H and Suratwala T I 2000 Nd-doped phosphate glasses for high-energy/high-peak-power lasers *J. Non-Cryst. Solids* **263–4** 318–41
[4] Weber H *et al* 1989 Advances in glasses for high average power laser systems *Proc. SPIE* **1021** 36–41
[5] Bell R J and Dean P 1970 Atomic vibrations in vitreous silica *Discuss. Faraday Soc.* **50** 55
[6] Hornung M *et al* 2013 High-intensity, high-contrast laser pulses generated from the fully diode-pumped Yb:glass laser system POLARIS *Opt. Lett.* **38** 718–20
[7] Sen S *et al* 2006 Direct spectroscopic observation of the atomic-scale mechanisms of clustering and homogenization of rare-earth dopant ions in vitreous silica *Phys. Rev.* B **74** 100201–14
[8] Fujimoto Y and Nakatsuka M 1997 A novel method for uniform dispersion of the rare earth ions in SiO2 glass using zeolite X *J. Non-Cryst. Solids* **215** 182–91
[9] Fujimoto Y *et al* 2005 Development of Nd-doped optical gain material based on silica glass with high thermal shock parameter for high-average-power laser *Japan. J. Appl. Phys.* **44** 1764–70
[10] Sato T *et al* 2006 Laser oscillation of Nd-doped silica glass with high thermal shock parameter *Japan. J. Appl. Phys.* **45** 6936–9
[11] Logvinkov S M, Semchenko G D and Kobyzeva D A 1996 Rearrangement of conodes of the phase diagram of the MgO-Al2O3-SiO2 system and its technological prospects *Refractories* **37** 378–81
[12] Wange P *et al* 2002 Microstructure-property relationship in high-strength MgO–Al2O3–SiO2–TiO2 glass-ceramics *J. Non-Cryst. Solids*. **298** 137–45
[13] Dittmer M, Müller M and Rüssel C 2010 Self-organized nanocrystallinity in MgO–Al2O3–SiO2 glasses with ZrO2 as nucleating agent *Mater. Chem. Phys.* **124** 1083–8
[14] Reben M and Li H 2011 Thermal stability and crystallization kinetics of MgO-Al2O3-B2O3-SiO2 glasses *Int. J. Appl. Glass Sci.* **2** 96–107
[15] Hunger A *et al* 2010 Young's moduli and microhardness of glass–ceramics in the system MgO/Al2O3/TiO2/ZrO2/SiO2 containing quartz nanocrystals *Mater. Chem. Phys.* **122** 502–6
[16] Dittmer M and Rüssel C 2011 Colorless and high strength MgO/Al2O3/SiO2 glass-ceramic dental material using zirconia as nucleating agent *J. Biomed. Mater. Res.* B **100B** 463–70
[17] Leturcq G *et al* 2011 Chemical durability of aluminosilicate glasses containing low solubility chemical elements *MRS Proc.* **506** 199
[18] Izumitani T, Matsukawa M and Miyade H 1987 Solubility of Pt in Nd phosphate laser glass *Laser Induced Damage in Optical Materials (NIST Special Publication* 756) ed H E Bennett, A H Guenther, D Milam, B E Newnan and M J Soileau (National Institute of Standards and Technology) **1988** 29–34
[19] Dittmer M *et al* 2011 Crystallization and mechanical properties of MgO/Al2O3/SiO2/ZrO2 glass-ceramics with and without the addition of yttria *Solid State Sci.* **13** 2146–53
[20] Hunger A *et al* 2008 Ultra-high thermal expansion glass–ceramics in the system MgO/Al2O3/TiO2/ZrO2/SiO2 by volume crystallization of cristobalite *J. Non-Cryst. Solids* **354** 5402–7
[21] Hunger A, Carl G and Rüssel C 2010 Formation of nano-crystalline quartz crystals from ZnO/MgO/Al2O3/TiO2/ZrO2/SiO2 glasses *Solid State Sci.* **12** 1570–4
[22] Koerner J *et al* 2012 Measurement of temperature-dependent absorption and emission spectra of Yb:YAG, Yb:LuAG, and Yb:CaF_2 between 20°C and 200°C and predictions on their influence on laser performance *J. Opt. Soc. Am.* B **29** 2493
[23] McCumber D 1964 Einstein relations connecting broadband emission and absorption spectra *Phys. Rev.* **136** A954–7
[24] Payne S A *et al* 1992 Infrared cross-section measurements for crystals doped with Er/sup 3+/, Tm/sup 3+/, and Ho/sup 3+ *IEEE J. Quantum Electron.* **28** 2619–30
[25] Herrmann A *et al* 2014 Structure and fluorescence properties of ternary alumino silicate glasses doped with samarium and europium *J. Mater. Chem.* C **2** 4328–37
[26] Kuhn S *et al* 2013 Sm3+-doped La2O3–Al2O3–SiO2-glasses: structure, fluorescence and thermal expansion *J. Mater. Sci.* **48** 8014–22
[27] Tiegel M *et al* 2013 Magnesium aluminosilicate glasses as potential laser host material for ultrahigh power laser systems *J. Mater. Chem.* C **1** 5031
[28] Bocker C *et al* 2011 Fluorine sites in glasses and transparent glass-ceramics of the system Na2O/K2O/Al2O3/SiO2/BaF2 *J. Solid State Chem.* **184** 405–10
[29] de Pablos-Martín A *et al* 2010 Design of oxy-fluoride glass-ceramics containing NaLaF4 nano-crystals *J. Non-Cryst. Solids* **356** 3071–9

5.4. [MT4] Fluorescence properties of Eu^{3+}-doped alumino silicate glasses

Andreas Herrmann, Stefan Kuhn, Mirko Tiegel, Christian Rüssel

Optical Materials, 37 (2014) 293-297, DOI: 10.1016/j.optmat.2014.06.011

	Dr. Andreas Herrmann	Stefan Kuhn	Mirko Tiegel	Prof. Dr. Christian Rüssel
Konzeption des Forschungsansatzes	☒	☒	☒	☒
Planung der Untersuchungen	☒	☒	☒	☐
Datenerhebung	☒	☒	☒	☐
Datenanalyse und -interpretation	☒	☒	☐	☐
Schreiben des Manuskripts	☒	☒	☒	☒
Vorschlag Anrechnung Publikationsäquivalente			0,5	

Optical Materials 37 (2014) 293–297

Contents lists available at ScienceDirect

Optical Materials

journal homepage: www.elsevier.com/locate/optmat

Fluorescence properties of Eu^{3+}-doped alumino silicate glasses

Andreas Herrmann *, Stefan Kuhn, Mirko Tiegel, Christian Rüssel

Otto-Schott-Institut, Jena University, Fraunhoferstr. 6, 07743 Jena, Germany

ARTICLE INFO

Article history:
Received 7 March 2014
Received in revised form 7 May 2014
Accepted 4 June 2014
Available online 11 July 2014

Keywords:
Europium III
Fluorescence
Alumino silicate glass
Refractive index
Optical basicity

ABSTRACT

Alumino silicate glasses of a very broad range of molar compositions doped with $1 \cdot 10^{20}$ Eu^{3+} cm^{-3} (about 0.2 mol% Eu_2O_3) were prepared. As network modifier oxides Li_2O, Na_2O, K_2O, MgO, CaO, SrO, BaO, ZnO, PbO, Y_2O_3 and La_2O_3 have been used. All glasses show relatively broad fluorescence excitation and emission spectra. For most glasses only a weak effect of the glass composition on the excitation and emission spectra is observed. Although the glasses should be structurally similar, notable differences are found for the fluorescence lifetimes. These increase steadily with decreasing mean atomic weight, decreasing refractive index and decreasing optical basicity of the glasses, which may be explained by local field effects. An exception from this rule are the strontium, barium and potassium containing glasses, which show significantly increased fluorescence lifetimes despite of their high refractive index, optical basicity and molecular weight. The non mono-exponential fluorescence decay curves as well as the fluorescence spectra indicate a massive change in the local surroundings of the doped rare earth ions for these glasses.

1. Introduction

Alumino silicate (AS) glasses are used in many technological fields because of their countless advantageous properties. Depending on composition these are e.g. good glass forming ability, high mechanical strength, high chemical durability, small coefficients of thermal expansion and high Young's moduli. Typical areas of application for AS glasses are display glasses for flat screens, technical fibers for polymer matrix composites, container glasses for high temperature chemical or bio-chemical applications and base glasses for glass–ceramics with excellent mechanical and thermo-mechanical properties as e.g. hard disc substrates, materials in dentistry, glass–ceramic cooktops or even telescope mirrors. For production of glass ceramics from these glasses nucleating agents have to be added to the composition. The very good glass forming ability of AS glasses in a broad compositional range furthermore allows tailoring of many physical properties (as e.g. refractive index, viscosity, coefficient of thermal expansion). Additionally, these glasses possess a high solubility for rare earth elements. However, so far only lanthanum alumino silicate glass is frequently considered for optical applications e.g. as optical fiber amplifiers or as fiber- and bulk laser material [1, 2 and references therein].

Within earlier publications, we started the systematical evaluation of alumino silicate glasses as potential laser host material, especially with respect to ultra high power laser applications. For these very general investigations, Sm^{3+} and Yb^{3+} ions have been used as dopants. Although systematic changes in the fluorescence behavior of these two ions depending on the composition of the glasses were found (i.e. fluorescence lifetime as a central laser parameter), the measurements were affected by OH^- quenching (Yb^{3+} and Sm^{3+}), by cross relaxation processes (Sm^{3+}), by reabsorption (Yb^{3+}) or generally show a high experimental error (Yb^{3+}) [3,4]. By contrast, the fluorescence of Eu^{3+} is not affected by these processes. For that reason the fluorescence properties of a great variety of Eu^{3+}-doped alumino silicate glasses are presented in the following.

2. Experimental procedures

The glasses were prepared from high purity raw materials (Fe < 10 ppm, other contaminating metals <0.5 ppm) SiO_2 (Sipur A1, Schott, Germany), Al_2O_3 (Ceralox, Condea Chemie, Germany), Li_2CO_3 (Chemapol, Czech Republic), Na_2CO_3 (Merck, Germany), MgO (Merck, Germany), $CaCO_3$ (Merck, Germany), $SrCO_3$ (Reachim, Ukraine), $BaCO_3$ (Reachim, Ukraine), ZnO (Merck, Germany), PbO (Chemapol, Czech Republic), Y_2O_3 (Sigma–Aldrich, Germany), $La_2O_3 \cdot H_2O$ (Laborchemie Apolda, Germany) and Eu_2O_3 (Ferak, Germany). Batches of 100–200 g were melted in covered platinum crucibles at temperatures in the range from 1600 to 1650 °C

* Corresponding author. Tel.: +49 3641948543; fax: +49 3641948502.
E-mail address: andreas.herrmann@uni-jena.de (A. Herrmann).

http://dx.doi.org/10.1016/j.optmat.2014.06.011
0925-3467/

depending on the individual glass composition. Special measures for additional homogenization of the melts have not been applied. After melting for at least 3 h, the samples were cast into preheated steel moulds and transferred into a muffle furnace, preheated to temperatures in the range from 720 to 920 °C depending on T_g of the glass. Subsequently the cooling furnace was switched off and the samples were allowed to cool (cooling rate: approximately 3 K/min).

Table 1 summarizes the chemical compositions of all prepared glasses. The samples were denoted according to their molar chemical composition. The doping concentration of Eu^{3+} was kept constant at $1 \cdot 10^{20}$ ions per cm^3 for all glass compositions which corresponds to about 0.2 mol% Eu_2O_3 depending on the density of the glass.

The glass transition temperatures T_g was measured using a dilatometer (DIL 402 PC, NETZSCH Gerätebau GmbH, Germany). For that purpose, cylindrical samples with a diameter of 8 mm and a length of about 20 mm had been prepared. A temperature range of 20–1000 °C and a heating rate of 5 K/min were used for these measurements. The densities were measured using a helium pycnometer (AccuPyc 1330, Micromeritics GmbH, Germany).

Fluorescence emission and excitation spectra were measured using a fluorescence spectrometer (RF-5301PC, SHIMADZU Japan); the samples were polished and had a thickness of 10 mm. The excitation spectra were recorded at an emission wavelength of about 613 nm while emission spectra were obtained using an excitation wavelength of about 464 nm (spectral resolution: 0.2 nm). Fluorescence lifetimes were measured using a home-made experimental setup. For excitation of the glass samples a high intensity pulsed InGaN-diode (LED 395-66-60-110, Roithner Lasertechnik GmbH, Austria) with an emission wavelength of 395 nm was used. The emitted fluorescence light was collected and focused by a lens array onto the entrance slit of a monochromator (H.25, HORIBA Jobin Yvon, France). The spectrum-sliced light is amplified by a photomultiplier tube (R5929, Hamamatsu Photonics K.K., Japan) connected to a digital storage oscilloscope (TDS2012, TEKTRONIX USA). This setup allows for wavelength specific lifetime measurements. Fluorescence lifetimes were measured for the strongest fluorescence transition of Eu^{3+} $^5D_0 \rightarrow {}^7F_2$ at around 613 nm.

3. Results and discussion

Table 1 summarizes the molar compositions, glass transition temperatures T_g, refractive indices n_e and densities ρ of all glasses. The density and the refractive index of the glasses increase with increasing atomic weight of the network modifier ion which is not surprising. However, a high refractive index is likely to be disadvantageous for laser applications because of increased second order effects [5] which might lead to self focusing and self-phase modulation which strongly deteriorate the temporal and spatial characteristics of the pulses [6].

Huge differences were found for the glass transition temperatures. In general, the glass transition temperatures are very high and lie in the range of 645–899 °C. The lowest T_g was found for the lead alumino silicate glass. A low T_g might be advantageous for the glass production because lower melting temperatures are possible. Hence better homogenization of the glasses might be facilitated due to lower viscosities.

The fluorescence emission spectra of six europium doped glasses are shown in Fig. 1. For comparison only the lithium-, magnesium-, yttrium- and lanthanum alumino silicate glasses are displayed (from top to bottom). A barium- and potassium alumino silicate glass have additionally been added to the graph. All spectra are normalized to their most intense peaks at around 613 nm. For clarity, the different spectra are shifted in vertical direction. Relatively narrow bands attributed to the f–f-transitions of Eu^{3+} are observed, which are broadened in comparison to the transitions observed in crystals due to the irregular glass structure and the attributed variation in the local sites of the Eu^{3+} ions. Fig. 1 shows the typical fluorescence emission lines of the Eu^{3+} ion. The most intense line at around 613 nm is attributed to the transition $^5D_0 \rightarrow {}^7F_2$. At around 576, 655 and 702 nm, the transitions $^5D_0 \rightarrow {}^7F_0$, $^5D_0 \rightarrow {}^7F_3$ and $^5D_0 \rightarrow {}^7F_4$ are respectively observed [7,8]. The band in the wavelength range between 580 and 600 nm is due to the transition $^5D_0 \rightarrow {}^7F_1$ which is split into several components [7]. The line shapes of most glasses, i.e. LiAS, MgAS, YAS and LaAS glasses, are hardly affected by compositional variations. Differences can be found for the barium (BaAS) and potassium (KAS) alumino silicate glasses. For these two samples the main peak at around 613 nm and the band at around 590 nm are notably narrowed. For the KAS sample this effect is especially well pronounced. The fluorescence emission spectra of Eu^{3+} furthermore allow an estimation of the symmetry of the local rare earth site [9]. This is possible since the transition $^5D_0 \rightarrow {}^7F_2$ (613 nm) is almost entirely electric dipole in nature and therefore sensitive to the local crystal field symmetry, while the transition $^5D_0 \rightarrow {}^7F_1$ at around 590 nm is an almost pure magnetic dipole transition which is not affected by local site symmetry [9]. Therefore the intensity ratio of the emission peaks at 590 and 613 nm, I_{590}/I_{613}, can be used as measure for the overall symmetry at the local Eu^{3+} site. A high ratio I_{590}/I_{613} indicates a high crystal field symmetry and vice versa [9]. Although the spectra are very similar, a deconvolution of the bands at 590 and 613 nm has been

Table 1
Molar compositions, transition temperatures T_g, density, refractive index n_e, fluorescence lifetimes ($1 \cdot 10^{20}$ Eu^{3+} cm^{-3}), symmetry ratios I_{590}/I_{615} and calculated optical basicities of all studied glass samples.

Sample name	Composition (mol%)			T_g (°C) ±5	Density (g/cm³) ±0.005	n_e ±0.005	τ_{Eu3+} (ms) ±0.05	I_{590}/I_{615}	Optical basicity
	$M_2O/MO/M_2O_3$	Al_2O_3	SiO_2						
LiAS1515	Li_2O: 15	15	70	820	2.36	1.521	2.07	0.2276	0.5374
KAS3010	K_2O: 30	10	60	660	2.48	1.512	2.56	0.2767	0.6408
MgAS1515	MgO: 15	15	70	831	2.44	1.520	2.05	0.2404	0.5306
MgAS3010	MgO: 30	10	60	796	2.56	1.548	2.08	0.2550	0.5508
CaAS2020	CaO: 20	20	60	868	2.61	1.557	1.94	0.2128	0.5695
ZnAS4010	ZnO: 40	10	50	700	3.42	1.633	1.97	0.2499	0.6126
SrAS3010	SrO: 30	10	60	785	3.12	1.628	2.10	0.2784	0.6042
BaAS3010	BaO: 30	10	60	770	3.54	1.606	2.17	0.2774	0.6125
PbAS2020	PbO: 20	20	60	645	3.66	1.659	1.71	0.2281	0.5885
YAS0823	Y_2O_3: 7.7	23.1	69.2	899	2.85	1.581	1.93	0.2535	0.5686
LaAS2525	La_2O_3: 25	25	50	862	4.28	1.745	1.68	0.2900	0.7275
LaAS1515	La_2O_3: 15	15	70	862	3.57	1.648	1.85	0.2689	0.6414
LaAS1030	La_2O_3: 10	30	60	873	3.31	1.625	1.87	0.2583	0.6144

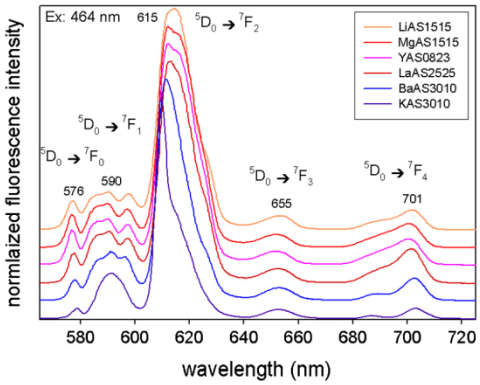

Fig. 1. Eu^{3+} emission spectra of different alumino silicate glasses doped with $1 \cdot 10^{20}$ Eu^{3+}/cm^3. Note that the different spectra have been shifted in vertical direction for clarity.

performed. For this, three Gaussian curves have been fitted to each of the two bands in the energy (wave number) scale. The peak at 576 nm has been added to this analysis to reduce the fit error. Finally, the ratio of the total areas of the two bands at 590 and 613 nm, I_{590}/I_{613} has been calculated. These values have been added to Table 1. In general, the rare earth site symmetry of all glasses presented here is very low. The highest I_{590}/I_{613} ratio is found for glasses with heavy network modifying ions such as LaAS2525, BaAS3010, SrAS3010 and KAS3010. An exception is the PbAS2020 sample which has a low symmetry. Low symmetry values are also found for CaAS2020 and LiAS1515 samples. In general, no clear correlation of the local site symmetry of the Eu^{3+} ions with the average atomic weight of the glass compositions can be found although a tendency to higher symmetry in glasses with high atomic weight can be observed.

The fluorescence excitation spectra which are shown in Fig. 2 are superimposed by several different effects. For clarity only 3 spectra are displayed. In general the excitation spectra consist of numerous relatively narrow bands, which correspond to the ground state absorption ($^7F_0$) of the levels $^5D_0$ at 588 nm, $^5D_1$ at 532 nm, $^5D_2$ at 469 nm, $^5D_3$ at 413 nm, $^5L_6$ at 396 nm and many more adjacent energy levels at lower wavelengths [8]. The excitation spectra of LiAS and LaAS glasses do not show notable differences except for the lower intensity of the near UV peaks below 400 nm in the lithium containing glass. This effect can be observed for all glasses of relatively low optical basicity, such as LiAS1515, MgAS1515, MgAS3010, CaAS2020, YAS0823 and – less pronounced – even for ZnAS4010. For these glasses notable amounts of Europium have been reduced to Eu^{2+} during the melting process which absorbs near UV radiation and therefore hinders the excitation of the Eu^{3+} ions in this wavelength range [7]. A similar effect is also found for zinc and lead containing samples (not shown). For these glasses, the effect is due to the broad absorption band of the zinc [10–12] or lead ions [7,13] in glasses between 200 and 400 nm. Notable differences in the shape and the relative peak sizes of the individual excitation bands are again found for the potassium alumino silicate glass. The excitation spectra of the SrAS and BaAS samples do not show any notable differences to the LaAS glass (not shown).

Fig. 3 shows the fluorescence decay curves of six Eu^{3+}-doped glass samples. After excitation at 395 nm by the high-power LED, fluorescence rises quickly to its maximum value (not shown), which is kept for several milliseconds (normalized fluorescence intensity level at $t < 0$). At $t = 0$, the diode is switched off and the fluorescence intensity of the samples drops with distinct characteristics. Due to the half-logarithmic scale, a mono-exponential decay appears as a straight line. The slope of this line corresponds to the inverse fluorescence lifetime. For most samples an almost perfect mono exponential decay is observed, which indicates an undisturbed fluorescence emission process and homogeneously distributed Eu^{3+} ions. The lifetimes vary between 1.7 ms (lanthanum alumino silicate) and 2.1 ms (lithium and magnesium alumino silicates). The decay curves of three samples show notable deviations from a mono-exponential decay; these samples are the strontium, barium and potassium containing glasses (Fig. 3). For these glasses a delayed decay and a higher fluorescence lifetime in comparison to all other glasses are found. Because of the non mono-exponential decay the fluorescence lifetime of these samples had to be determined by the barycenter method, described e.g. in Ref. [14]. The fluorescence lifetime values of all glasses are included in Table 1. For most samples, the fluorescence lifetime decreases steadily with increasing atomic weight of the network modifier ions and therefore also with increasing refractive index of the glasses. The same result that has also been found for Sm^{3+} and Yb^{3+} doped alumino silicate glasses [3,4]. An effect of the phonon energy of the glass matrix can be ruled out. Detailed studies on this subject in lanthanum and magnesium alumino silicate glasses did not show any systematic influence of the maximum phonon energy on the fluorescence lifetimes of the doped rare earth elements [1,15]. Furthermore it can be shown easily

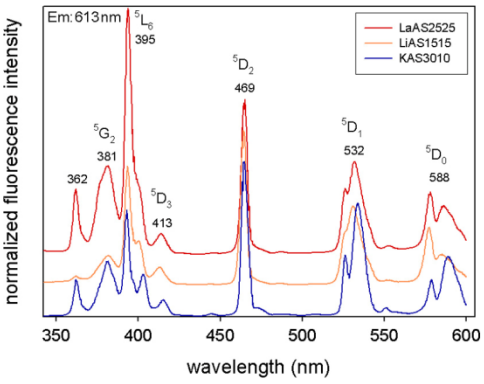

Fig. 2. Eu^{3+} excitation spectra of three different alumino silicate glasses doped with $1 \cdot 10^{20}$ Eu^{3+}/cm^3. Note that the different spectra have been shifted in vertical direction for clarity.

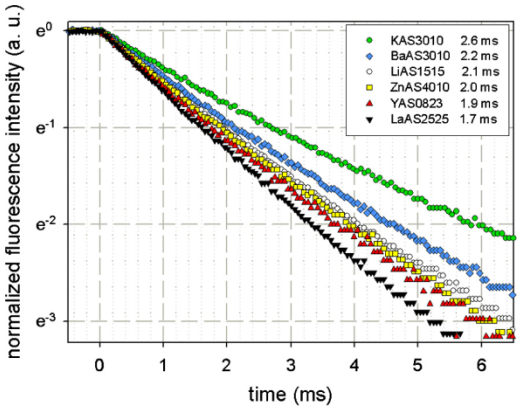

Fig. 3. Fluorescence decay curves of the $^5D_0$ energy level of Eu^{3+} and decay times (inset) for different glass compositions.

by applying the so called energy-gap law [16], that a phonon energy cutoff of about 1250 cm^{-1} [1,3,15] has no effect on the fluorescence decay rates of rare earth elements with an energy gap as high as 12,000 cm^{-1} as it is the case for Eu^{3+}.

However, strontium, barium and potassium containing samples, which have not been investigated in earlier publications show significantly increased fluorescence lifetimes despite of their relatively high refractive indices. From Fig. 3 it can clearly be seen that the fluorescence decay curves of these glasses have no mono exponential shape, which is a clear indicator for different local sites of the Eu^{3+} ions and for a massive structural change in the surrounding of a notable fraction of Eu^{3+} ions. Recent experiments with Sm^{3+} doped barium and potassium alumino silicate glasses show similar effects (not published data). Obviously network modifying ions that are larger in size than the doped rare earth ions, which is the case for Sr^{2+}, Ba^{2+} and K^{+} [17], affect their homogeneous distribution. However, Na^{+}, Ca^{2+} and La^{3+} possess about the same ionic radius as Eu^{3+} and Sm^{3+} [17] and might not have the same structural effect in alumino silicate glasses as the larger ions.

Fig. 4 shows the fluorescence lifetimes of Eu^{3+}-doped samples in dependence of the measured refractive indices n_e together with a least-square fit of the so called real cavity model. This model is based on the Purcell effect which describes the effect of the refractive index n of the surrounding dielectric media on the spontaneous emission rates A^{diel} of atoms [18]. The real cavity model is one of various theoretically derived models that predict this dependence [19–25]. In general it can be written as: $A^{diel}(n) = n \cdot l(n)^2 \cdot A_0$. Here, A_0 is the vacuum spontaneous emission rate and l is the dielectric local-field correction factor which differs for the various models. For the real-cavity model it is defined as $l(n) = 3n^2/(2n^2 + 1)$ [24,25]. Since $n \geqslant 1$, the spontaneous emission rate is increased (and the lifetime of the excited state is decreased) by the dielectric medium around the emitter with increasing n, and accordingly with increasing interaction of the emitter and the surrounding dielectric medium. As can be seen in Fig. 4, this model fits very well to the measured data as long as Sr^{2+}, Ba^{2+} and K^{+} containing samples are excluded from the fit (the data point of the KAS sample is by far out of range of the diagram and therefore not displayed). On the other hand it seems to fit also for sodium borosilicate glasses of the Pyrex type (e.g. Duran). This data point is additionally added to the graph [26]. However, due to phase separation effects this glass type does not allow for high rare earth doping concentrations [26]. As discussed earlier [3 and references therein], rare earth ions are likely to enter depolymerized regions of the aluminosilicate network. These regions are formed by the network modifying ions, which also determine the refractive index of the glass. Therefore a close relationship between electron density, polarizability (refractive index) and fluorescence lifetime can be expected. On the other hand this argumentation, including the real cavity model, implies that the interaction of the doped Eu^{3+} ions and their local surrounding must be notably diminished in strontium, barium and potassium alumino silicate glasses since their fluorescence lifetime is notably increased in these samples. For that reason, a notable amount of rare earth ions should occupy sites of lower polarizability and lower local electron density in these glasses which implies a massive structural change in the local surrounding of these Eu^{3+} ions. For this reason the fluorescence lifetime values have also been compared to the symmetry values. As can be seen from Table 1, a general tendency to lower lifetimes with increasing symmetry at the Eu^{3+} sites can be observed. But again, the SrAS, BaAS and KAS samples do not follow that trend. All of these samples show high symmetry values and high fluorescence lifetimes. Furthermore it has been tried to correlate the fluorescence lifetimes with the optical basicity of the glasses (Fig. 5). The optical basicities have been calculated according to Refs. [27,28]. The basicity data is also included in Table 1. As can be seen, the lifetime dependence on the optical basicity is very similar to Fig. 4, but in this case an almost linear dependence could be assumed. Obviously high fluorescence lifetimes are favoured in glasses of low optical basicity and vice versa. Again the strontium, barium and potassium containing glasses (as well as the lead containing glass) stand out from this rule. The data point for the potassium containing glass is by far out of range of the graph and therefore not displayed. However, as explained above, the dependency of the lifetime on the refractive index can theoretically be derived while the optical basicity is based on phenomenological observations. Nevertheless, with no doubt polarizability (refractive index) and optical basicity from a physical point of view are similar parameters [28].

Besides their advantageous properties alumino silicate glasses can also provide relatively long fluorescence lifetimes of doped rare earth ions. Obviously glasses of low atomic weight, low refractive index and low optical basicity provide relatively high lifetime values. Surprisingly, network modifying ions with large atomic radii such as Sr^{2+}, Ba^{2+} and K^{+} also lead to an increase in the fluorescence lifetime of the doped rare earth ions despite of the relatively high refractive index of these glasses. For these, fluorescence spectra as well as decay curves indicate a massive change in the local surroundings of the dopants. However, this effect might be useful for optical fiber applications where certain differences in the refractive indices of the core and cladding are required while high fluorescence lifetimes have to be maintained.

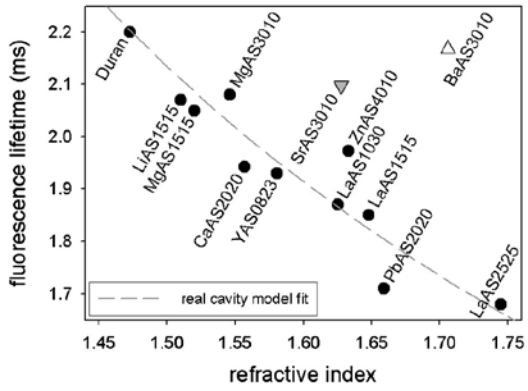

Fig. 4. Fluorescence lifetimes of ternary alumino silicate glasses doped with $1 \cdot 10^{20}$ cm^{-3} Eu^{3+} in dependence of the measured refractive index n_e of the glass composition. The data has been fitted with the real cavity model. The data point for the KAS3010 sample (2.56 ms) is by far out of range of the diagram and therefore not included.

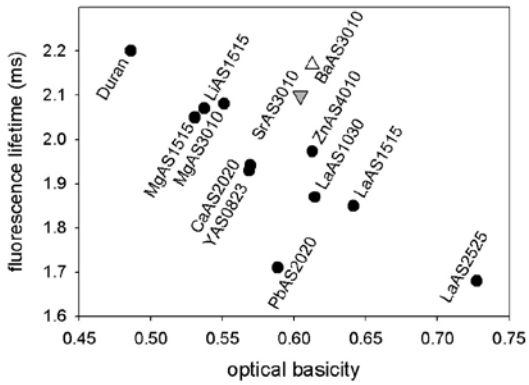

Fig. 5. Fluorescence lifetimes of ternary alumino silicate glasses doped with $1 \cdot 10^{20}$ cm^{-3} Eu^{3+} as a function of the calculated optical basicities of the glasses.

4. Conclusions

Alumino silicate glasses of a great variety of molar compositions doped with $1 \cdot 10^{20}$ Eu^{3+} cm^{-3} (about 0.2 mol% Eu_2O_3) were prepared and investigated with respect to their fluorescence properties. The glasses show broad fluorescence excitation and emission spectra that are hardly affected by the glass composition. Notable differences in the spectra are only found for strontium, barium and potassium alumino silicate glasses. Although the glasses should be structurally very similar, significant differences in the fluorescence lifetimes were found. Generally the fluorescence lifetime increases steadily with decreasing atomic weight, decreasing refractive index and decreasing optical basicity of the glasses. However, exceptions from this rule are again the strontium, barium and potassium alumino silicate glasses. Depending on the atomic radii of the network modifying ions, these glasses show a much higher fluorescence lifetime despite of their relatively high refractive indices and high optical basicities. Fluorescence spectra as well as decay curves indicate a massive change in the local surroundings of the doped rare earth ions for these glasses.

Acknowledgment

This work was supported by the European Social Fund (ESF) through the Thuringian Ministry of Economy, Employment and Technology (Project Number 2011 FGR 0122).

References

[1] S. Kuhn, A. Herrmann, J. Hein, M.C. Kaluza, C. Rüssel, Sm^{3+}-doped La_2O_3–Al_2O_3–SiO_2-glasses – structure, fluorescence and thermal expansion, J. Mater. Sci. 48 (2013) 8014–8022, http://dx.doi.org/10.1007/s10853-013-7613-1.
[2] D. Litzkendorf, S. Grimm, K. Schuster, et al., Study of lanthanum aluminum silicate glasses for passive and active optical fibers, Int. J. Appl. Glass Sci. 3 (2012) 321–331.
[3] A. Herrmann, S. Kuhn, M. Tiegel, C. Rüssel, J. Körner, D. Klöpfel, J. Hein, M.C. Kaluza, Structure and fluorescence properties of ternary alumino silicate glasses doped with samarium and europium, J. Mater. Chem. C 2 (2014) 4328–4337.
[4] M. Tiegel, S. Kuhn, A. Herrmann, C. Rüssel, J. Körner, D. Klöpfel, R. Seifert, J. Hein, M.C. Kaluza, Fluorescence and thermal stress properties of Yb^{3+}-doped alumino silicate glasses for ultra high peak power laser applications, Laser Phys. Lett. (in preparation).
[5] M. Sheik-Bahae, E.W. Van Stryland, Optical nonlinearities in the transparency region of bulk semiconductors, Nonlinear Opt. Semicond. 58 (1999) 257–318.
[6] T. Töpfer, J. Hein, J. Philipps, D. Ehrt, R. Sauerbrey, Tailoring the nonlinear refractive index of fluoride-phosphate glasses for laser applications, Appl. Phys. B 71 (2000) 203–206.
[7] G. Blasse, B.C. Grabmaier, Luminescent Materials, Springer, Berlin and New York, 1994.
[8] W. Carnall, P. Fields, K.J. Rajnak, Chem. Phys. 49 (1968) 4424–4442, http://dx.doi.org/10.1063/1.1669893.
[9] F.S. Richardson, J.D. Saxe, S.A. Davis, T.R. Faulkner, Mol. Phys. 42 (1981) 1401–1429.
[10] D. Ehrt, H.T. Vu, A. Herrmann, G. Völksch, Luminescent ZnO–Al_2O_3–SiO_2 glasses and glass ceramics, Adv. Mater. Res. 39 (40) (2008) 231–236.
[11] G. Qian, M. Nikl, J. Bei, J. Pejchal, S. Baccaro, R. Giorgi, A. Cecilia, G. Chen, Temperature dependence of photoluminescence in ZnO-containing glasses, Opt. Mater. 30 (2007) 91–94.
[12] G. Chen, M. Nikl, N. Solovieva, A. Beitlerova, J. Rao, Y. Yang, Y. Zhang, X. Jiang, C. Zhu, Photoluminescent properties of nanocrystallized zinc borosilicate glasses, Radiat. Meas. 38 (2004) 771–774.
[13] D. Ehrt, Photoluminescence in the UV–VIS region of polyvalent ions in glasses, J. Non-Cryst. Solids 348 (2004) 22–29.
[14] L. Jyothi, V. Venkatramu, P. Babu, C.K. Jayasankar, M. Bettinelli, G. Mariotto, A. Speghini, Composition and concentration dependence of spectroscopic properties of Nd^{3+}-doped tellurite and metaborate glasses, Opt. Mater. 33 (2011) 928–936.
[15] M. Tiegel, A. Herrmann, C. Rüssel, J. Körner, D. Klöpfel, J. Hein, M.C. Kaluza, Magnesium aluminosilicate glasses as potential laser host material for ultrahigh power laser systems, J. Mater. Chem. C 1 (2013) 5031–5039, http://dx.doi.org/10.1039/c3tc30761a.
[16] M.P. Hehlen, N.J. Cockroft, T.R. Gosnell, A.J. Bruce, Spectroscopic properties of Er^{3+}- and Yb^{3+}-doped soda–lime silicate and aluminosilicate glasses, Phys. Rev. B 56 (1997) 9302–9318.
[17] A.F. Hollemann, E. Wieberg, Lehrbuch der Anorganischen Chemie, de Gruyter, Berlin and New York, 1995.
[18] E.M. Purcell, Spontaneous emission probabilities at radio frequencies, Phys. Rev. 69 (1946), http://dx.doi.org/10.1103/PhysRev. 69.674.2. 674–674.
[19] R.J. Glauber, M. Lewenstein, Quantum optics of dielectric media, Phys. Rev. A 43 (1991) 467–491.
[20] P. de Vries, A. Lagendijk, Resonant scattering and spontaneous emission in dielectrics: microscopic derivation of local-field effects, Phys. Rev. Lett. 81 (1998) 1381–1384.
[21] M.E. Crenshaw, C.M. Bowden, Effects of local fields on spontaneous emission in dielectric media, Phys. Rev. Lett. 85 (2000) 1851–1854, http://dx.doi.org/10.1103/PhysRevLett. 85.1851.
[22] P.R. Berman, P.W. Milonni, Microscopic theory of modified spontaneous emission in a dielectric, Phys. Rev. Lett. 92 (2004) 0536011–0536014, http://dx.doi.org/10.1103/PhysRevLett. 92.053601.
[23] M.E. Crenshaw, The quantized field in a dielectric and application to the radiative decay of an embedded atom, Phys. Lett. A 358 (2006) 438–442, http://dx.doi.org/10.1016/j.physleta.2006.05.049.
[24] C.-K. Duan, M.F. Reid, Z. Wang, Local field effects on the radiative lifetime of emitters in surrounding media: virtual- or real-cavity model?, Phys Lett. A 343 (2005) 474–480, http://dx.doi.org/10.1016/j.physleta.2005.06.037.
[25] D. Toptygin, Effects of the solvent refractive index and its dispersion on the radiative decay rate and extinction coefficient of a fluorescent solute, J. Fluoresc. 13 (2003) 201–219.
[26] A. Herrmann, S. Fibikar, D. Ehrt, Time-resolved fluorescence measurements on Eu^{3+}- and Eu^{2+}-doped glasses, J. Non-Cryst. Solids 355 (2009) 2093–2101.
[27] J.A. Duffy, A review of optical basicity and its applications to oxidic systems, Geochim. Cosmochim. Acta 57 (1993) 3961–3970.
[28] V. Dimitrov, T. Komatsu, An interpretation of optical properties of oxides and oxide glasses in terms of the electronic ion polarizability and average single bond strength, J. Univ. Chem. Technol. Metall. 45 (2010) 219–250.

5.5. [MT5] Spectroscopic properties of cerium-doped aluminosilicate glasses

Andreas Herrmann, Hosam A. Othman, Achraf A. Assadi, Mirko Tiegel, Stefan Kuhn, Christian Rüssel

Optical Materials Express, 5 (2015) 720-732, DOI: 10.1364/OME.5.000720

	Dr. Andreas Herrmann	Dr. Hosam A. Othman	Achraf A. Assadi	Mirko Tiegel	Stefan Kuhn	Prof. Dr. Christian Rüssel
Konzeption des Forschungsansatzes	☒	☒	☐	☒	☒	☒
Planung der Untersuchungen	☒	☒	☒	☒	☐	☐
Datenerhebung	☒	☒	☒	☒	☒	☐
Datenanalyse und -interpretation	☒	☒	☒	☒	☐	☐
Schreiben des Manuskripts	☒	☒	☐	☒	☒	☒
Vorschlag Anrechnung Publikationsäquivalente				0,75		

Spectroscopic properties of cerium-doped aluminosilicate glasses

Andreas Herrmann,[1] Hosam A. Othman,[2] Achraf A. Assadi,[3] Mirko Tiegel,[1] Stefan Kuhn[1] and Christian Rüssel[1]

[1]*Otto Schott Institut für Materialforschung, Jena University, Fraunhoferstr. 6, 07743 Jena, Germany*
[2]*Faculty of Science, Menoufia University, Shibin el-Kom, Egypt*
[3]*Laboratoire Géoressources, Matériaux, Environnement et Changements Globaux, Faculty of Sciences of Sfax, Sfax University, 3018 Sfax, Tunisia*
[*]*Andreas.Herrmann@uni-jena.de*

Abstract: The spectroscopic properties of cerium ions in various aluminosilicate glasses modified by Mg^{2+}, Ca^{2+}, Ba^{2+} and Na^{+} were investigated in order to optimize these for the potential utilization as Ce^{3+}/Yb^{3+} quantum cutting material. An increasing optical basicity of the glasses results in a shift in the peak position of the 5d-4f emission of Ce^{3+} to longer wavelengths and in a decrease in the Ce^{3+} fluorescence intensity due to decreasing Ce^{3+}/Ce^{4+} ratios. Argon-bubbling of the melt and supplying argon as melting atmosphere and/or using small amounts of metallic aluminum powder as raw material led to an almost complete reduction of Ce^{4+} to Ce^{3+}. This resulted in much higher intensities of the Ce^{3+} fluorescence emission which runs parallel to a decreasing charge transfer absorption of Ce^{4+}. From the absorption spectra of these samples extinction coefficients for Ce^{4+} and Ce^{3+} were calculated. For this purpose, an additional sample was prepared by using oxygen bubbling of the melt. An increasing cerium concentration shifts the Ce^{3+} emission peak position to longer wavelengths, while up to $2 \cdot 10^{20}$ ions per cm^3 only a slight increase in the Ce^{3+} emission intensity was observed. At higher dopant concentrations, a drastic decrease in the Ce^{3+} fluorescence emission is observed which is most likely attributed to an increasing Ce^{4+} concentration. High intensity Ce^{3+} blue emission matching the spectroscopic requirements for potential quantum cutting in Ce^{3+}/Yb^{3+} codoped glasses could be achieved with a barium aluminosilicate glass.

OCIS codes: (160.2540) Fluorescent and luminescent materials; (160.2750) Glass and other amorphous materials; (160.4670) Optical materials; (160.5690) Rare-earth-doped materials.

References and links

1. J. Chen, H. Guo, Z. Li, H. Zhang, and Y. Zhuang, "Near-infrared quantum cutting in Ce^{3+}, Yb^{3+} co-doped YBO_3 phosphors by cooperative energy transfer," Opt. Mater. **32**(9), 998–1001 (2010).
2. H. Zhang, J. Chen, and H. Guo, "Efficient near-infrared quantum cutting by Ce^{3+}-Yb^{3+} couple in $GdBO_3$ phosphors," J. Rare Earths **29**(9), 822–825 (2011).
3. S. F. Zou, Z. L. Zhang, F. Zhang, and Y. L. Mao, "High efficient quantum cutting in Ce^{3+}/Yb^{3+} co-doped oxyfluoride glasses," J. Alloy. Comp. **572**, 110–112 (2013).
4. T. Förster, "Experimentelle und theoretische Untersuchung des zwischenmolekularen Übergangs von Elektronenanregungsenergie," Z. Naturforschung **4a**, 321–327 (1949).
5. D. L. Dexter, "A theory of sensitized luminescence in solids," J. Chem. Phys. **21**(5), 836–850 (1953).
6. P. Vergeer, T. J. H. Vlugt, M. H. F. Kox, M. I. den Hertog, J. P. J. M. van der Eerden, and A. Meijerink, "Quantum cutting by cooperative energy transfer in $Yb_xY_{1-x}PO_4$:Tb^{3+}," Phys. Rev. B **71**(1), 0141901 (2005).
7. D. L. Dexter, "Cooperative optical absorption in solids," Phys. Rev. **126**(6), 1962–1967 (1962).
8. M. Tiegel, A. Herrmann, S. Kuhn, C. Rüssel, J. Körner, D. Klöpfel, R. Seifert, J. Hein, and M. C. Kaluza, "Fluorescence and thermal stress properties of Yb^{3+}-doped alumino silicate glasses for ultra high peak power laser applications," Laser Phys. Lett. **11**(11), 115811 (2014).
9. H. Scholze, *Glass - Nature, Structure, and Properties* (Springer, 1991).

#231149 - $15.00 USD Received 22 Dec 2014; revised 3 Feb 2015; accepted 3 Feb 2015; published 9 Mar 2015

10. A. Herrmann, S. Kuhn, M. Tiegel, C. Rüssel, J. Körner, D. Klöpfel, J. Hein, and M. C. Kaluza, "Structure and Fluorescence Properties of Ternary Alumino Silicate Glasses doped with Samarium and Europium," J. Mater. Chem. C **2**(21), 4328–4337 (2014).
11. J. E. Ritter, Jr. and C. L. Sherburne, "Dynamic and Static Fatigue of Silicate Glasses," J. Am. Ceram. Soc. **54**(12), 601–605 (1971).
12. M. Tiegel, A. Herrmann, C. Rüssel, J. Körner, D. Klöpfel, J. Hein, and M. C. Kaluza, "Magnesium aluminosilicate glasses as potential laser host material for ultrahigh power laser systems," J. Mater. Chem. C **1**(33), 5031–5039 (2013).
13. A. Paul and R. W. Douglas, "Cerous Ceric Equilibrium in Binary Alkali Borate and Alkali Silicate Glasses," Phys. Chem. Glasses **6**, 212–215 (1965).
14. H. D. Schreiber, H. V. Lauer, Jr., and T. Thanyasiri, "The redox state of cerium in basaltic magmas: an experimental study of iron-cerium interactions in silicate melts," Geochim. Cosmochim. Acta **44**(10), 1599–1612 (1980).
15. V. Gottardi, G. Paoletti, and M. Tornati, "The ratio Ce3+/Ce4+ in the melting of different glasses and its influence on their properties," Advances in Glass Technology, VI International Congress in Glass, Washington D.C. 412–423 (1962).
16. W. D. Johnston, "Oxidation-Reduction Equilibria in Molten Na_2O $2SiO_2$ Glass," J. Am. Ceram. Soc. **48**(4), 184–190 (1965).
17. A. Paul, M. Mulholland, and M. S. Zaman, "Ultraviolet absorption of cerium(Ill) and cerium(IV) in some simple glasses," J. Mater. Sci. **11**(11), 2082–2086 (1976).
18. J. Mendham, R. C. Denney, J. D. Barnes, and M. J. K. Thomas, *Vogel's Quantitative Chemical Analysis (6th ed.)*, (Pearson Education Limited: Harlow, 2000).
19. D. J. Smythe, J. M. Brenan, N. R. Bennett, T. Regier, and G. S. Henderson, "Quantitative determination of cerium oxidation states in alkali-aluminosilicate glasses using M4,5-edge XANES," J. Non-Cryst. Solids **378**, 258–264 (2013).
20. A. M. Efimov, N. V. Nikonorov, A. I. Ignatiev, and E. S. Postnikov, "Quantitative UV–VIS spectroscopic studies of photo-thermo-refractive glasses. II. Manifestations of Ce^{3+} and Ce(IV) valence states in the UV absorption spectrum of cerium-doped photo-thermo-refractive matrix glasses," J. Non-Cryst. Solids **361**, 26–37 (2013).
21. H. Ebendorff-Heidepriem and D. Ehrt, "Formation and UV absorption of cerium, europium and terbium ions in different valencies in glasses," Opt. Mater. **15**(1), 7–25 (2000).
22. S. E. Paje, M. A. García, M. A. Villegas, and J. Llopis, "Cerium doped soda-lime-silicate glasses: effects of silver ion-exchange on optical properties," Opt. Mater. **17**(4), 459–469 (2001).
23. A. M. Efimov, A. I. Ignatev, N. V. Nikonorov, and E. S. Postnikov, "Spectral components that form UV absorption spectrum of Ce^{3+} and Ce(IV) valence states in matrix of photothermorefractive glasses," Opt. Spectrosc. **111**(3), 426–433 (2011).
24. M.-L. Brandily-Anne, J. Lumeau, L. Glebova, and L. B. Glebov, "Specific absorption spectra of cerium in multicomponent silicate glasses," J. Non-Cryst. Solids **356**(44-49), 2337–2343 (2010).
25. P. Dorenbos, "5d-level energies of Ce^{3+} and the crystalline environment. III. Oxides containing ionic complexes," Phys. Rev. B **64**(12), 125117 (2001).
26. P. Dorenbos, "Relating the energy of the [Xe]5*d*1 configuration of Ce^{3+} in inorganic compounds with anion polarizability and cation electronegativity," Phys. Rev. B **65**(23), 2351101–2351106 (2002).
27. J. A. Duffy, "A review of optical basicity and its applications to oxidic systems," Geochim. Cosmochim. Acta **57**(16), 3961–3970 (1993).
28. V. Dimitrov and T. Komatsu, "An interpretation of optical properties of oxides and oxide glasses in terms of the electronic ion polarizability and average single bond strength," J. Univ. Chem. Tech. Met. **45**, 219–250 (2010).
29. N. J. Weber, "Optical spectra of Ce^{3+} and Ce^{3+}-sensitized fluorescence in $YAlO_3$," J. Appl. Phys. **44**(7), 3205–3208 (1973).
30. R. Reisfeld, "Spectra and energy transfer of rare earths in inorganic glasses," Structure and Bonding **13**, 53–98 (1973).
31. G. Blasse and B. C. Grabmaier, *Luminescent Materials* (Springer, 1994).
32. A. Herrmann, S. Fibikar, and D. Ehrt, "Time-resolved fluorescence measurements on Eu^{3+}- and Eu^{2+}-doped glasses," J. Non-Cryst. Solids **355**(43-44), 2093–2101 (2009).
33. G. A. Slack, S. L. Dole, V. Tsoukala, and G. S. Nolas, "Optical absorption spectrum of trivalent cerium in Y2O3, Ba2GdTaO6, ThO2, and related compounds," J. Opt. Soc. Am. B **11**(6), 961–974 (1994).

Introduction

Cerium doped glasses are attractive materials for a broad range of applications. Cerium ions can act as sensitizer in luminescent glasses as e.g. scintillator or laser glasses, they are widely used as sensitizer in photo-thermo-refractive glasses, they are often used to decrease photo-darkening in optical fibers or as decolorizing agent for container glass. Furthermore, most white emitting LEDs are based on Ce^{3+}-doped yttrium-aluminum-garnet (YAG) phosphors which act as wavelength converter.

Recently Ce^{3+} was proposed as sensitizer ion for quantum cutting materials due to its high absorption cross section and strong fluorescence emission [1, 2]. Quantum Cutting (QC) is

#231149 - $15.00 USD Received 22 Dec 2014; revised 3 Feb 2015; accepted 3 Feb 2015; published 9 Mar 2015

the emission of two or more low energy photons upon the absorption of one high energy photon. This effect attained great attention due to its potential utilization in the improvement of photonic materials. Efficient NIR QC in an UV excited photonic material will result in quantum efficiencies higher than unity and therefore increase the quantum yield of these materials. Possible applications are e.g. the improvement of solar cells or wavelength converters for optical sensors. Up to now mostly crystalline quantum cutting materials are described in literature, but lately S. F. Zou et al. have shown that QC is also possible in glasses [3]. To achieve QC, Ce^{3+}-Yb^{3+} codoping in oxyfluoride glasses has been used in this case. For energy transfer between fluorophores, the transfer efficiency mainly depends on the spectral overlap of the emission spectrum of the sensitizer ion and the absorption spectrum of the acceptor ion [4, 5]. In principle this is also valid for energy transfer in QC materials [6], but here the self-convoluted absorption spectrum of the acceptor ion has to be used [7]. However, the spectral overlap between sensitizer and acceptor ion was not high in Ref. [3]. A further optimization of the spectral overlap should increase the efficiency of the quantum cutting material. This can be achieved by the variation of the chemical composition of the host glass since the transitions involved in the Ce^{3+} fluorescence are parity allowed 4f-5d electric dipole transitions which are strongly dependent on the local surrounding of the Ce^{3+} sites. This is not only the reason of the strong absorption and emission of Ce^{3+} but also allows the shift of the Ce^{3+} absorption and emission spectra over a very broad spectral range. An optimal QC energy transfer from Ce^{3+} to Yb^{3+} should be obtained if the Ce^{3+} emission wavelength matches with twice the energy of the Yb^{3+} absorption in the same host [6, 7], which is about 465 nm in aluminosilicate glasses [8]. Aluminosilicate glasses are very promising host matrices for utilization of this effect since they offer chemical stability over an exceptionally broad compositional range [e.g 9, 10]. Furthermore they offer a high chemical durability, high mechanical strength, high rare earth solubility, relatively small coefficients of thermal expansion and low production costs [e.g 8–12].

Besides the spectroscopic properties of the Ce^{3+} doped host material also the red-ox state of the cerium ions is crucial for its utilization as QC sensitizer. As a polyvalent ion cerium might occur in glasses as Ce^{3+} and Ce^{4+}. The ratio of the concentrations of these two oxidation states mainly depends on the composition of the glass [13, 14], the oxygen activity of the melt which might also be affected by the furnace atmosphere [14–16] and the temperature of melting [14, 16, 18]. As in the case of all other polyvalent ions, also Ce^{3+} and Ce^{4+} form an equilibrium with the physically dissolved oxygen of the melt according to $4\ Ce^{3+} + O_2 \leftrightarrow 4\ Ce^{4+} + 2\ O^{2-}$. The equilibrium is shifted to Ce^{3+} with increasing temperature, decreasing basicity and the application of reducing melting conditions. In principle, the equilibrium constants of redox reactions can be determined by equilibration experiments [18] or, however, using electrochemical measurements. Smythe et al. presented a calibration method for the quantitative determination of Ce^{3+}/Ce^{4+}-ratios in alkali-aluminosilicate glasses using Ce $M_{4,5}$-edge X-ray absorption near edge structure (XANES) spectroscopy [19]. It was further tried to separate the Ce^{3+} and Ce^{4+} absorption bands by spectroscopic methods [17, 20–24]. This is difficult since Ce^{3+} and Ce^{4+} ions both show broad-band and largely overlapping near UV absorption. Furthermore, up to now a clear evidence of any Ce^{4+} fluorescence emission has not been found, which could help to separate the absorption bands via fluorescence excitation measurements. However, only one of these workgroups applied reducing and oxidizing melting conditions to enable a clear separation of the Ce^{3+} and Ce^{4+} absorption bands [21]. Since this work was done in phosphate and fluoride phosphate glasses of relatively low optical basicity, and low melting temperature only small amounts of Ce^{4+} could be obtained.

For effective Ce^{3+}-Yb^{3+} quantum cutting, glasses of relatively high optical basicity have to be used. In these materials, the co-existence of Ce^{4+} which has an extremely strong and broad charge transfer transition would dramatically decrease the absorption of UV photons by Ce^{3+} ions. This would result in very low Ce^{3+} emission intensities and in low quantum yields even at high energy transfer rates to the acceptor ion. Therefore a detailed knowledge of the influence of the host matrix, the melting conditions and the overall cerium concentration on

#231149 - $15.00 USD Received 22 Dec 2014; revised 3 Feb 2015; accepted 3 Feb 2015; published 9 Mar 2015

the spectral properties of Ce^{3+} and the Ce^{3+}/Ce^{4+} ratio is needed. This paper presents a systematical study on the spectral properties of Ce^{3+} and Ce^{4+} in aluminosilicate glasses, which is of particular importance for the development of QC materials as well as for the research on photo-thermo-refractive glasses.

Experimental procedure

All glasses were prepared from high purity raw materials (Fe < 10 ppm, other contaminating metals < 0.5 ppm) SiO_2 (Sipur A1, Schott, Germany), Al_2O_3 (Ceralox, Condea Chemie, Germany), MgO (Merck, Germany), $CaCO_3$ (Merck, Germany), Na_2CO_3 (Merck, Germany), and $BaCO_3$ (VK Labor- und Feinchemikalien, Germany). The batches were melted in covered platinum crucibles (non-reducing melts) or corundum crucibles (reducing melts) at temperatures in the range from 1550 to 1650°C depending on the individual glass composition. After melting for 2 h, the samples were cast into brass moulds and transferred into a muffle furnace, preheated to temperatures in the range from 720 to 920°C. Subsequently, the cooling furnace was switched off and the samples were allowed to cool (cooling rate: approximately 3 K/min).

Starting with a magnesium aluminosilicate glass, different glass compositions of increasing optical basicities have been melted. Table 1 summarizes the chemical compositions, densities and calculated optical basicities of all prepared glasses. Two series of glass samples were prepared; in the first series the cerium concentration was kept constant at $1 \cdot 10^{19}$ ions per cm^3 (about 0.04 mol% CeO_2) while varying the glass composition; for the second glass series the glass composition was kept constant (BaAS3510) while the cerium concentration was varied between $5 \cdot 10^{18}$ and $5 \cdot 10^{20}$ ions per cm^3. The samples were denoted according to their molar chemical composition. Glass samples were doped with cerium ions using CeO_2 as an additive to the raw materials.

The density of each glass sample was measured using an AccPyc 1330 pycnometer (Micromeritics, Germany). Fluorescence emission and excitation spectra were measured using a fluorescence spectrometer RF-5301PC (SHIMADZU, Japan). For these investigations, the samples were cut and polished (thickness 10 mm). Cerium excitation spectra were recorded at the wavelength of the emission peak maximum while emission spectra were obtained using the wavelength of the excitation peak maximum (spectral resolution: 0.2 nm). Optical absorption spectra were recorded using a commercial double beam spectrometer UV-3102PC (SHIMADZU, Japan) in the wavelength range of 190–3,200 nm with an error of about 1%. For these measurements, polished samples with a thickness of 0.1 to 1 mm were used.

Table 1. The compositions of all studied samples, their densities and calculated optical basicities (after: [28 and references therein]).

sample name	chemical composition (mol%)						theoretical optical basicity Λ_{th}	density
	Na_2O	MgO	CaO	BaO	Al_2O_3	SiO_2		(g/cm^3) ± 0.001
MgAS2020	0	20	0	0	20	60	0.55	2.550
CaAS3020	0	0	30	0	20	50	0.60	2.712
CaNaAS251015	10	0	25	0	15	50	0.62	2.868
CaBaAS251013	0	0	25	10	13	52	0.62	3.048
BaAS3510	0	0	0	35	10	55	0.64	3.729

#231149 - $15.00 USD Received 22 Dec 2014; revised 3 Feb 2015; accepted 3 Feb 2015; published 9 Mar 2015

Results and discussion

The effect of glass composition

Figure 1 shows the fluorescence emission and excitation spectra recorded from various glass compositions all doped with a cerium concentration of $1 \cdot 10^{19}$ ions per cm^3 which corresponds to about 0.04 mol% CeO_2 depending on the density of the glass. All curves show a pronounced maximum. The peak emission and excitation of the magnesium containing glass MgAS2020 occur at the smallest wavelengths (385 and 340 nm, respectively) while those of the barium containing glass BaAS3510 are observed at the largest wavelengths (445 and 365 nm, respectively). The intensity of the emission spectrum is largest in the magnesium containing sample MgAS2020, and decreases within the series CaAS3020, CaBaAS251013, CaNaAS251015. Within this series, a continuous decrease of the peak intensity with increasing wavelength of the peak maximum is observed. The ternary barium aluminosilicate glass is observed at the largest wavelength, however, it shows a clearly more intense fluorescence emission than the glasses CaBaAS251013 and CaNaAS251015. Obviously, glasses of larger optical basicity show emission at lower wavenumbers / larger wavelengths (see Table 1). The optical basicity is a phenomenological measure of the electron donor power of an oxidic compound. It is closely related to the polarizability of the material and can be calculated from experimentally determined or theoretically derived basicity values of the individual oxides [27]. For the calculation of the theoretical basicities of the glass compositions the averaged partial basicity values of Duffy and Lebouteiller/Courtine given in Ref. [28]. have been used. The observed dependency on the chemical composition of the glasses can be explained as follows: An increasing optical basicity of the glass composition is related to an increasing polarizability at the local rare earth sites. According to Dorenbos [25, 26] an increasing polarizability results in an increasing shift of the $5d^1$ energy level of Ce^{3+} to lower energies which is equivalent to a red-shift of the absorption and emission spectra. In particular the polarizability is reported to increase in the order $Mg^{2+} < Ca^{2+} < Na^{+} < Ba^{2+}$ [25] which exactly resembles the order of the optical basicities of the respective oxides [27, 28]. The splitting of the $5d^1$ energy level has a further influence on the spectral position of the absorption/emission peaks. Stronger splitting results in an additional red shift of the spectra. The splitting is reported to be mainly dependent on the Ce^{3+} coordination number and Ce-O bond length but independent of the shift of the $5d^1$ level [25]. Hence, varying the glass composition in order to increase the optical basicity results in the desired shift to longer wavelengths of the Ce^{3+} emission as seen in Fig. 1. Furthermore, it can be seen that the Ce^{3+} emission spectra consist of two components (non-symmetrical shape of the emission spectra). This effect is due to the two $4f^1$ energy levels ($^2F_{5/2}$ and $^2F_{7/2}$) which are the final states of the fluorescence transition $5d^1 \rightarrow 4f^1$. $^2F_{5/2}$ is the ground state while the $^2F_{7/2}$ level is located at around 2,000 cm^{-1} [29] which corresponds very well to the spectra.

Figure 1 additionally includes an energy-doubled absorption spectrum of Yb^{3+} doped MgAS2020 glass (grey short-dashed line, doping concentration $1 \cdot 10^{20}$ ions per cm^3). The peak is due to the ground state ($^2F_{7/2}$) absorption of the 3-fold splitted $^2F_{5/2}$ level of the Yb^{3+} ion. Since this transition is an f-f transition it is – in contrast to the f-d transitions of Ce^{3+} – hardly affected by the glass composition [8]. Its distinctive tall peak is located at about 980 nm in aluminosilicate glasses, the broader subpeak is observed at a smaller wavelength of about 930 nm [8] (in Fig. 1 displayed at 490 and 465 nm, respectively). The largest overlap between the Ce^{3+} emission and the energy-doubled Yb^{3+} absorption in principle may be obtained by the high basicity BaAS3510 glass which shows the Ce^{3+} emission peak at around 445 nm. However, by melting under air only a relatively small fluorescence emission intensity is obtained with this glass composition.

#231149 - $15.00 USD Received 22 Dec 2014; revised 3 Feb 2015; accepted 3 Feb 2015; published 9 Mar 2015

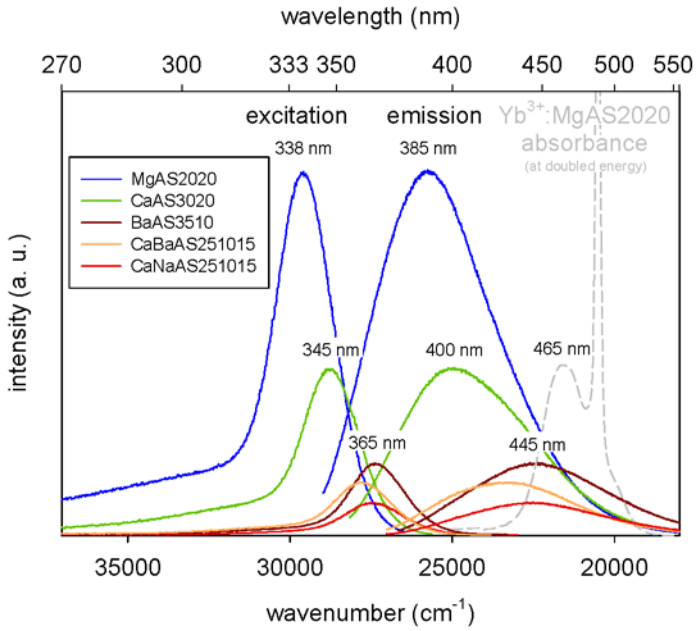

Fig. 1. Ce^{3+} excitation (left) and emission spectra (right) of various cerium doped aluminosilicate glasses of relatively high optical basicity. The grey short-dashed curve is the Yb^{3+} absorption spectrum in the MgAS2020 glass at doubled energy.

The notable decrease in Ce^{3+} fluorescence intensity of glasses with higher optical basicity is in agreement with the literature where a shift of red-ox equilibria to the higher oxidation state with increasing basicity has often been described [13, 14] (see also introduction section). Therefore under constant melting conditions, the Ce^{4+} concentration should be higher in glasses of higher optical basicity. Due to the large spectral overlap of the absorption spectra of Ce^{3+} and Ce^{4+} and the strong charge transfer absorption of Ce^{4+} more radiation is absorbed by Ce^{4+} which does not result in fluorescence emission in these glasses.

The effect of reducing melting conditions

In order to further evaluate the effect of Ce^{4+} and to increase the emission intensity of Ce^{3+} in high basicity glasses, three different reduction techniques were applied in this work: melting with argon bubbling for 1 h (curve b in Fig. 2), melting with argon bubbling for 1 h under argon atmosphere (curve c in Fig. 2) and replacing a small part of the aluminum oxide by metallic aluminum powder in the batch (curve d in Fig. 2). For the latter, 0.5 mol% of Al_2O_3 were replaced by 1 mol% Al-powder. The glass composition of the highest optical basicity BaAS3510 and a cerium doping concentration of $1 \cdot 10^{19}$ cm^{-3} were used for these experiments. In Fig. 2 the fluorescence excitation and emission spectra of the reduced samples (curves b, c, d) are compared to the unreduced sample (curve a). As expected, reduction of the melt results in an increased Ce^{3+} fluorescence intensity. Obviously, argon bubbling under air only slightly decreased the Ce^{4+} concentration. Curves c and d (bubbling with argon under argon atmosphere and reducing by Al-powder respectively) show maxima which are in an almost perfect agreement. This indicates an almost complete reduction of Ce^{4+} to Ce^{3+} in both cases. Overall, the Ce^{3+} fluorescence intensity increased by a factor of about 2.4 in these two samples in comparison to the unreduced sample.

#231149 - $15.00 USD Received 22 Dec 2014; revised 3 Feb 2015; accepted 3 Feb 2015; published 9 Mar 2015

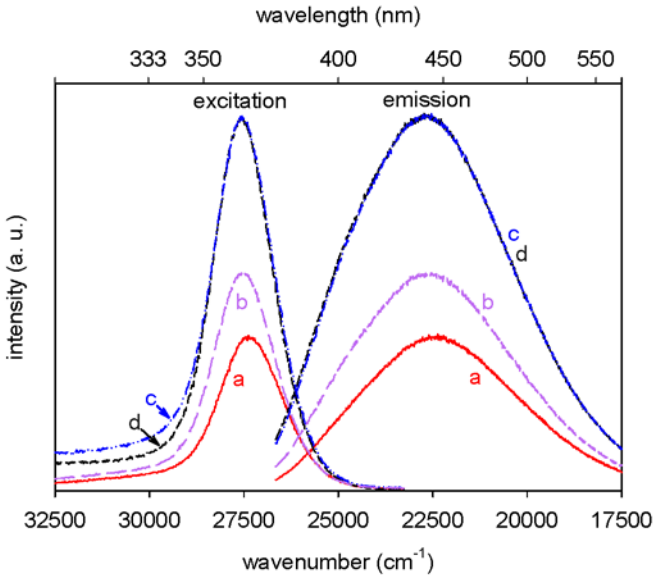

Fig. 2. Excitation (left) and emission spectra (right) of barium aluminosilicate glasses doped with $1 \cdot 10^{19}$ cerium ions/cm^3 prepared under different melting conditions a) unreduced, b) reduced by Ar bubbling, c) reduced by Ar bubbling in Ar atmosphere, and d) reduced by adding aluminum powder to the batch.

Figure 3 shows the absorption spectra of BaAS3510 glass samples doped with $1 \cdot 10^{19}$ cerium ions per cm^3, melted under reducing (long-dashed line), not reducing (full line) and oxidizing conditions (short-dashed line). For oxidation, the melt was bubbled with oxygen for 2 hours and subsequently casted without refining. An oxidized sample (oxygen bubbling) and a reduced sample (argon bubbling) of this series are shown in Fig. 4 (sample thickness 1 cm, sample size about 3 × 2 cm). Although the doping concentration is very low, the oxidized sample shows a clear yellow/brownish coloring while the reduced sample is clear and colorless.

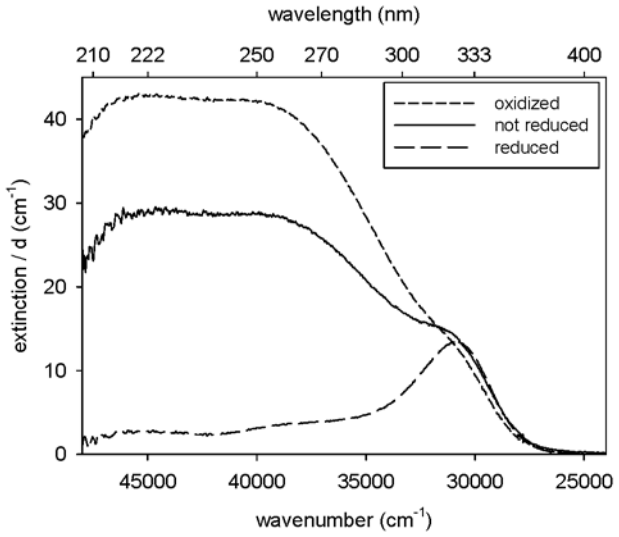

Fig. 3. UV-VIS absorption spectra of cerium doped BaAS3510 glasses ($1 \cdot 10^{19}$ ions per cm^3) prepared using reducing, non-reducing and oxidizing melting conditions. The spectra of the undoped samples (not shown) have been subtracted from the respective spectra of the cerium doped samples.

#231149 - $15.00 USD Received 22 Dec 2014; revised 3 Feb 2015; accepted 3 Feb 2015; published 9 Mar 2015

To separate the optical absorption due to Ce^{3+} and Ce^{4+} ions from the absorption of impurities, the spectra of reduced, oxidized and unreduced blank glass samples have been measured and subtracted from the respective spectra of doped samples in Fig. 3. At a wavenumber of about 31,000 cm^{-1}, the most intense Ce^{3+} absorption peak ($4f^1 \rightarrow 5d^1$) is observed which is clearly visible for the reduced and not reduced samples. For the oxidized sample, this peak is much smaller. However, since the $5d^1$ energy level of Ce^{3+} is split into 5 sublevels [21, 29–31], four more Ce^{3+} absorption bands should be visible. On the other hand, it is well known that the charge transfer transition of Ce^{4+} is also located in this spectral range (see spectra of not reduced and oxidized samples). Therefore, it is difficult to decide whether the spectrum of the reduced sample solely represents the absorption of Ce^{3+} or a superposition of transitions of both Ce^{3+} and Ce^{4+} ions in the range from 47,000 to 31,000 cm^{-1}. In Fig. 2 Ce^{3+} fluorescence spectra of two strongly reduced samples are shown which are in very good agreement, although they had been produced by completely different methods. This is a hint that the maximum possible amount of Ce^{3+} has already been achieved in theses samples. To further evaluate this assumption, samples of different cerium concentrations have been prepared with the aluminum powder reduction method. Up to a concentration of $2 \cdot 10^{20}$ cm^{-3} all these spectra have almost the same shape (not shown). Samples of higher cerium concentration could unfortunately not be measured, due to the too strong absorption of Ce^{3+}, even at a sample thickness of only 0.1 mm. From these measurements it can be concluded that the reduction potential of 1 mol% aluminum powder is sufficient to reduce the entire cerium concentration to Ce^{3+}. In fact 1 mol% CeO_2 corresponds to a concentration of about $2.5 \cdot 10^{20}$ cerium ions per cm^3 in this glass. It should further be mentioned that one mol% metallic aluminum should be sufficient to reduce 3 mol% CeO_2 ($2\ Al + 6\ CeO_2 \rightarrow Al_2O_3 + 3\ Ce_2O_3$), however, a part of the metal might also be oxidized e.g. by CO_2 from the used raw materials.

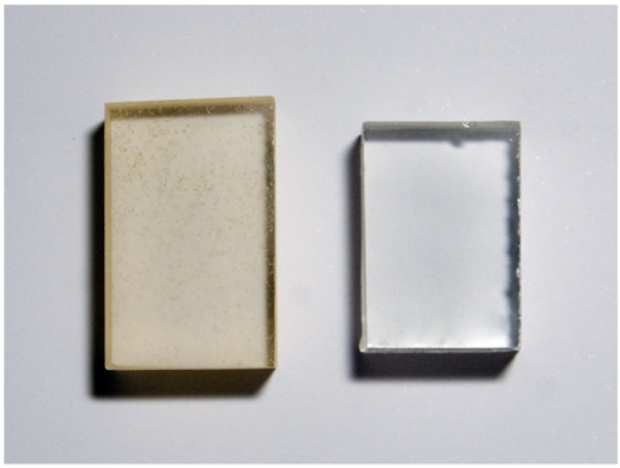

Fig. 4. An oxidized (oxygen bubbling, left) and a reduced BaAS3510 sample (argon bubbling, right). Sample thickness 1 cm, sample size about 2 × 3 cm. Overall cerium doping concentration $1 \cdot 10^{19}$ ions per cm^3. The oxidized sample clearly shows a yellow/brownish coloring.

Ebendorff-Heidepriem and Ehrt [21] also reported a complete reduction of cerium to Ce^{3+} (1.5 and $2 \cdot 10^{19}$ cm^{-3}) in phosphate and fluoride phosphate glasses by melting with the addition of sugar to the batch or by remelting the glasses in carbon crucibles under argon atmosphere. In both cases, melting temperatures of 1100 °C have been used. Johnston [16] reports that the percentage of Ce^{4+} in a sodium silicate glass could be reduced from 68 to 22% only by applying CO_2 atmosphere instead of melting in air at 1085 °C. A further hint that all of the cerium could be reduced by using the presented methods at low cerium concentrations can be found in Ref. [14]: Schreiber et al. measured the red-ox equilibria of different ions as

#231149 - $15.00 USD Received 22 Dec 2014; revised 3 Feb 2015; accepted 3 Feb 2015; published 9 Mar 2015

e.g. $Eu^{2+/3+}$, $Fe^{2+/3+}$ and $Ce^{3+/4+}$ in aluminosilicate glasses at 1500 °C. It is stated that cerium has the highest reduction potential of these ions and therefore is much easier to reduce than e.g. europium. In an earlier work on the fluorescence properties of europium, we reported an almost complete reduction of Eu^{3+} to Eu^{2+} in borosilicate glasses by using similar, strongly reducing melting conditions [32]. Although the glass composition had a lower optical basicity in that case it might be a further indirect hint that all of the cerium could be reduced to Ce^{3+} in the present experiments. However, in order to further evaluate the measured absorption spectra, they were deconvoluted using curves of Gaussian shape.

Figures 5, 6 and 7 represent three examples of deconvolution of absorption spectra of a reduced, a not reduced and an oxidized cerium doped sample respectively (BaAS3510, $1 \cdot 10^{19}$ $Ce^{3+/4+}$ cm^{-3}, also displayed in Fig. 3). Since it can be assumed that most of the cerium is reduced to Ce^{3+} in the reduced sample (Fig. 5) it has been tried to fit 5 Gaussian peaks to the spectrum since the $5d^1$ level is split up into 5 components as explained earlier. The positions of the peaks are about 30,000, 30,700, 32,000, 37,200 and 45,700 cm^{-1}. Especially the relative spectral position of the three peaks of lower energies corresponds well to literature data, e.g. 33,000, 34,500 and 36,400 cm^{-1} in $YAlO_3$ [29]. The peak positions of the two peaks observed at higher energies of about 37,200 and 45,700 cm^{-1} still fit relatively well (41,900 and 45,500 cm^{-1} [29]). Similar Ce^{3+} f-d band positions are also reported for borax glasses [30]. In phosphate and fluoride phosphate glasses, the band positions are reported to be more equally distributed between 34,000 and 49,000 cm^{-1} [21]. However, Ce^{3+} band positions and line widths can be much different for different host materials [21, 25, 26, 29, 30, 33]. Furthermore, especially for the high energy band, the reliability of the measurements and fits is relatively low since in this spectral range also the absorption of the glass matrix is observed. In addition, here the charge transfer absorption of Ce^{4+} is located, which consists of 2 bands [21, 23]. Therefore, also a superposition of Ce^{4+} and Ce^{3+} absorption bands could be observed here, which cannot be separated clearly.

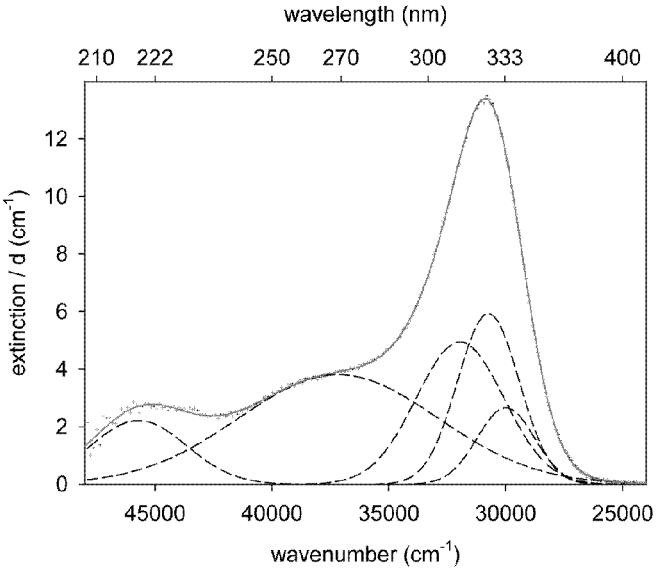

Fig. 5. Example of deconvolution of the optical absorption spectrum of a cerium doped BaAS3510 sample ($1 \cdot 10^{19}$ ions per cm^3) melted under reducing conditions. All five peaks are attributed to Ce^{3+}.

Figure 6 shows the deconvolution of the absorption spectrum of the unreduced sample. As can be seen the absorption at wavenumbers above 35,000 cm^{-1} strongly increased in intensity. To separate the absorption bands of Ce^{4+} and Ce^{3+} in this spectrum, the bands of Ce^{3+} obtained from the deconvolution in Fig. 5 have been added at the same spectral positions.

#231149 - $15.00 USD Received 22 Dec 2014; revised 3 Feb 2015; accepted 3 Feb 2015; published 9 Mar 2015

Then two more peaks at higher energies have been added which resemble the 2 band absorption of Ce^{4+}. While keeping the positions, relative intensities and shape of the five assumed Ce^{3+} peaks constant, it has been tried to fit the two additional Ce^{4+} peaks to the spectrum. This approach worked reasonably well. Under the assumption that the reduced sample (Fig. 5) contains solely Ce^{3+}, a molar extinction coefficient of 807 $l \cdot mol^{-1} \cdot cm^{-1}$ for Ce^{3+} at a wavelength of 324 nm was calculated. Using this result, the deconvolution shown in Fig. 6 furthermore enables to calculate the extinction coefficient of Ce^{4+}. According to the fit, the intensity of the Ce^{3+} peak decreased to 67% in comparison to the reduced sample. In turn this means that the Ce^{4+} concentration in the not reduced sample is $0.33 \cdot 10^{19}$ cm^{-3} and a molar extinction coefficient of 4,627 $l \cdot mol^{-1} \cdot cm^{-1}$ can be calculated for Ce^{4+} at 250 nm in this sample. In the same way the extinction coefficient of Ce^{4+} can also be calculated from the absorption spectrum of the oxidized sample (Fig. 7). Here, a Ce^{4+} concentration of $0.53 \cdot 10^{19}$ cm^{-3} and an extinction coefficient of 4,843 $l \cdot mol^{-1} \cdot cm^{-1}$ at 250 nm was calculated. These results are summarized in Table 2. The relative difference of less than 5% for these two calculations proves, that the assumptions that the reduced sample (Fig. 5) only contains Ce^{3+} and the Ce^{3+} extinction coefficient is about 807 $l \cdot mol^{-1} \cdot cm^{-1}$ are justified. The average value of these two molar extinction coefficient values is 4,735 $l \cdot mol^{-1} \cdot cm^{-1}$. However, it must be pointed out that the relative intensities of the two Ce^{4+} peaks are obviously not the same in the two deconvolutions shown in Figs. 6 and 7. In analogy, a slight difference in the peak positions of these two peaks in both deconvolutions is observed. From the absorption spectra reported by Ebendorff-Heidepriem and Ehrt [21], a molar extinction coefficient of about 710 $l \cdot mol^{-1} \cdot cm^{-1}$ at 290 nm can be deduced for Ce^{3+} in a phosphate glass, and a value of about 470 $l \cdot mol^{-1} \cdot cm^{-1}$ at 265 nm for a fluoride phosphate glass. Especially the value for the phosphate glass is fairly close to our result. However, the reported extinction coefficients for Ce^{4+} are much lower than in the glasses presented here (2,230 and 720 $l \cdot mol^{-1} \cdot cm^{-1}$ for phosphate and fluoride phosphate glass respectively). This might be a hint that not all cerium occurred as Ce^{3+} in those samples; most likely due to the much lower melting temperature of these glass compositions.

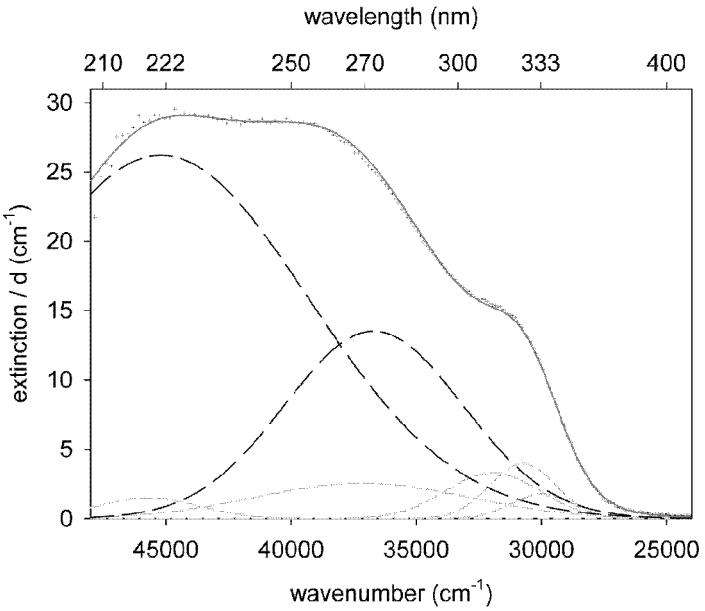

Fig. 6. Example of deconvolution of the optical absorption spectrum of a cerium doped BaAS3510 sample ($1 \cdot 10^{19}$ ions per cm^3) melted under not reducing conditions. The five short-dashed grey peaks are attributed to Ce^{3+} (see Fig. 5), while the two long-dashed black peaks represent the two-band Ce^{4+} absorption.

#231149 - $15.00 USD Received 22 Dec 2014; revised 3 Feb 2015; accepted 3 Feb 2015; published 9 Mar 2015

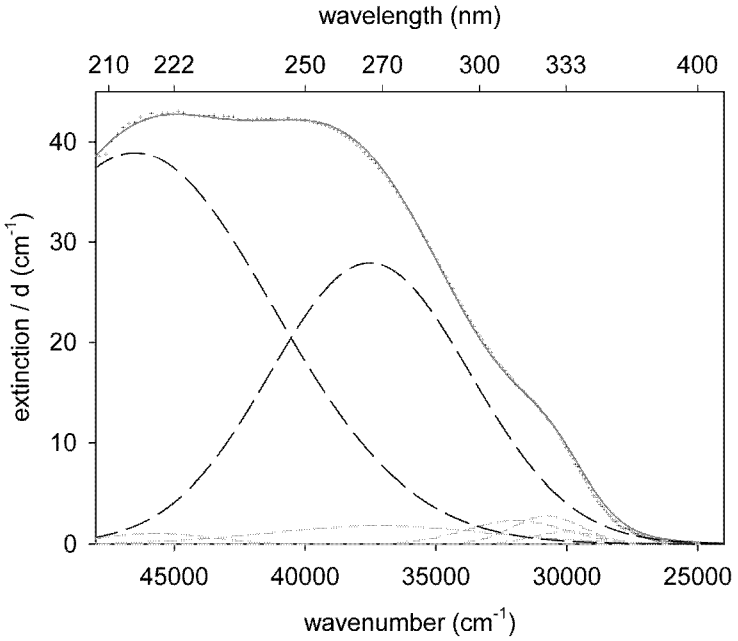

Fig. 7. Example of deconvolution of the optical absorption spectrum of a cerium doped BaAS3510 sample ($1 \cdot 10^{19}$ ions per cm^3) melted under oxidizing conditions. The five short-dashed grey peaks are attributed to Ce^{3+} (see Fig. 5), while the two long-dashed black peaks represent the two-band Ce^{4+} absorption.

From Fig. 7, it is also obvious that the low energy absorption peak of Ce^{4+} extends far into the visible range resulting in the yellow/brownish coloring of this glass (left sample in Fig. 4). As a result, the following conclusions can be drawn: The extinction coefficient of Ce^{4+} can roughly be estimated to be about 6 times larger than the extinction coefficient of Ce^{3+} at their respective peak wavelengths. Due to the extremely broad Ce^{4+} absorption peak at around 37,000 cm^{-1}, the absorption spectrum of Ce^{4+} extends far into the visible range of the spectrum. Therefore the yellow/brownish coloring of the samples is due to the Ce^{4+} absorption although the peak positions of the Ce^{4+} bands are located at much higher energies than the Ce^{3+} absorption.

Table 2. Calculated molar extinction coefficients of $Ce^{3+/4+}$ at the respective peak absorption wavelengths in barium aluminosilicate glasses melted under different conditions

sample name	estimated cerium concentration (ions /cm^3)	calculated molar extinction coefficient (l / (cm·mol))	wavelength (nm)
BaAS3510 reduced	Ce^{3+}: $1 \cdot 10^{19}$	807	324
BaAS3510 not reduced	Ce^{3+}: $0.67 \cdot 10^{19}$	807	324
	Ce^{4+}: $0.33 \cdot 10^{19}$	4,843	250
BaAS3510 oxidized	Ce^{3+}: $0.47 \cdot 10^{19}$	807	324
	Ce^{4+}: $0.53 \cdot 10^{19}$	4,627	250

The effect of cerium concentration

Excitation and emission spectra of samples with different cerium concentrations are shown in Fig. 8. All of these samples are of the glass composition BaAS3510 and have been melted using 1 mol% metallic aluminum powder as reducing agent replacing 0.5 mol% of Al_2O_3 in the batch. With increasing cerium concentration, the intensities in the spectra increase while the peak position is slightly shifted towards lower wavenumbers / higher wavelengths. The

#231149 - $15.00 USD Received 22 Dec 2014; revised 3 Feb 2015; accepted 3 Feb 2015; published 9 Mar 2015

spectral shift indicates an increase of the optical basicity with increasing cerium concentration.

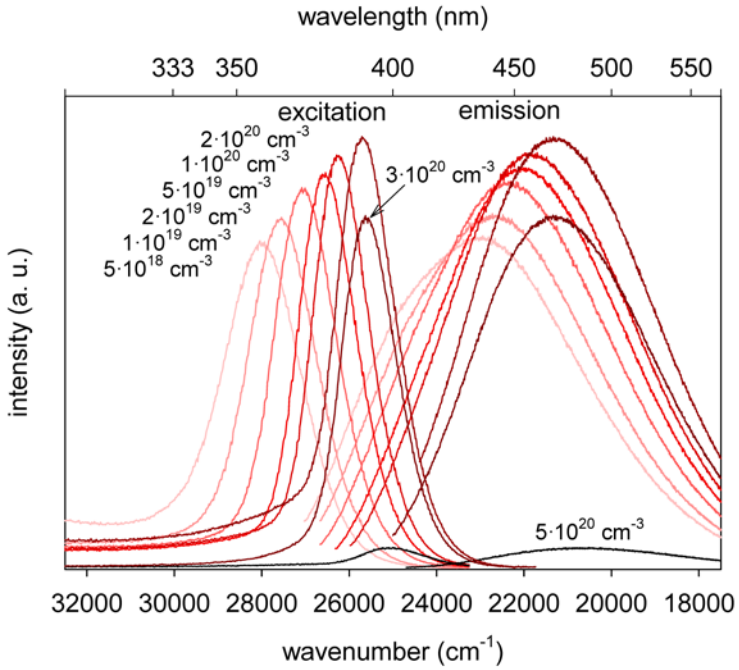

Fig. 8. Ce^{3+} excitation (left) and emission spectra (right) of BaAS3510 glasses with different cerium concentrations between $5 \cdot 10^{18}$ and $5 \cdot 10^{20}$ cm^{-3}.

The intensity increase up to a concentration of $2 \cdot 10^{20}$ ions per cm^3 can be attributed to the increasing Ce^{3+} concentration and therefore to a higher quantity of radiation centers. Nevertheless, the intensity increase is much lower than the respective Ce^{3+} concentration increase. Furthermore the above mentioned shift of the spectra due to the increasing optical basicity is much too large to be solely attributed to the relatively small increase in cerium concentration. Possibly these effects are due to clustering of the cerium ions in these glasses which would result in an increased local basicity (spectral shift) due to the high optical basicity of cerium oxide (0.65 [28]) and increased concentration quenching (non-proportional intensity increase) at the cerium sites. However, further work is needed to fully understand this effect. A further increase in the cerium concentration to $5 \cdot 10^{20}$ ions per cm^3 (about 2 mol% CeO_2) results in a drastic decrease of the emission intensity. At this point, the concentration of cerium exceeds the concentration of metallic aluminum in the batch necessary to reduce all Ce^{4+} and hence a fairly high concentration of Ce^{4+} is still present. This is supported by the color of the glass samples. While the samples with low cerium concentrations are colorless, samples of higher cerium concentration tend to be yellow/brownish. The sample with $5 \cdot 10^{20}$ cerium ions per cm^3 even appears light brown. The coloring is due to the broad charge transfer absorption band of Ce^{4+} which extends far into the visible part of the spectrum as shown earlier. Concentration quenching might play an additional role in the intensity decrease at cerium concentrations above $2 \cdot 10^{20}$ ions per cm^3.

Conclusion

The effect of the glass composition, optical basicity and melting conditions on the Ce^{3+}/Ce^{4+} ratio and the spectral properties and intensity of the Ce^{3+} fluorescence was studied in aluminosilicate glasses. In samples of high optical basicity, the Ce^{3+} excitation and emission peak positions shift towards longer wavelengths while the Ce^{3+}/Ce^{4+} ratio decreases. Increasing amounts of Ce^{4+} can efficiently hinder the excitation of Ce^{3+} due to their broad and

#231149 - $15.00 USD Received 22 Dec 2014; revised 3 Feb 2015; accepted 3 Feb 2015; published 9 Mar 2015

very intensive charge transfer absorption. The application of strongly reducing melting conditions can counteract this effect. High intensity blue emission matching the spectroscopic requirements for potential quantum cutting in Ce^{3+}/Yb^{3+} codoped glasses could be achieved with a barium aluminosilicate glass. The molar extinction coefficients of Ce^{3+} and Ce^{4+} at their respective absorption peaks were calculated to be around 807 and 4,735 $l \cdot mol^{-1} \cdot cm^{-1}$, respectively.

Acknowledgments

This work was supported by the European Social Fund (ESF) through the Thuringian Ministry of Economy, Employment and Technology (project number 2011 FGR 0122).

#231149 - $15.00 USD Received 22 Dec 2014; revised 3 Feb 2015; accepted 3 Feb 2015; published 9 Mar 2015

5.6. [MT6] Young's modulus, Vickers hardness and indentation fracture toughness of alumino silicate glasses

Mirko Tiegel; Reza Hosseinabadi; Stefan Kuhn; Andreas Herrmann; Christian Rüssel

Ceramics International, (2015), DOI: 10.1016/j.ceramint.2015.01.144

	Mirko Tiegel	Reza Hosseinabhadi	Stefan Kuhn	Dr. Andreas Herrmann	Prof. Dr. Christian Rüssel
Konzeption des Forschungsansatzes	☒	☐	☐	☒	☒
Planung der Untersuchungen	☒	☒	☐	☐	☐
Datenerhebung	☒	☒	☐	☐	☐
Datenanalyse und -interpretation	☒	☐	☐	☐	☐
Schreiben des Manuskripts	☒	☐	☒	☒	☒
Vorschlag Anrechnung Publikationsäquivalente	1,0				

ARTICLE IN PRESS

Available online at www.sciencedirect.com

ScienceDirect

Ceramics International ▮ (▮▮▮▮) ▮▮▮–▮▮▮

CERAMICS INTERNATIONAL

www.elsevier.com/locate/ceramint

Young's modulus, Vickers hardness and indentation fracture toughness of alumino silicate glasses

Mirko Tiegel*, Reza Hosseinabadi, Stefan Kuhn, Andreas Herrmann, Christian Rüssel

Otto-Schott-Institut für Materialforschung, Jena University, Fraunhoferstraße 6, 07743 Jena, Germany

Received 5 November 2014; received in revised form 28 January 2015; accepted 28 January 2015

Abstract

A wide range of alumino silicate glasses with different network modifier ions (Li, Mg, Na, Ca, Zn, La, Ba, Sr, and Pb) was prepared. The glasses were studied with respect to their mechanical properties: Poisson's ratio, Young's modulus, Vickers hardness and indentation fracture toughness. These properties were mostly affected by the field strength of network modifier ions. All determined properties increase with increasing field strength of the network modifier ions. The mixed modifier alumino silicate glasses with zinc and magnesium show a positive deviation from linearity with two maxima. Lanthanum containing glasses show larger values of mechanical properties for higher lanthanum concentrations. For magnesium alumino silicate glasses the mechanical properties get smaller with increasing SiO_2 concentration; an effect of the magnesium concentration is not observed. Furthermore, if up to 9 mol% MgO is replaced by MgF_2 the mechanical properties are not significantly affected. Compared to models predicting Young's moduli of all studied glass compositions, significant deviations are found.

Keywords: C. Mechanical properties; C. Hardness; D. Glass

1. Introduction

The mechanical properties of alumino silicate glasses are of great importance due to their numerous industrial applications, e.g. as chemically strengthened cover glasses in personal electronic devices [1], as glass for glass fiber reinforced composite materials [2], as scaffolds for bone repair [3] and for modern design purposes [4]. Recently, they have also been proposed as bulk laser materials [5,6] for high power applications. So in recent years, many models have been developed to theoretically describe the relationship between the properties and the composition of these glasses. There are commonly accepted calculation models for hardness [7] and elastic modulus [8,9], but as shown in this article, values calculated using these models differ considerably from the measured values.

Studies on the glass structure of alumino silicates with magic-angle spinning nuclear magnectic resonance (MAS-NMR) techniques [10] and molecular dynamic simulations (MD) [11,12] show that the aluminum is mostly incorporated into the glass network as $[AlO_4]^-$ tetrahedra which act as network forming species. The negative charge of $[AlO_4]^-$ tetrahedra is compensated by positively charged cations. As the formation of Al–O–Al linkages is energetically less favorable than Si–O–Al linkages, these Al–O–Al linkages scarcely occur [13] (Al/Al avoidance principle). The principle is put into perspective by investigations on Si/Al ratios much smaller than unity [14]. In peralkaline or metaluminous compositions, the ratio of aluminum to network modifier is smaller than 1. For these glasses it is assumed that *all* aluminum units form tetrahedra with 4/2 bridging-oxygen. The remaining concentrations of network modifier ions form non-bridging-oxygen sites by splitting up the Si–O–Si bridges. Hence, the average number of bridging-oxygen per network forming $[SiO_4]$ and $[AlO_4]^-$ tetrahedron BO/T can directly be calculated from the chemical composition and is a simple measurement of the connectivity and rigidity of the glasses.

Crack resistance of glass is an important mechanical property. Cook and Pharr [15] stated a lack of generality in indentation-cracking behavior due to the complexity and diversity of the indentation cracking patterns. They showed that shape and

*Corresponding author. Tel.: +493641948524.
E-mail address: mirko.tiegel@uni-jena.de (M. Tiegel).

http://dx.doi.org/10.1016/j.ceramint.2015.01.144
0272-8842/

Please cite this article as: M. Tiegel, et al., Young's modulus, Vickers hardness and indentation fracture toughness of alumino silicate glasses, Ceramics International (2015), http://dx.doi.org/10.1016/j.ceramint.2015.01.144

Table 1
Chemical compositions of the studied samples, the hereof calculated values of the mean number of bridging oxygen per network forming unit, and Poisson's ratio, ν, Young's-moduli, E, Vickers hardness, H_v, and indentation fracture toughness, K_c.

Sample	Composition (mol%)			BO/T	ν	E (GPa)	H_v (GPa)	K_c (MPa m$^{1/2}$)
	M_xO_y MF_z	Al_2O_3	SiO_2		±0.02	±3	±0.2	±0.05
Pb	20 PbO	20	60	4	0.249	77	5.58	0.59
Zn	20 ZnO	20	60	4	0.256	97	6.85	1.18
Ca	20 CaO	20	60	4	0.257	100	6.79	0.94
Li	20 Li_2O	20	60	4	0.227	83	6.18	1.01
Na	20 Na_2O	20	60	4	0.200	72	5.96	0.57
La	9 La_2O_3	21	70	3.89	0.254	103	6.95	0.97
BaMg	10 BaO; 10 MgO	20	60	4	0.250	88	6.67	0.85
CaMg	10 CaO; 10 MgO	20	60	4	0.260	95	7.02	0.97
SrMg	10 SrO; 10 MgO	20	60	4	0.251	93	6.79	0.92
ZnMg	10 ZnO; 10 MgO	20	60	4	0.249	99	7.00	1.07
Mg	20 MgO	20	60	4	0.255	102	7.15	1.16
Mg30	30 MgO	10	60	3.5	0.254	96	7.48	0.95
Mg45	45 MgO	5	50	2.67	0.281	104	7.35	0.92
Mg37	37 MgO	13	50	3.37	0.268	107	7.85	0.99
Mg15	15 MgO	14	71	3.98	0.241	91	7.34	1.08
Mg20OH	20 MgO	20	60	4	0.253	101	7.27	1.06
La20	20 La_2O_3	20	60	3.2	0.285	102	7.22	0.74
La15	15 La_2O_3	15	70	3.4	0.266	94	7.12	0.75
La16	16 La_2O_3	24	60	3.56	0.278	115	7.18	0.82
La25	25 La_2O_3	25	50	3	0.300	110	7.64	0.74
La12	12 La_2O_3	28	60	3.86	0.283	94	7.32	0.76
Zn03Mg17	3 ZnO; 17 MgO	20	60	4	0.260	102	7.42	1.75
Zn05Mg15	5 ZnO; 15 MgO	20	60	4	0.260	102	7.33	1.44
Zn15Mg05	15 ZnO; 5 MgO	20	60	4	0.260	100	7.13	1.46
Mg-F1.5	18.5 MgO; 1.5 MgF_2	20	60	4	0.258	96	7.08	1.07
Mg-F3	17 MgO; 3 MgF_2	20	60	4	0.258	103	7.17	1.09
Mg-F9	11 MgO; 9 MgF_2	20	60	4	0.247	98	7.08	1.10

sequence of a crack were strongly affected by the material parameter Young's modulus divided by hardness E/H. According to Yamane and Mackenzie [16], the resistance of a glass to deformation during indentation is a result of three distinct processes: plastic (shear) flow, densification and elastic deformation. With detailed investigations [16–19] of the densification vs. shear contribution of the indentation a better understanding of the deformation mechanism was reached. According to Kato [20] a clear correlation between the crack resistance and Vickers hardness, fracture toughness or "brittleness" cannot be found. But glasses with a larger densification around the indentation show higher crack resistance. Rouxel et al. [21,22] ascertained that the resistance of glasses toward corner cracks is related to Poisson's ratio ν. The authors distinguish between resilient glasses ($0.15 < \nu < 0.20$), semi-resilient glasses ($0.20 < \nu < 0.25$), easily damaged glasses ($0.25 < \nu < 0.33$) and highly resilient glasses ($0.33 < \nu$). Investigations on the compositional dependence of mechanical properties show deviations from linearity within mixed modifier oxide glasses. Both positive [4,23–25] and negative [4,22,26–28] deviations were found.

In this article, a simple correlation between field strength of the network modifier ions and the (measured) values for Young's modulus, Vickers hardness and indentation fracture toughness is demonstrated. For this a large variety of alumino silicate glasses with different network modifier ions has been studied. Furthermore, the influence of network modifier concentration, the addition of fluorine and the effect of mixed modifiers oxides were studied.

2. Experimental procedures

The glasses were prepared from reagent grade raw materials. The raw materials used were SiO_2 (Sipur A1, Bremthaler Quarzitwerk, Germany), Al_2O_3 (Pengda Munich, Germany), MgO (Merck, Germany), ZnO (Heubach, Germany), Li_2CO_3 (Sigma-Aldrich, USA), $La_2O_3 \cdot H_2O$ (Laborchemie Apolda, Germany), $BaCO_3$ (Reachim, USSR), $CaCO_3$ (Merck, Germany), $SrCO_3$ (Ferak, Germany), $PbCO_3$ (Merck, Germany), Na_2CO_3 (Merck, Germany), and MgF_2 (Chemiewerk Nünchritz, Germany). For the preparation of all the samples magnesium oxide and aluminum oxide were used except for the sample Mg20/OH which was prepared from magnesium carbonate hydroxide and aluminum hydroxide. The chemical compositions of the glasses calculated from the batch composition are summarized in Table 1. For alkali and alkaline earth alumino silicate glasses, the molar composition is 20 mol% network modifier oxide, 20 mol% Al_2O_3 and 60 mol% SiO_2. For the lanthanum, magnesium and zinc magnesium containing glasses, other chemical compositions have also been prepared.

Please cite this article as: M. Tiegel, et al., Young's modulus, Vickers hardness and indentation fracture toughness of alumino silicate glasses, Ceramics International (2015), http://dx.doi.org/10.1016/j.ceramint.2015.01.144

The glasses were melted in covered dispersion hardened platinum (DPH) crucibles at temperatures in the range from 1450 to 1610 °C depending on the individual glass composition for 3 h. Finally, samples were cast into preheated steel molds and transferred into a muffle furnace, preheated to temperatures in the range of 600–920 °C depending on the glass transition temperature T_g of the glasses. Subsequently, the cooling furnace was switched off and the samples were allowed to cool (cooling rate: approximately 3 K min^{-1}). Table 1 summarizes the chemical compositions of all prepared glasses. Elemental analyses of the fluorine containing glasses revealed a fluorine loss of up to 35% which apparently occurred during the melting of the glasses. This effect is well-known and has previously been described in the literature [29].

The glass transition temperatures T_g were measured by dilatometry in the temperature range of 20–1000 °C using a heating rate of 5 K min^{-1} (dilatometer DIL 402 PC, NETZSCH Gerätebau GmbH, Germany). For that purpose, cylindrical samples with a diameter of 8 mm and a length of about 20 mm had been prepared. The densities were measured using a helium pycnometer (AccuPyc 1330, Micromeritics GmbH, Germany).

Samples, which were polished at the surface, were examined for Vickers hardness (micro-hardness) using a Duramin-1 microhardness tester (Struers GmbH, Germany) and a load F of 1.96 N with a loading time of 10 s. All measurements are done at 20 °C and at relative humidity $<70\%$. Immediately after each loading the indentation was analyzed. Ten indentations in different areas of each sample were conducted in order to increase the accuracy of measurement. The hardness was calculated by the Duramin software using the following equation:

$$H_v = 1.8544\frac{F}{d^2} \quad (1)$$

where H_v is Vickers hardness, F is the supplied force, and d is the average value of the measured diagonals of the indentation mark. The standard deviations of hardness measurements were less or equal to 0.2 GPa.

In order to measure the indentation fracture toughness K_c, the indentation was done using the same equipment with a load F of 9.81 or 19.6 N. Immediately after each loading the lengths of 10 cracks were measured and the crack toughness was obtained by the following formula introduced by Anstis et al. [30]:

$$K_c = 0.016\frac{F(E/H_v)^{0.5}}{c^{1.5}} \quad (2)$$

where E is Young's modulus, H_v is the hardness and c is the average distance from the middle of the indentation to the end of the cracks. The standard deviations of the indentation fracture toughness were less or equal to ± 0.05 MPa m$^{1/2}$.

Finally, to measure Young's modulus, the ultrasound technique by Krautkrämer [31] was used. Glass samples were cut into 17–25 mm long cylinders with the same diameter of the transducer (Ø15 mm). Using the USD 15 (Krautkrämer-Branson, Austria), the longitudinal and shear (transverse) acoustic velocities were measured. In order to prevent the ultrasound to propagate in the air, the space between transducer and sample was filled with honey. Then Poisson's ratio can be obtained by using the following equation:

$$v = \frac{(1/2)c_l^2 - c_t^2}{c_l^2 - c_t^2} \quad (3)$$

where c_t is the shear (transverse) and c_l is the longitudinal velocity. Finally, the shear modulus G and Young's modulus E can be obtained with the following equation:

$$G = \rho c_t^2 \quad (5)$$

$$E = 2G(1+v) \quad (6)$$

where ρ is the density of the glass sample. The standard deviations of Young's modulus measurements were less or equal to ± 3 GPa.

3. Results and discussion

All glasses are visually transparent and clear. Elemental analyses of the fluorine substituted glasses Mg–F revealed a fluorine loss of up to 35% which apparently occurred during the melting of the glasses.

Fig. 1 shows the measured values of Poisson's ratio, Young's moduli, Vickers hardness and indentation fracture toughness in dependence of the average field strength of network modifier ions of the glass composition. The field strengths F are calculated with the following equation according to Dietzel [32]:

$$F = \frac{Z}{(r + r_{O^{2-}})^2} \quad (7)$$

where Z is the valency of the network modifier, r is the ionic radius of the network modifier (tabulated radii of sixfold-coordinated cations in Ref. [33]) and $r_{O^{2-}}$ is the radius of oxygen ions.

From the determined values of all four properties, a trend to higher values can be seen for increased field strengths of the network modifier ions. In particular, a linear dependency for Vickers hardness and a trend for Young's modulus and indentation fracture toughness can be found. Glasses with higher field strength of modifier ions, but with the same network modifier concentrations, have a more rigid structure and therefore show higher values of Poisson's ratio, hardness, Young's modulus and indentation fracture toughness.

It should be mentioned that Eq. (2) is mostly used to evaluate the indentation fracture toughness from indentations, however, also other models are reported in the literature [34]. If for example the model of Niihara [35] is used, the values of the fracture toughness are approximately 40% smaller; however, they show the same trend. This is also illustrated in Fig. 1d.

Young's modulus and indentation fracture toughness of lithium containing alumino silicate glass samples are much larger than expected from a linear correlation of Young's modulus or indentation fracture toughness versus field strength. On the other hand Young's modulus, indentation fracture toughness and hardness of lead and the lanthanum containing samples are notably smaller than expected from a linear correlation. Also zinc containing glass samples show comparatively small hardness values. DeGuire and Brown [36] have reported that the elastic properties

Please cite this article as: M. Tiegel, et al., Young's modulus, Vickers hardness and indentation fracture toughness of alumino silicate glasses, Ceramics International (2015), http://dx.doi.org/10.1016/j.ceramint.2015.01.144

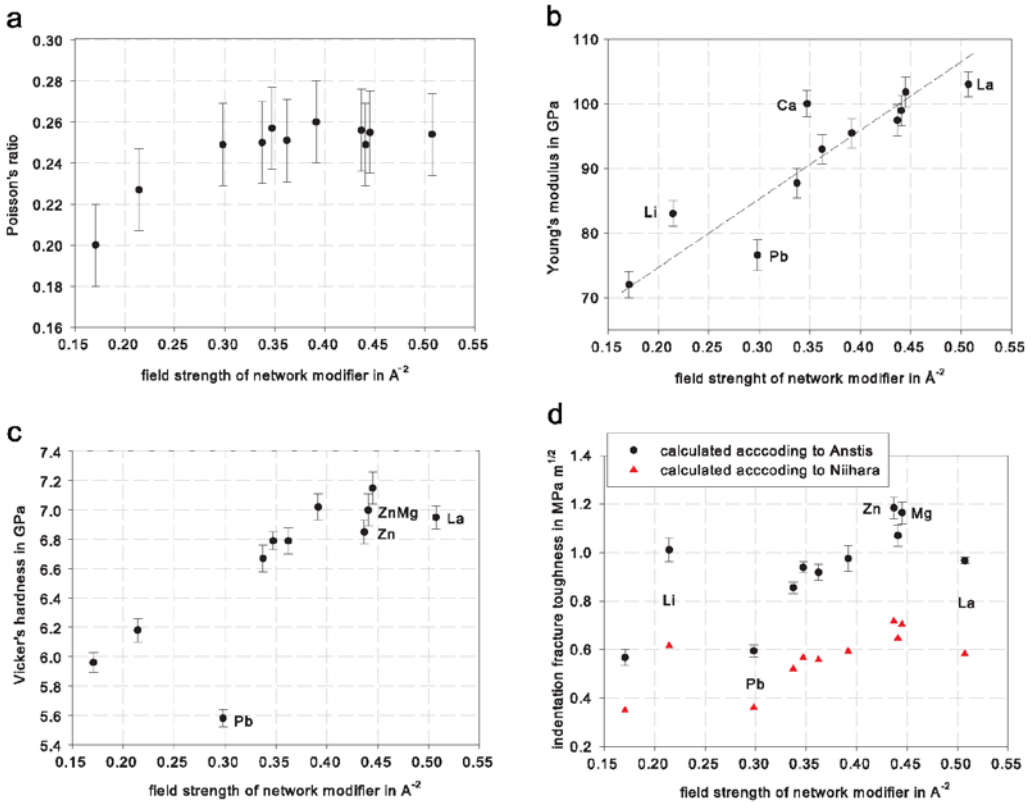

Fig. 1. Poisson's ratio (a), Young's-moduli (b), Vickers hardness (c) and indentation fracture toughness (d) of alumino silicate glasses with 20 mol% M_xO, 20 mol% Al_2O_3 and 60 mol% SiO_2 as a function of field strength of the network modifier ions.

of lithium silicate and lithium aluminosilicate glasses depend on the oxygen packaging density. In comparison to sodium and potassium containing glasses, the oxygen packing densities and Young's moduli increase, if silicon is substituted by lithium or aluminum and lithium. XPS investigations on the incorporation of lead in lead silicate glasses reported by Wang [37] show that the structural behavior of lead strongly depends on its concentration. At low lead concentrations, the metallic feature of lead will dominate and it will play the role of a network modifier. While increasing the concentration of lead, the degree of covalency of the Pb–O bonds rises and the rigidity of the glass structure increases.

The lanthanum containing aluminosilicate glass sample La has a smaller number of bridging-oxygen per network forming tetrahedron than the other alumino silicate glasses. Hence, in the case of the lanthanum containing glasses, more non-bridging-oxygen sites occur and reduce the connectivity and decrease the rigidity of the glass structure. This results in a decrease of Young's moduli, indentation fracture toughness and hardness which is discussed below for some lanthanum and magnesium aluminosilicate glass compositions. Also the properties of magnesium and zinc aluminosilicate glass composition mixtures are investigated in more detail.

In Fig. 2, the results for 6 different magnesium alumino silicate glass compositions are shown. All glasses have a ratio of magnesium oxide to aluminum oxide larger or equal to 1, therefore all samples have a peralkaline or metaluminous composition. Peralkaline compositions with more magnesium oxide than aluminum oxide have non-bridging-oxygen sites due to the excess of magnesium. The higher the excess of magnesium, the larger the number of non-bridging-oxygen sites, the lower the number of bridging-oxygen per tetrahedron (BO/T) the more pronounced is the weakening of the glass structure. In Fig. 2 the measured results are plotted against the BO/T-number, however, for Poisson's ratio, Young's modulus and hardness they do not show the expected dependence, while a general trend to higher Poisson's ratios can be found for lower BO/T-numbers; no clear correlation can be found for Young's modulus and hardness. By contrast, the indentation fracture toughness increases with a more connected structure. It can be stated that the SiO_2-concentration determines Poisson's ratio and Young's modulus of the magnesium alumino silicate glasses. The lowest modulus and Poisson's ratio has the sample Mg15 with the highest concentration of SiO_2. The highest Young's moduli and Poisson's ratios were measured for the samples Mg45 and Mg37 with the lowest concentration of SiO_2 and with the lowest number of bridging-oxygen per tetrahedron. Also the hardness values do not show a significant dependence on connectivity. The values are approximately the same (7.3 ± 0.1 GPa) except for Mg37 with a hardness of 7.8 ± 0.1 GPa. Another aspect of the glass structure of magnesium containing alumino silicate glasses has to be mentioned: according to McMillan and Kirkpatrick [38] aluminum

Please cite this article as: M. Tiegel, et al., Young's modulus, Vickers hardness and indentation fracture toughness of alumino silicate glasses, Ceramics International (2015), http://dx.doi.org/10.1016/j.ceramint.2015.01.144

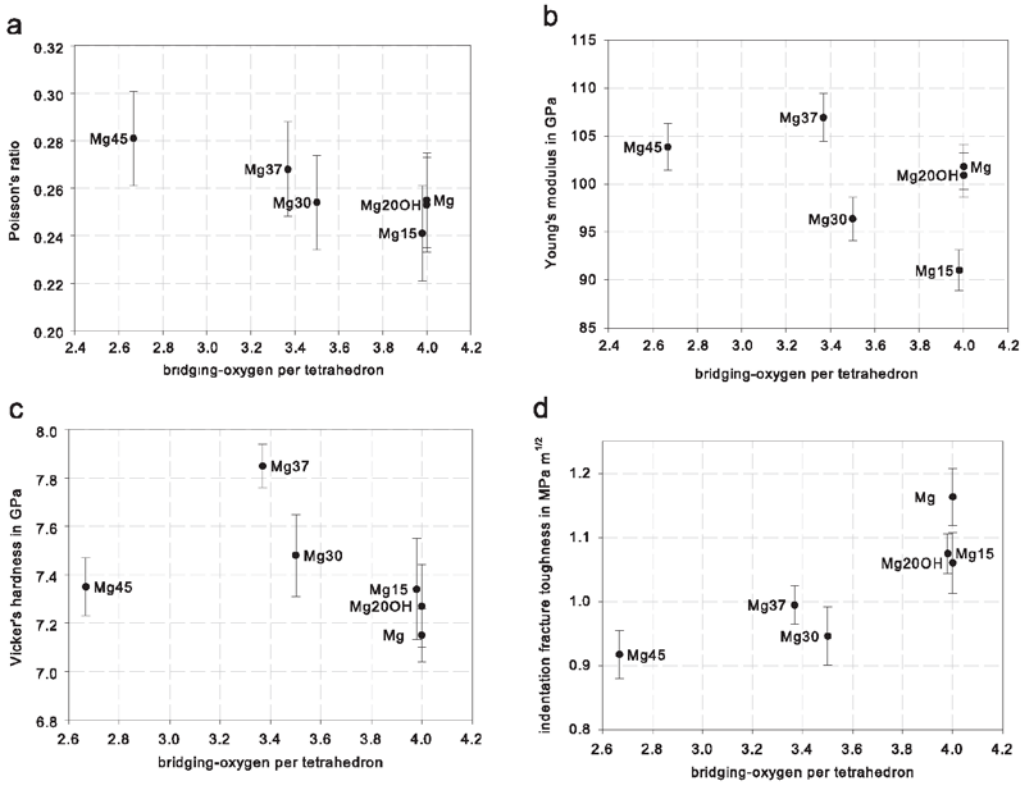

Fig. 2. Poisson's ratio (a), Young's moduli (b), Vickers hardness (c) and indentation fracture toughness (d) of magnesium alumino silicate glasses with different molar compositions as a function of the theoretically calculated bridging-oxygen per tetrahedron.

might also be present in five- and sixfold coordination in metaluminous and peralkaline magnesium containing glasses. They reported the occurrence of five- and sixfold coordinated aluminum species in mildly peraluminous magnesium alumino silicate glasses with MgO/Al_2O_3 ratio slightly larger than unity (1.1–1.2). $[AlO_5]$ and $[AlO_6]$ species will decrease the connectivity and rigidity of the glasses. Samples Mg and Mg15 possess a MgO/Al_2O_3 ratio equal to unity, nevertheless they could exhibit some aluminum with a coordination number bigger than four. That might be an explanation for their lower Young's moduli and Poisson's ratio. Smedskjaer et al. [39] reported that Young's moduli and hardness do not always run parallel. Because of the complexity of the deformation processes occurring under indentation, the hardness is not only controlled by the average bond strength, but generally by the number of rigid bonding constraints associated with the network forming species [40].

The OH-containing raw materials of Mg20/OH lead to an increase of water concentration of the resulting glass ($E/d = 3$ cm^{-1} at ≈ 2800 nm). In comparison to sample Mg ($E/d = 1$ cm^{-1} at ≈ 2800 nm) which has the same concentrations of Mg, Al and Si, Poisson's ratio, indentation fracture toughness and Young's modulus are slightly lower and the hardness higher. This could be seen as a hint to the formation of additional non-bridging-oxygen sites by OH groups which affect the connectivity of the glass structure.

Fig. 3 presents the results of the lanthanum alumino silicate glass compositions. In these lanthanum is acting as a network modifier [41,42]. All glasses are compositions with an excess of lanthanum compensating the negative charges of $[AlO_4]^-$ tetrahedra and creating non-bridging oxygen sites. The higher the excess of lanthanum, the higher is the quantity of non-bridging-oxygen sites. According to Stebbins [43], who investigated lanthanum alumino silicate glasses with triple-quantum magic-angle spinning (3QMAS) NMR techniques, small but significant quantities of five- and sixfold coordinated Al are present in the glass structure of those glasses. This is explained by the high field strength of the lanthanum (0.51 for 6-coordination). In Fig. 3 the measured mechanical properties are plotted against the BO/T-number. The values of Young's modulus vary between 94 and 115 GPa but without showing a distinct correlation with the BO/T–ratio. Poisson's ratio and hardness measurements show a trend to lower values with increasing number of bridging-oxygen per tetrahedron. This trend is disturbed by the sample La12, which has a significantly higher Vickers hardness (7.32 GPa) and Poisson's ratio (0.283). Furthermore, this sample has the highest concentration of aluminum oxide. However, all three properties show a trend to higher values with lower connectivity. The indentation fracture toughness of these lanthanum alumino silicate glasses is within the limits of error the same for all samples (0.75 MPa $m^{1/2}$). Only sample La with the lowest excess of lanthanum and the highest theoretical connectivity has a higher

Please cite this article as: M. Tiegel, et al., Young's modulus, Vickers hardness and indentation fracture toughness of alumino silicate glasses, Ceramics International (2015), http://dx.doi.org/10.1016/j.ceramint.2015.01.144

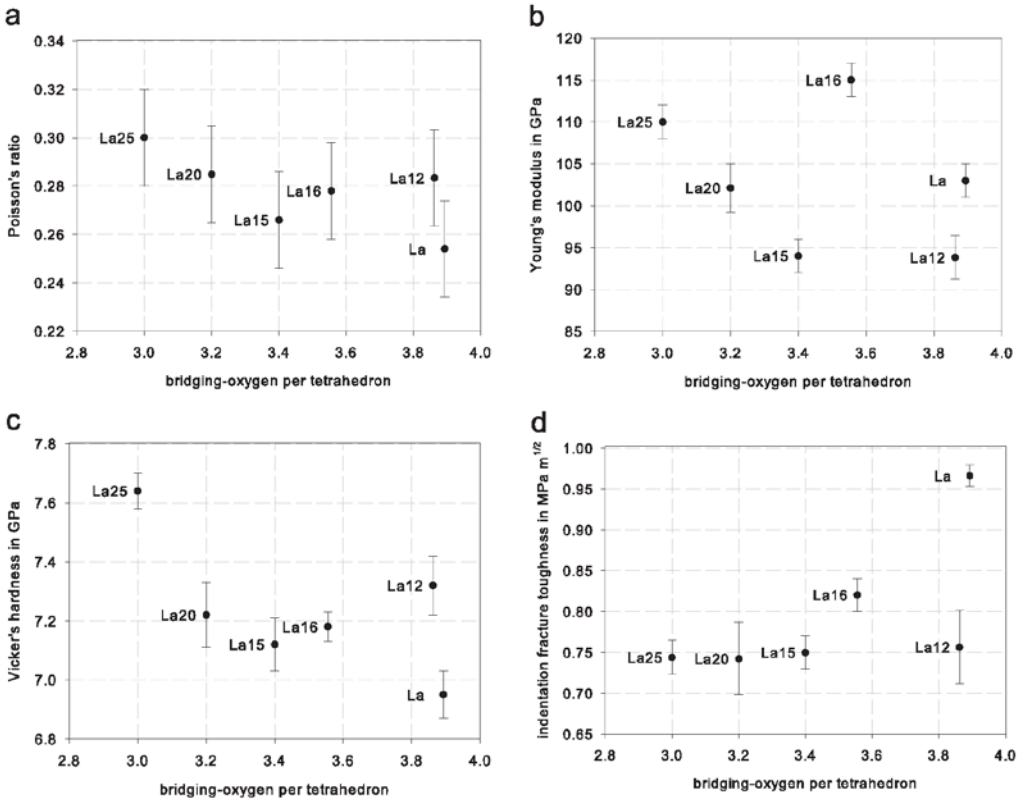

Fig. 3. Poisson's ratio (a), Young's moduli (b), Vickers hardness (c) and indentation fracture toughness (d) of lanthanum alumino silicate glasses with different molar compositions as a function of the theoretical bridging-oxygen sites per tetrahedron.

toughness of 0.97 MPa $m^{1/2}$. In comparison to the magnesium containing alumino silicate glasses, the lanthanum containing glasses have a more complex dependence of their mechanical properties on the chemical composition. This is due to the higher polarizability, larger radius and higher field strength of the lanthanum ion.

Fig. 4 shows the results for zinc magnesium alumino silicate glasses in which magnesium is replaced by zinc. All compositions have 20 mol% (MgO+ZnO), 20 mol% Al_2O_3 and 60 mol% SiO_2 and hence a theoretical network connectivity of 4 BO/T, i.e. in theory these glasses should not contain any non-bridging oxygen sites. Within this series, the alumino silicate glass solely containing magnesium has a higher Young's modulus and hardness than the alumino silicate glass containing only zinc, whereas the indentation fracture toughness is nearly the same. There are no differences in the measured values of Poisson's ratio for all magnesium and zinc alumino silicate samples. The alumino silicate glass containing equimolar concentrations of zinc and magnesium (ZnMg) has a Young's modulus and a hardness lying in between those of the pure ternary glasses. The indentation fracture toughness of ZnMg is within the error the same. Surprisingly, all other glasses with compositions between the respective pure ternary glasses and the 1 to 1 mixed glass have even higher values for all measured properties. A positive deviation from linearity is located between the pure glasses and the ZnMg glass. In the literature [44] a deviation of the materials properties from a linear function of the cationic composition is often denoted as mixed ionic effect. In this case, the mixed alkaline earth effect has already been reported especially for kinetic properties, such as diffusivity or ionic conductivity. A simple explanation for this could be the filling of interstices in the glass structure. In a glass structure, the interstices have different sizes. Smaller sites can better be filled by smaller cations, while larger cations are better incorporated in larger sites. In summary, each type of network modifying cation is incorporated in that site, it fits best. The interstices are therefore filled in a structurally more advantageous manner in mixed modifier glasses. It is concluded that no "simple mechanism" can be responsible for the observed nonlinearities [45]. Moreover, it is pointed out, that the deviation from linearity of certain properties must be intimately connected to microscopic structural changes. In the case of Mg/Ca and Ca/Li sodium alumino silicate glasses [46,47] negative deviations from linearity of Young's moduli and Vickers hardness and positive [48] deviations in Na/K alumino silicate glasses have been reported in the literature. The origin of this effect is then discussed in terms of glass structure and bonding. The deviation from linearity must be linked to the compactness of the glass network when two types of network modifier ions co-exist. It is said that the origin of this structural compactness needs to be further investigated. Since the cation radii and field strength of zinc (88 pm, 0.437 $Å^{-2}$) and magnesium (86 pm, 0.445 $Å^{-2}$) are similar in size in comparison to the

Please cite this article as: M. Tiegel, et al., Young's modulus, Vickers hardness and indentation fracture toughness of alumino silicate glasses, Ceramics International (2015), http://dx.doi.org/10.1016/j.ceramint.2015.01.144

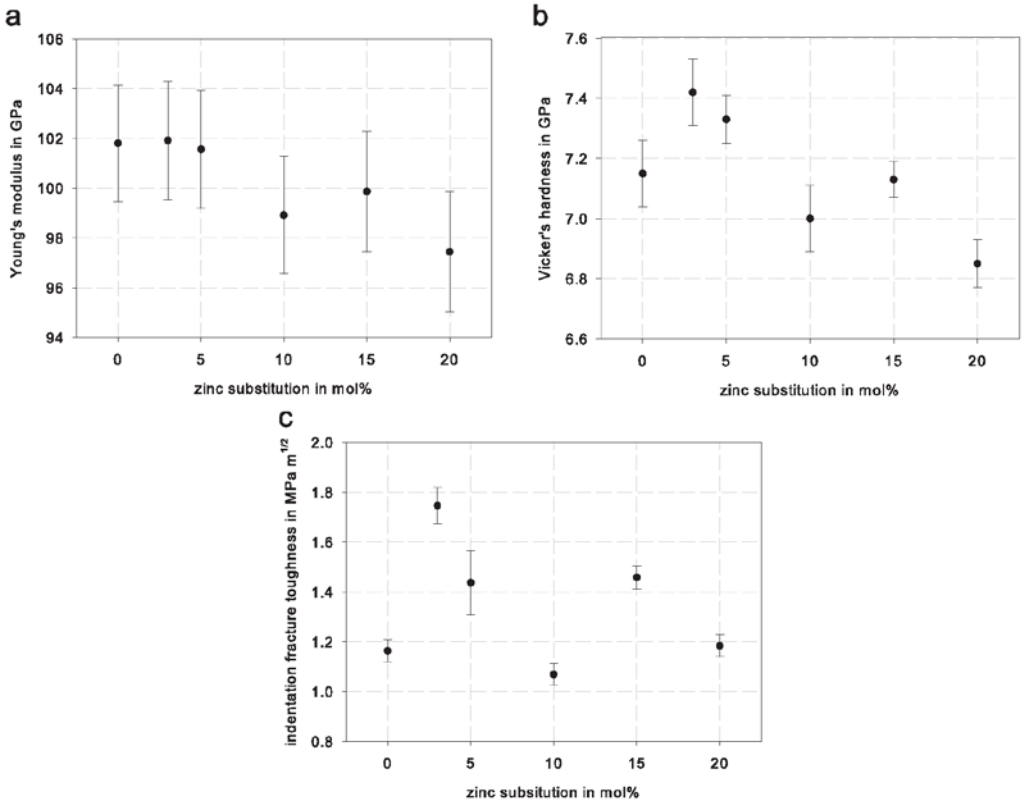

Fig. 4. Young's moduli (a), Vickers hardness (b) and indentation fracture toughness (c) of the zinc substituted magnesium alumino silicate glasses.

systems in the literature with magnesium and calcium (114 pm, 0.347 $Å^{-2}$) as well as sodium (116 pm, 0.171 $Å^{-2}$) and potassium (152 pm, 0.129 $Å^{-2}$), the mixed ionic effect is even more complicated.

Magnesium alumino silicate glasses with different concentrations of MgF_2 instead of MgO have also been investigated. Surprisingly, the mechanical properties do not systematically change with MgF_2-concentrations of up to 9 mol%. It seems that these comparatively small fluorine concentrations do not affect the structural rigidity of the glasses. Furthermore, the fluorine loss during melting of up to 35% has to be considered. The structural role of fluoride seems to depend sensitively on the aluminum concentration, while in alkali or alkaline earth silicates, fluoride is reported to be incorporated as Ca–F units [10] in the corresponding alumosilicate glasses Al–F–Ca structural units are observed using solid state NMR. Since fluorine is incorporated in alumino silicate glasses forming aluminum oxyfluoride species $[AlO_xF_y]^{n-}$, the concentration of bridging-oxygen sites according to Refs. [10,49,50] should remain constant.

In addition to the measurements, it was tried to calculate the mechanical properties using various empirical models. Fig. 5 shows the relative deviation of calculated Young's modulus values from the measured ones. Nine different models, all reported in the literature [51], were used for this. For the model of Makishima [8] predicted and additionally measured values of the density were used for the calculations. As can be seen in Fig. 5 the models of Priven, published in 1998, and Demkina have the best accuracy and precision. However, calculated Young's moduli tend to be smaller than the measured values for all models except that of Makishima which uses the measured densities. The model of Makishima calculates Young's moduli of oxide glasses in terms of the packing density of chemical compositions and the dissociation energy of oxide constituents per unit volume. Hwa et al. reported comparisons of measured Young's modulus with values calculated by Makishima model for low-silica calcium alumino silicate [52] and lanthanum alumino silicate glasses [53]. Both comparisons show 5–20% lower calculated Young's moduli than measured values. All models cannot reflect anomalous structure and bonding species within the glass network such as higher coordination numbers of aluminum promoted by high field strengths of network modifier ions and mixed ionic effects.

4. Conclusion

Alumino silicate glasses with the molar composition 20 mol% Al_2O_3, 60 mol% SiO_2 and 20 mol% M_xO as well as magnesium alumino silicate glasses and lanthanum alumino silicate glasses with different compositions were prepared and investigated with respect to their mechanical properties: Poisson's ratio, Young's modulus, hardness and indentation fracture toughness. Also the effects of mixed magnesium and zinc concentrations as well as of

Please cite this article as: M. Tiegel, et al., Young's modulus, Vickers hardness and indentation fracture toughness of alumino silicate glasses, Ceramics International (2015), http://dx.doi.org/10.1016/j.ceramint.2015.01.144

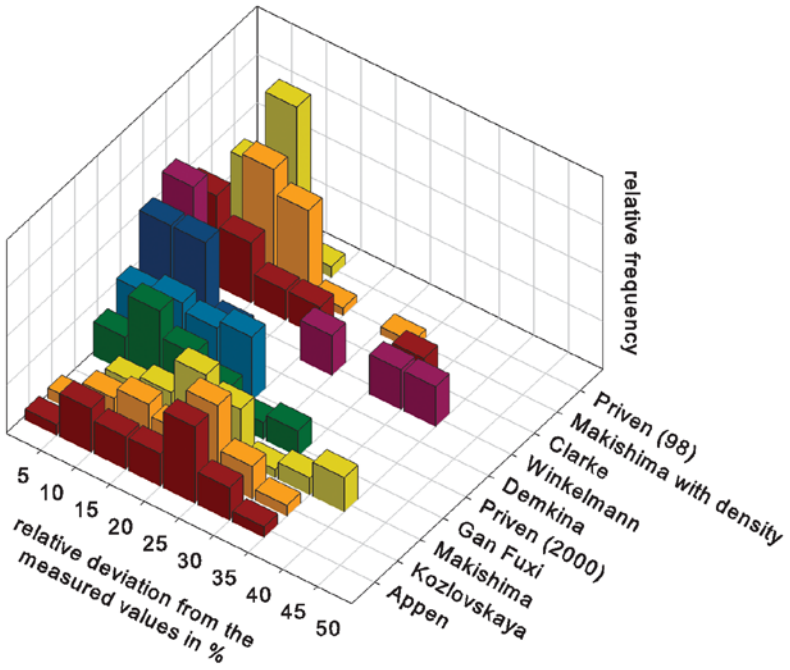

Fig. 5. Relative frequencies of deviations of measured Young's moduli from the values predicted by different models.

a partial substitution of oxides by fluorides were studied. The mechanical properties depend on the glass structure and the type of the network modifier ion.

All studied mechanical properties increase with increasing field strength of network modifier ions. In quaternary magnesium zinc alumino silicate glasses, mechanical properties of the 1 to 1 mixture lie in between the solely zinc and magnesium containing glasses. The mechanical properties of the other mixed zinc magnesium alumino silicate glasses are larger than expected for a linear dependence from the magnesium to zinc ratio.

Furthermore, the rigidity of the glass structure and therefore the concentration and structural role of the network modifier oxide or intermediate oxides affect the mechanical properties of the alumino silicate glasses. In lanthanum alumino silicate glasses, higher values for all measured mechanical properties are obtained for higher lanthanum concentrations.

The effect of the degree of network connectivity, i.e. the number of non-bridging-oxygen sites per network forming tetrahedron was evaluated on magnesium alumino silicate glasses with different MgO concentrations. A clear correlation between rigidity of the glass structure and Poisson's ratio, Young's modulus and hardness was not found for these glasses. Here, the highest values are found for glasses with the lowest concentration of SiO_2. By contrast, higher concentrations of water in the glasses (higher number of non-bridging-oxygen sites) result in a decrease of all studied mechanical properties. Surprisingly, if up to 9 mol% MgO is replaced by MgF_2 the mechanical properties are not significantly affected.

The calculation of Young's moduli by using nine different models leads to the conclusion that all of them predict smaller values than measured. The smallest deviation from measured values is achieved by the models of Priven, published in 1998, and Demkina for most glass compositions.

Acknowledgments

This work was supported by the European Social Fund (ESF) through the Thuringian Ministry of Economy, Employment and Technology (Project number 2011 FGR 0122).

References

[1] A.K. Varshneya, Chemical strengthening of glass: lessons learned and yet to be learned, Int. J. Appl. Glass Sci. 1 (2) (2010) 131–142.
[2] A. Smrcek, Compositions of Industrial Glasses, in: F.T. Wallenberger, P.A. Bingham (Eds.), Fiberglass and Glass Technology, Springer, New York, 2010, pp. 229–266.
[3] Q. Fu, E. Saiz, M.N. Rahaman, A.P. Tomsia, Toward strong and tough glass and ceramic scaffolds for bone repair, Adv. Funct. Mater. 23 (44) (2013) 5461–5476.
[4] R.J. Hand, D.R. Tadjiev, Mechanical properties of silicate glasses as a function of composition, J. Non-Cryst. Solids 356 (44–49) (2010) 2417–2423.
[5] J.H. Campbell, J.S. Hayden, A. Marker, High-power solid-state lasers: a laser glass perspective, Int. J. Appl. Glass Sci. 2 (1) (2011) 3–29.
[6] M. Tiegel, A. Herrmann, S. Kuhn, C. Rüssel, J. Körner, D. Klöpfel, R. Seifert, J. Hein, M.C. Kaluza, Fluorescence and thermal stress properties of Yb^{3+}-doped alumino silicate glasses for ultra high peak power laser applications, Laser Phys. Lett. 11 (11) (2014) 115811.
[7] M. Yamane, J.D. Mackenzie, Vicker's Hardness of glass, J. Non-Cryst. Solids 15 (2) (1974) 153–164.
[8] A. Makishima, J.D. Mackenzie, Direct caluclation of Young's modulus of glass, J. Non-Cryst. Solids 12 (1973) 35–45.
[9] A. Makishima, J.D. Mackenzie, Calculation of bulk modulus, shear modulus and Poisson's ratio of glass, J. Non-Cryst. Solids 17 (1975) 147–157.

Please cite this article as: M. Tiegel, et al., Young's modulus, Vickers hardness and indentation fracture toughness of alumino silicate glasses, Ceramics International (2015), http://dx.doi.org/10.1016/j.ceramint.2015.01.144

[10] A. Stamboulis, R.G. Hill, R.V. Law, Characterization of the structure of calcium alumino-silicate and calcium fluoro-alumino-silicate glasses by magic angle spinning nuclear magnetic resonance (MAS-NMR), J. Non-Cryst. Solids 333 (1) (2004) 101–107.
[11] P. Ganster, M. Benoit, W. Kob, J.-M. Delaye, Structural properties of a calcium aluminosilicate glass from molecular-dynamics simulations: a finite size effects study, J. Chem. Phys. 120 (21) (2004) 10172–10181.
[12] T.F. Soules, Molecular dynamic calculations of glass structure and diffusion in glass, J. Non-Cryst. Solids 49 (1–3) (1982) 29–52.
[13] E.R. Myers, V. Heine, M.T. Dove, Thermodynamics of Al/Al avoidance in the ordering of Al/Si tetrahedral framework structures, Phys. Chem. Miner. 25 (6) (1998) 457–464.
[14] J.F. Stebbins, S.K. Lee, J.V. Oglesby, Al–O–Al oxygen sites in crystalline aluminates and aluminosilicate glasses: high-resolution oxygen-17 NMR results, Am. Mineral. 84 (5–6) (1999) 983–986.
[15] R.F. Cook, G.M. Pharr, Direct observation and analysis of indentation cracking in glasses and ceramics, J. Am. Ceram. Soc. 73 (4) (1990) 787–817.
[16] S. Yoshida, A. Hidaka, J. Matsuoka, Crack initiation behavior of sodium aluminosilicate glasses, J. Non-Cryst. Solids 344 (1–2) (2004) 37–43.
[17] Y. Kato, H. Yamazaki, S. Itakura, S. Yoshida, J. Matsuoka, Load dependence of densification in glass during Vickers indentation test, J. Ceram. Soc. Jpn. 119 (1386) (2011) 110–115.
[18] J.-P. Guin, T. Rouxel, J.-C. Sanglebœuf, I. Melscoët, J. Lucas, Hardness, toughness, and scratchability of germanium–selenium chalcogenide glasses, J. Am. Ceram. Soc. 85 (6) (2002) 1545–1552.
[19] A. Winterstein-Beckmann, D. Möncke, D. Palles, E.I. Kamitsos, L. Wondraczek, A Raman-spectroscopic study of indentation-induced structural changes in technical alkali-borosilicate glasses with varying silicate network connectivity, J. Non-Cryst. Solids 405 (2014) 196–206.
[20] Y. Kato, H. Yamazaki, S. Yoshida, J. Matsuoka, Effect of densification on crack initiation under Vickers indentation test, J. Non-Cryst. Solids 356 (35–36) (2010) 1768–1773.
[21] T. Rouxel, P. Sellappan, F. Célarié, P. Houizot, J.-C. Sanglebœuf, Toward glasses with better indentation cracking resistance, Comptes Rendus Méc. 342 (1) (2014) 46–51.
[22] P. Sellappan, T. Rouxel, F. Celarie, E. Becker, P. Houizot, R. Conradt, Composition dependence of indentation deformation and indentation cracking in glass, Acta Mater. 61 (16) (2013) 5949–5965.
[23] A. Mohajerani, J.W. Zwanziger, Mixed alkali effect on Vickers hardness and cracking, J. Non-Cryst. Solids 358 (12–13) (2012) 1474–1479.
[24] J. Kjeldsen, M.M. Smedskjaer, J.C. Mauro, R.E. Youngman, L. Huang, Y. Yue, Mixed alkaline earth effect in sodium aluminosilicate glasses, J. Non-Cryst. Solids 369 (0) (2013) 61–68.
[25] A. Faivre, F. Despetis, F. Guillaume, P. Solignac, M. Ramonda, Role of mobile cations on microplasticity in alumino-phosphate glasses, J. Am. Ceram. Soc. 93 (10) (2010) 2986–2989.
[26] S. Deriano, T. Rouxel, M. Lefloch, B. Beuneu, Structure and mechanical properties of alkali–alkaline earth-silicate glasses, Phys. Chem. Glasses 45 (1) (2004) 37–44.
[27] S. Yoshida, J.-C. Sanglebœuf, T. Rouxel, Quantitative evaluation of indentation-induced densification in glass, J. Mater. Res. 20 (12) (2005) 3404–3412.
[28] K. Hirao, M. Yoshimoto, N. Soga, K. Tanaka, Densification of magnesium and calcium metaphosphate glasses, J. Non-Cryst. Solids 130 (1) (1991) 78–84.
[29] M. Tiegel, A. Herrmann, C. Russel, J. Korner, D. Klopfel, J. Hein, M.C. Kaluza, Magnesium aluminosilicate glasses as potential laser host material for ultrahigh power laser systems, J. Mater. Chem. C 1 (33) (2013) 5031–5039.
[30] G.R. Anstis, P. Chantikul, B.R. Lawn, D.B. Marshall, A critical evaluation of indentation techniques for measuring fracture toughness: I, direct crack measurements, J. Am. Ceram. Soc. 64 (9) (1981) 533–538.
[31] J. Krautkrämer, H. Krautkrämer, Ultrasonic Testing of Materials, Springer, Berlin, Germany, 1969.
[32] A. Dietzel, Die Kationenfeldstärken und ihre Beziehungen zu Entglasungsvorgängen, zur Verbindungsbildung und zu den Schmelzpunkten von Silicaten, Z. Elektrochem. Angew. Phys. Chem. 48 (1) (1942) 9–23.
[33] N. Wiberg, Lehrbuch der Anorganischen Chemie, de Gruyter, Berlin, 2007.
[34] J.J. Kruzic, D.K. Kim, K.J. Koester, R.O. Ritchie, Indentation techniques for evaluating the fracture toughness of biomaterials and hard tissues, J. Mech. Behav. Biomed. Mater. 2 (4) (2009) 384–395.
[35] K. Niihara, R. Morena, D.P.H. Hasselman, Evaluation of KIc of brittle solids by the indentation method with low crack-to-indent ratios, J. Mater. Scie. Lett. 1 (1) (1982) 13–16.
[36] M.R. DeGuire, S.D. Brown, Dependence of Young's modulus on volume and structure in alkali silicate and alkali aluminosilicate glasses, J. Am. Ceram. Soc. 67 (4) (2006) 270–273.
[37] P.W. Wang, L.P. Zhang, Structural role of lead in lead silicate glasses derived from XPS spectra, J. Non-Cryst. Solids 194 (1–2) (1996) 129–134.
[38] P.F. McMillan, R.J. Kirkpatrick, Al coordination in magnesium aluminosilicate glasses, Am. Mineral. 77 (7–8) (1992) 898–900.
[39] M.M. Smedskjaer, J.C. Mauro, J. Kjeldsen, Y. Yue, Microscopic origins of compositional trends in aluminosilicate glass properties, J. American Ceram. Soc. 96 (5) (2013) 1436–1443.
[40] M.M. Smedskjaer, J.C. Mauro, Y. Yue, Prediction of glass hardness using temperature-dependent constraint theory, Phys. Rev. Lett. 105 (11) (2010) 115503.
[41] S. Kuhn, A. Herrmann, J. Hein, M. Kaluza, C. Rüssel, Sm^{3+}-doped La_2O_3–Al_2O_3–SiO_2-glasses: structure, fluorescence and thermal expansion, J. Mater. Sci. 48 (22) (2013) 8014–8022.
[42] A. Aronne, S. Esposito, P. Pernice, FTIR and DTA study of lanthanum aluminosilicate glasses, Mater. Chem. Phys. 51 (2) (1997) 163–168.
[43] T. Schaller, J.F. Stebbins, The structural role of lanthanum and yttrium in aluminosilicate glasses: a ^{27}Al and ^{17}O MAS NMR study, J. Phys. Chem. B 102 (52) (1998) 10690–10697.
[44] K.J. Rao, D.C. Conductivity, in: K.J. Rao (Ed.), Structural Chemistry of Glasses, Elsevier Science Ltd, Oxford, 2002, pp. 203–261 (Chapter 6).
[45] J.-O. Byun, B.-H. Kim, K.-S. Hong, H.-J. Jung, S.-W. Lee, A.A. Izyneev, Properties and structure of $RO \cdot Na_2O \cdot Al_2O_3 \cdot P_2O_5$ (R=Mg, Ca, Sr, Ba) glasses, J. Non-Cryst. Solids 190 (3) (1995) 288–295.
[46] J. Kjeldsen, M.M. Smedskjaer, J.C. Mauro, R.E. Youngman, L.P. Huang, Y.Z. Yue, Mixed alkaline earth effect in sodium aluminosilicate glasses, J. Non-Cryst. Solids 369 (2013) 61–68.
[47] J. Kjeldsen, M.M. Smedskjaer, J.C. Mauro, Y.Z. Yue, Hardness and incipient plasticity in silicate glasses: origin of the mixed modifier effect, Appl. Phys. Lett. 104 (5) (2014) 051913.
[48] J. Kjeldsen, M.M. Smedskjaer, J.C. Mauro, Y. Yue, On the origin of the mixed alkali effect on indentation in silicate glasses, J. Non-Cryst. Solids 406 (2014) 22–26.
[49] S.C. Kohn, R. Dupree, M.G. Mortuza, C.M.B. Henderson, NMR evidence for five- and six-coordinated aluminum fluoride complexes in F-bearing aluminosilicate glasses, Am. Mineral. 76 (1–2) (1991) 309–312.
[50] J.F. Stebbins, S. Kroeker, S.K. Lee, T.J. Kiczenski, Quantification of five- and six-coordinated aluminum ions in aluminosilicate and fluoride-containing glasses by high-field, high-resolution ^{27}Al NMR, J. Non-Cryst. Solids 275 (1–2) (2000) 1–6.
[51] A.I. Priven, O.V. Mazurin, Comparison of methods used for the calculation of density, refractive index and thermal expansion of oxide glasses, Glass Technol. 44 (4) (2003) 156–166.
[52] L.-G. Hwa, K.-J. Hsieh, L.-C. Liu, Elastic moduli of low-silica calcium alumino-silicate glasses, Mater. Chem. Phys. 78 (1) (2003) 105–110.
[53] L.G. Hwa, T.H. Lee, S.P. Szu, Elastic properties of lanthanum aluminosilicate glasses, Mater. Res. Bull. 39 (1) (2004) 33–40.

Please cite this article as: M. Tiegel, et al., Young's modulus, Vickers hardness and indentation fracture toughness of alumino silicate glasses, Ceramics International (2015), http://dx.doi.org/10.1016/j.ceramint.2015.01.144

Literaturverzeichnis

[1] T.H. Maiman, Stimulated Optical Radiation in Ruby, Nature, 187 (1960) 493-494.

[2] P.P. Sorokin, M.J. Stevenson, Stimulated Infrared Emission from Trivalent Uranium, Physical Review Letters, 5 (1960) 557-559.

[3] A. Javan, W.R. Bennett, D.R. Herriott, Population Inversion and Continuous Optical Maser Oscillation in a Gas Discharge Containing a He-Ne Mixture, Physical Review Letters, 6 (1961) 106-110.

[4] E. Snitzer, Optical Maser Action of Nd^{+3} in a Barium Crown Glass, Physical Review Letters, 7 (1961) 444-446.

[5] J.H. Campbell, J.S. Hayden, A. Marker, High-Power Solid-State Lasers: a Laser Glass Perspective, International Journal of Applied Glass Science, 2 (2011) 3-29.

[6] M.D. Perry, G. Mourou, Terawatt to Petawatt Subpicosecond Lasers, Science, 264 (1994) 917-924.

[7] M.C. Kaluza, Laser-Based Particle Acceleration, Optik & Photonik, 5 (2010) 56-59.

[8] W. Koechner, M. Bass, Solid state lasers: a graduate text, Springer, New York, USA, 2003.

[9] Das POLARIS-Lasersystem, Institut für Optik und Quantenelektronik, Friedrich-Schiller-Universität Jena, http://www.ioq.uni-jena.de/Lasersysteme/POLARIS.html.

[10] S. Paoloni, J. Hein, T. Töpfer, H.G. Walther, R. Sauerbrey, D. Ehrt, W. Wintzer, Laser beam induced optical aberrations in phosphate and fluoride phosphate glasses, Applied Physics B, 78 (2004) 415-419.

[11] M. Dittmer, M. Müller, C. Rüssel, Self-organized nanocrystallinity in $MgO–Al_2O_3–SiO_2$ glasses with ZrO_2 as nucleating agent, Materials Chemistry and Physics, 124 (2010) 1083-1088.

[12] S.M. Logvinkov, G.D. Semchenko, D.A. Kobyzeva, Rearrangement of conodes of the phase diagram of the $MgO-Al_2O_3-SiO_2$ system and its technological prospects, Refractories, 37 (1996) 378-381.

[13] P. Wange, T. Höche, C. Rüssel, J. Dieter Schnapp, Microstructure-property relationship in high-strength $MgO–Al_2O_3–SiO_2–TiO_2$ glass-ceramics, Journal of Non-Crystalline Solids, 298 (2002) 137-145.

[14] G. Leturcq, G. Berger, T. Advocat, C. Fillet, C. Halgand, E. Vernaz, Chemical Durability of Aluminosilicate Glasses Containing Low Solubility Chemical Elements, MRS Proceedings, 506 (2011).

[15] T. Izumitani, M. Matsukawa, H. Miyade, Solubility of Pt in Nd Phosphate Laser Glass, ASTM International, (1988) 29-29-26.

[16] Y. Fujimoto, M. Nakatsuka, A novel method for uniform dispersion of the rare earth ions in SiO2 glass using zeolite X, Journal of Non-Crystalline Solids, 215 (1997) 182-191.

[17] Y. Fujimoto, H. Yoshida, M. Nakatsuka, T. Ueda, A. Fujinoki, Development of Nd-doped Optical Gain Material Based on Silica Glass with High Thermal Shock Parameter for High-Average-Power Laser, Japanese Journal of Applied Physics, 44 (2005) 1764-1770.

[18] T. Sato, Y. Fujimoto, T. Ueda, A. Fujinoki, H. Okada, H. Yoshida, K. Sumimura, M. Nakatsuka, Laser Oscillation of Nd-Doped Silica Glass with High Thermal Shock Parameter, Japanese Journal of Applied Physics, 45 (2006) 6936-6939.

[19] J. Chen, H. Guo, Z. Li, H. Zhang, Y. Zhuang, Near-infrared quantum cutting in Ce^{3+}, Yb^{3+} co-doped YBO_3 phosphors by cooperative energy transfer, Optical Materials, 32 (2010) 998-1001.

[20] Z. Wu, C. Romano, A. Marcelli, A. Mottana, G. Cibin, G. Della Ventura, G. Giuli, P. Courtial, D.B. Dingwell, Evidence for Al/Si tetrahedral network in aluminosilicate glasses from Al *K*-edge x-ray-absorption spectroscopy, Physical Review B, 60 (1999) 9216-9219.

[21] A. Stamboulis, R.G. Hill, R.V. Law, Characterization of the structure of calcium alumino-silicate and calcium fluoro-alumino-silicate glasses by magic angle spinning nuclear magnetic resonance (MAS-NMR), Journal of Non-Crystalline Solids, 333 (2004) 101-107.

[22] P. Ganster, M. Benoit, W. Kob, J.-M. Delaye, Structural properties of a calcium aluminosilicate glass from molecular-dynamics simulations: A finite size effects study, The Journal of Chemical Physics, 120 (2004) 10172-10181.

[23] T.F. Soules, Molecular dynamic calculations of glass structure and diffusion in glass, Journal of Non-Crystalline Solids, 49 (1982) 29-52.

[24] W. Loewenstein, The distribution of aluminum in the tetrahedra of silicates and aluminates, American Mineralogist, 39 (1954) 92-96.

[25] S.K. Lee, J.F. Stebbins, Al–O–Al and Si–O–Si sites in framework aluminosilicate glasses with Si/Al=1: quantification of framework disorder, Journal of Non-Crystalline Solids, 270 (2000) 260-264.

[26] S. Takahashi, D.R. Neuville, H. Takebe, Thermal properties, density and structure of percalcic and peraluminus $CaO–Al_2O_3–SiO_2$ glasses, Journal of Non-Crystalline Solids, 411 (2015) 5-12.

[27] D.M. Zirl, S.H. Garofalini, Structure of Sodium Aluminosilicate Glasses, Journal of the American Ceramic Society, 73 (1990) 2848-2856.

[28] S.K. Sharma, J.A. Philpotts, D.W. Matson, Ring distributions in alkali- and alkaline-earth aluminosilicate framework glasses- a raman spectroscopic study, Journal of Non-Crystalline Solids, 71 (1985) 403-410.

[29] D.W. Matson, S.K. Sharma, J.A. Philpotts, Raman spectra of some tectosilicates and of glasses along the orthoclase-anorthite and nepheline-anorthite joins, American Mineralogist, 71 (1986) 694-704.

[30] D.R. Neuville, L. Cormier, D. Massiot, Al environment in tectosilicate and peraluminous glasses: A ^{27}Al MQ-MAS NMR, Raman, and XANES investigation, Geochimica et Cosmochimica Acta, 68 (2004) 5071-5079.

[31] L.M. Thompson, J.F. Stebbins, Non-bridging oxygen and high-coordinated aluminum in metaluminous and peraluminous calcium and potassium aluminosilicate glasses: High-resolution ^{17}O and ^{27}Al MAS NMR results, American Mineralogist, 96 (2011) 841-853.

[32] J.F. Stebbins, Z. Xu, NMR evidence for excess non-bridging oxygen in an aluminosilicate glass, Nature, 390 (1997) 60-62.

[33] D.R. Neuville, L. Cormier, D. Massiot, Al coordination and speciation in calcium aluminosilicate glasses: Effects of composition determined by ^{27}Al MQ-MAS NMR and Raman spectroscopy, Chemical Geology, 229 (2006) 173-185.

[34] D.R. Neuville, L. Cormier, V. Montouillout, D. Massiot, Local Al site distribution in aluminosilicate glasses by ^{27}Al MQMAS NMR, Journal of Non-Crystalline Solids, 353 (2007) 180-184.

[35] T. Schaller, J.F. Stebbins, The Structural Role of Lanthanum and Yttrium in Aluminosilicate Glasses: A ^{27}Al and ^{17}O MAS NMR Study, The Journal of Physical Chemistry B, 102 (1998) 10690-10697.

[36] J.T. Kohli, J.E. Shelby, J.S. Frye, A structural investigation of yttrium aluminosilicate glasses using ^{29}Si and ^{27}Al magic angle spinning nuclear magnetic resonance, Physics and chemistry of glasses, 33 (1992) 73-78.

[37] S.C. Kohn, R. Dupree, M.G. Mortuza, C.M.B. Henderson, NMR evidence for five- and six-coordinated aluminum fluoride complexes in F-bearing aluminosilicate glasses, American Mineralogist, 76 (1991) 309-312.

[38] J.F. Stebbins, S. Kroeker, S.K. Lee, T.J. Kiczenski, Quantification of five- and six-coordinated aluminum ions in aluminosilicate and fluoride-containing glasses by high-field, high-resolution ^{27}Al NMR, Journal of Non-Crystalline Solids, 275 (2000) 1-6.

[39] C.W. Ponader, G.E. Brown Jr, Rare earth elements in silicate glassmelt systems: I. Effects of composition on the coordination environments of La, Gd, and Yb, Geochimica et Cosmochimica Acta, 53 (1989) 2893-2903.

[40] J.E. Shelby, J.T. Kohli, Rare-Earth Aluminosilicate Glasses, Journal of the American Ceramic Society, 73 (1990) 39-42.

[41] I. Bardez, D. Caurant, P. Loiseau, N. Baffier, J.L. Dussossoy, C. Gervais, F. Ribot, D.R. Neuville, Structural characterisation of rare earth rich glasses for nuclear waste immobilisation, Physics and Chemistry of Glasses, 46 (2005) 320-329.

[42] N. Wiberg, Lehrbuch der Anorganischen Chemie, de Gruyter, Berlin, 2007.

[43] G. Blasse, B.C. Grabmaier, Luminescent Materials, Springer Berlin Heidelberg1994.

[44] S. Cotton, Lanthanide and actinide chemistry, John Wiley & Sons Ltd, Chichester, England, 2006.

[45] W.F. Krupke, Ytterbium solid-state lasers. The first decade, Selected Topics in Quantum Electronics, IEEE Journal of, 6 (2000) 1287-1296.

[46] A. Paul, M. Mulholland, M.S. Zaman, Ultraviolet absorption of cerium(III) and cerium(IV) in some simple glasses, Journal of Materials Science, 11 (1976) 2082-2086.

[47] M.J. Weber, Optical spectra of Ce^{3+} and Ce^{3+}-sensitized fluorescence in $YAlO_3$, Journal of Applied Physics, 44 (1973) 3205-3208.

[48] W.T. Carnall, P.R. Fields, K. Rajnak, Electronic Energy Levels in the Trivalent Lanthanide Aquo Ions. I. Pr^{3+}, Nd^{3+}, Pm^{3+}, Sm^{3+}, Dy^{3+}, Ho^{3+}, Er^{3+}, and Tm^{3+}, The Journal of Chemical Physics, 49 (1968) 4424-4442.

[49] W.T. Carnall, P.R. Fields, K. Rajnak, Electronic Energy Levels of the Trivalent Lanthanide Aquo Ions. IV. Eu3+, The Journal of Chemical Physics, 49 (1968) 4450-4455.

[50] A. Paul, R.W. Douglas, Cerous-ceric equilibrium in binary alkali borate and alkali silicate glasses, Physics and Chemistry of Glasses, 6 (1965) 212-215.

[51] H.D. Schreiber, H.V. Lauer Jr, T. Thanyasiri, The redox state of cerium in basaltic magmas: an experimental study of iron-cerium interactions in silicate melts, Geochimica et Cosmochimica Acta, 44 (1980) 1599-1612.

[52] V. Gottardi, G. Paoletti, M. Tornati, The ratio Ce^{3+}/Ce^{4+} in the melting of different glasses and its influence on their properties, Advances in Glass Technology, VI International Congress in GlassWashington D.C., 1962, pp. 412-423.

[53] W.D. Johnston, Oxidation-Reduction Equilibria in Molten $Na_2O.2SiO_2$ Glass, Journal of the American Ceramic Society, 48 (1965) 184-190.

[54] A.I. Vogel, J. Mendham, Vogel's textbook of quantitative chemical analysis, Prentice Hall, Harlow, 2000.

[55] F. Goubin, X. Rocquefelte, M.-H. Whangbo, Y. Montardi, R. Brec, S. Jobic, Experimental and Theoretical Characterization of the Optical Properties of CeO_2, $SrCeO_3$, and Sr_2CeO_4 Containing Ce^{4+} (f^0) Ions, Chemistry of Materials, 16 (2004) 662-669.

[56] N.V. Skorodumova, R. Ahuja, S.I. Simak, I.A. Abrikosov, B. Johansson, B.I. Lundqvist, Electronic, bonding, and optical properties of CeO_2 and Ce_2O_3 from first principles, Physical Review B, 64 (2001) 115108.

[57] F. Marabelli, P. Wachter, Covalent insulator CeO_2: Optical reflectivity measurements, Physical Review B, 36 (1987) 1238-1243.

[58] H. Ebendorff-Heidepriem, D. Ehrt, Formation and UV absorption of cerium, europium and terbium ions in different valencies in glasses, Optical Materials, 15 (2000) 7-25.

[59] A.M. Efimov, A.I. Ignatiev, N.V. Nikonorov, E.S. Postnikov, Quantitative UV–VIS spectroscopic studies of photo-thermo-refractive glasses. II. Manifestations of Ce^{3+} and Ce(IV) valence states in the UV absorption spectrum of cerium-doped photo-thermo-refractive matrix glasses, Journal of Non-Crystalline Solids, 361 (2013) 26-37.

[60] Y. Yang, L. Liu, M. Li, C. Mi, Y. Liu, X. Su, J. Zhang, F. Yu, X. Li, S. Cai, Near-Infrared Quantum Cutting in Ce^{3+}, Yb^{3+}Doped $Gd(PO_3)_3$ Phosphors, Science of Advanced Materials, 7 (2015) 1304-1309.

[61] J. Zhou, Y. Teng, S. Zhou, J. Qiu, Quantum Cutting in Luminescent Glasses and Glass Ceramics, International Journal of Applied Glass Science, 3 (2012) 299-308.

[62] T. Förster, Experimentelle und theoretische Untersuchung des zwischenmolekularen Übergangs von Elektronenanregungsenergie, Zeitschrift für Naturforschung, 4a (1949) 321-327.

[63] D.L. Dexter, A theory of sensitized luminescence in solids, The Journal of Chemical Physics, 21 (1953) 836-850.

[64] P. Vergeer, T.J.H. Vlugt, M.H.F. Kox, M.I. den Hertog, J.P.J.M. van der Eerden, A. Meijerink, Quantum cutting by cooperative energy transfer in $Yb_xY_{1-x}PO_4 : Tb^{3+}$, Physical Review B, 71 (2005) 014119.

[65] D.L. Dexter, Cooperative Optical Absorption in Solids, Physical Review, 126 (1962) 1962-1967.

[66] W. Schmidt, Optische Spektroskopie: eine Einführung, 2 ed., Wiley-VCH, Weinheim, Germany, 2000.

[67] J.R. Lakowicz, Principles of Fluorescence Spectroscopy, 3 ed., Springer, New York, USA, 2006.

[68] E.M. Purcell, Spontaneous Emission Probabilities at Radio Frequencies, in: E. Burstein, C. Weisbuch (Eds.) Confined Electrons and Photons, Springer US1995, pp. 839-839.

[69] R.J. Glauber, M. Lewenstein, Quantum optics of dielectric media, Physical Review A, 43 (1991) 467-491.

[70] P. de Vries, A. Lagendijk, Resonant Scattering and Spontaneous Emission in Dielectrics: Microscopic Derivation of Local-Field Effects, Physical Review Letters, 81 (1998) 1381-1384.

[71] M.E. Crenshaw, C.M. Bowden, Effects of Local Fields on Spontaneous Emission in Dielectric Media, Physical Review Letters, 85 (2000) 1851-1854.

[72] P.R. Berman, P.W. Milonni, Microscopic Theory of Modified Spontaneous Emission in a Dielectric, Physical Review Letters, 92 (2004) 053601.

[73] M.E. Crenshaw, The quantized field in a dielectric and application to the radiative decay of an embedded atom, Physics Letters A, 358 (2006) 438-442.

[74] C.-K. Duan, M.F. Reid, Z. Wang, Local field effects on the radiative lifetime of emitters in surrounding media: Virtual- or real-cavity model?, Physics Letters A, 343 (2005) 474-480.

[75] D. Toptygin, Effects of the Solvent Refractive Index and Its Dispersion on the Radiative Decay Rate and Extinction Coefficient of a Fluorescent Solute, Journal of Fluorescence, 13 (2003) 201-219.

[76] H.W. Moos, Spectroscopic relaxation processes of rare earth ions in crystals, Journal of Luminescence, 1–2 (1970) 106-121.

[77] C.B. Layne, Multiphonon relaxation and excitation transfer in rare-earth doped glasses, California Univ., Lawrence Livermore Lab, Livermore (USA), 1975.

[78] J.M.F. van Dijk, M.F.H. Schuurmans, On the nonradiative and radiative decay rates and a modified exponential energy gap law for 4f–4f transitions in rare-earth ions, The Journal of Chemical Physics, 78 (1983) 5317-5323.

[79] C.B. Layne, W.H. Lowdermilk, M.J. Weber, Multiphonon relaxation of rare-earth ions in oxide glasses, Physical Review B, 16 (1977) 10-20.

[80] J.A. Duffy, M.D. Ingram, Establishment of an optical scale for Lewis basicity in inorganic oxyacids, molten salts, and glasses, Journal of the American Chemical Society, 93 (1971) 6448-6454.

[81] J.A. Duffy, A review of optical basicity and its applications to oxidic systems, Geochimica et Cosmochimica Acta, 57 (1993) 3961-3970.

[82] J.A. Duffy, M.D. Ingram, Comments on the application of optical basicity to glass, Journal of Non-Crystalline Solids, 144 (1992) 76-80.

[83] J.E. Marion, Appropriate use of the strength parameter in solid-state slab laser design, Journal of Applied Physics, 62 (1987) 1595-1604.

[84] J.B. Wachtman, W.R. Cannon, M.J. Matthewson, Mechanical Properties of Ceramics, 2 ed., John Wiley & Sons, Inc.2009.

[85] R.J. Bell, P. Dean, Atomic vibrations in vitreous silica, Discussions of the Faraday Society, 50 (1970) 55.

[86] W. Mozgawa, M. Handke, W. Jastrzębski, Vibrational spectra of aluminosilicate structural clusters, Journal of Molecular Structure, 704 (2004) 247-257.

[87] W. Mozgawa, W. Jastrzębski, M. Handke, Vibrational spectra of D4R and D6R structural units, Journal of Molecular Structure, 744-747 (2005) 663-670.

[88] K.J. Rao, Chapter 6 - D.C. conductivity, in: K.J. Rao (Ed.) Structural Chemistry of Glasses, Elsevier Science Ltd, Oxford, 2002, pp. 203-261.

[89] J. Kjeldsen, M.M. Smedskjaer, J.C. Mauro, R.E. Youngman, L.P. Huang, Y.Z. Yue, Mixed alkaline earth effect in sodium aluminosilicate glasses, Journal of Non-Crystalline Solids, 369 (2013) 61-68.

[90] J. Kjeldsen, M.M. Smedskjaer, J.C. Mauro, Y.Z. Yue, Hardness and incipient plasticity in silicate glasses: Origin of the mixed modifier effect, Appl. Phys. Lett., 104 (2014) 051913.

[91] J. Kjeldsen, M.M. Smedskjaer, J.C. Mauro, Y. Yue, On the origin of the mixed alkali effect on indentation in silicate glasses, Journal of Non-Crystalline Solids, 406 (2014) 22-26.

[92] A. Herrmann, D. Ehrt, Time-resolved fluorescence measurements on Dy^{3+} and Sm^{3+} doped glasses, Journal of Non-Crystalline Solids, 354 (2008) 916-926.

[93] F.S. Richardson, J.D. Saxe, S.A. Davis, T.R. Faulkner, Intensity calculations on hypersensitive f-f transitions in nine-coordinate lanthanide systems of trigonal symmetry, Molecular Physics, 42 (1981) 1401-1429.

[94] D. Ehrt, H.T. Vu, A. Herrmann, G. Völksch, Luminescent ZnO-Al_2O_3-SiO_2 Glasses and Glass Ceramics, Advanced Materials Research, 39-40 (2008) 231-236.

[95] G. Qian, M. Nikl, J. Bei, J. Pejchal, S. Baccaro, R. Giorgi, A. Cecilia, G. Chen, Temperature dependence of photoluminescence in ZnO-containing glasses, Optical Materials, 30 (2007) 91-94.

[96] G. Chen, M. Nikl, N. Solovieva, A. Beitlerova, J. Rao, Y. Yang, Y. Zhang, X. Jiang, C. Zhu, Photoluminescent properties of nanocrystallized zinc borosilicate glasses, Radiation Measurements, 38 (2004) 771-774.

[97] D. Ehrt, Photoluminescence in the UV–VIS region of polyvalent ions in glasses, Journal of Non-Crystalline Solids, 348 (2004) 22-29.

[98] H. Scholze, Eigenschaften des Glases, Glas, Springer Berlin Heidelberg1977, pp. 122-290.

[99] B.F. Aull, H. Jenssen, Vibronic interactions in Nd:YAG resulting in nonreciprocity of absorption and stimulated emission cross sections, Quantum Electronics, IEEE Journal of, 18 (1982) 925-930.

[100] P. Dorenbos, 5d-level energies of Ce^{3+} and the crystalline environment. III. Oxides containing ionic complexes, Physical Review B, 64 (2001) 125117.

[101] P. Dorenbos, Relating the energy of the $[Xe]5d^1$ configuration of Ce^{3+} in inorganic compounds with anion polarizability and cation electronegativity, Physical Review B, 65 (2002) 235110.

Danksagung

Mein Dank gilt all denen, die zum Gelingen dieser Arbeit beigetragen haben.

Besonderer Dank gebührt Herrn Prof. Dr. Christian Rüssel für die interessante Themenstellung sowie die fachliche Betreuung während der vergangenen drei Jahre.

Ebenfalls bedanke ich mich bei Herrn Dr. Andreas Herrmann für die immerwährende freundschaftliche Unterstützung, die kreativen Diskussionen und die Messungen der Fluoreszenz. Auch gilt großer Dank Herrn Stefan Kuhn, mit dessen Arbeit gemeinsam eine kontinuierliche Weiterentwicklung der untersuchten Aluminosilicatgläser möglich war. Weiterhin danke ich allen Mitarbeitern des Otto-Schott-Instituts für Materialforschung, die mich in den letzten drei Jahren unterstützt haben. Speziell herausstellen möchte ich Herrn Thomas Kittel für die beständige Unterstützung in Fragen der Glastechnologie, Mikroskopie und Homogenitätsuntersuchungen, Frau Gabriele Möller, die unzählige Proben feinoptisch bearbeitet hat, sowie Herrn Dietmar Güttler, Frau Steffi Ebbinghaus und Herrn Christian Thieme für Dilatometrie- und DTA-Messungen. Außerdem möchte ich meinen Dank gegenüber den Gaststudenten und –wissenschaftlern Herrn Dr. Hosam A. Othman, Herrn Reza Hosseinabadi und Herrn Achraf A. Assadi für ihre tatkräftige Hilfe ausdrücken.

Für ein sehr angenehmes und kinderreiches Arbeitsklima und inspirierende Diskussionen danke ich meinen Laborkollegen Martina, Ulli, Antje und Hacki.

Des Weiteren möchte ich mich bei den Mitarbeitern und Studenten des Institutes für Optik und Quantenelektronik in Jena für die zahlreichen Fluoreszenzmessungen und Lasertests von Ytterbium-dotierten Proben bedanken. Insbesondere gilt Herrn Dr. Jörg Körner, Herrn Dr. Joachim Hein und Herrn Prof. Dr. Malte C. Kaluza mein Dank für anregende Diskussionen und die gute Zusammenarbeit im Forschungsprojekt ALASKA. Auch bedanke ich mich beim Unternehmensbeirat für die hilfreichen Diskussionen in den Projektworkshops. Dabei gilt großer Dank Herrn Dr. Andreas Gebhardt für weitergehende Untersuchungen im technischen Maßstab und für die kostengünstige und kurzfristige Lieferung von Rohstoffen.

Schließlich danke ich Frau HDoz. Dr. Doris Ehrt für ihre Unterstützung mit hilfreichen Ratschlägen aus ihrem großen Erfahrungsschatz.

Der größte Dank gebührt meiner Mutter, meiner gesamten Familie und meinen Freund, ohne die diese Arbeit nicht möglich gewesen wäre.

Lebenslauf

Persönliche Daten

Name	Tiegel
Vorname	Mirko
Anschrift	Wiesenweg 45
	06712 Kretzschau
Geburtsdatum	09. September 1986
Geburtsort	Zeitz

Schulausbildung

Juli 1997 - März 2006	CJD Christophorusschule Droyßig in Droyßig
Schulabschluss	allgemeine Hochschulreife

Akademische Ausbildung

Oktober 2006 – November 2011	Chemiestudium an der Friedrich-Schiller-Universität Jena Diplomarbeit: „Herstellung von Glasfasern aus Vorformen mit verschiedenen Profilen an einer neuaufgebauten Ziehanlage“ Abschluss: Diplom in Chemie
seit Januar 2012	Promotion am Otto-Schott-Institut für Materialforschung an der Friedrich-Schiller-Universität Jena Arbeitsgruppe: Prof. Dr. C. Rüssel

Ort, Datum . . . . . .

Unterschrift . . . . . .

Bestätigung des Einverständnisses der Koautoren

Die Koautoren der in dieser kumulativen Dissertation verwendeten Manuskripte sind sowohl über die Nutzung, als auch über die angegebenen Eigenanteile informiert und stimmen dem zu.

Ort, Datum . . . . . .

Unterschrift . . . . . .

Selbstständigkeitserklärung

Ich erkläre, dass ich die vorliegende Arbeit selbstständig und unter Verwendung der angegebenen Hilfsmittel, persönlichen Mitteilungen und Quellen angefertigt habe.

Ort, Datum . . . . . .

Unterschrift . . . . . .